LBL-1226

THE QUESTION OF EQUILIBRIUM AT A PHASE BOUNDARY DURING THE CRYSTAL GROWTH FROM THE MELT

RECEIVED
LAWRENCE
RADIATION LABORATORY

LIBRARY AND
DOCUMENTS SECTION

Tsung-Shen Thomas Shih

(M. S. Thesis)

September 1972

AEC Contract No. W-7405-eng-48

For Reference

Not to be taken from this room

DISCLAIMER

This document was prepared as an account of work sponsored by the United States Government. While this document is believed to contain correct information, neither the United States Government nor any agency thereof, nor the Regents of the University of California, nor any of their employees, makes any warranty, express or implied, or assumes any legal responsibility for the accuracy, completeness, or usefulness of any information, apparatus, product, or process disclosed, or represents that its use would not infringe privately owned rights. Reference herein to any specific commercial product, process, or service by its trade name, trademark, manufacturer, or otherwise, does not necessarily constitute or imply its endorsement, recommendation, or favoring by the United States Government or any agency thereof, or the Regents of the University of California. The views and opinions of authors expressed herein do not necessarily state or reflect those of the United States Government or any agency thereof or the Regents of the University of California.

THE QUESTION OF EQUILIBRIUM AT A PHASE BOUNDARY DURING THE CRYSTAL GROWTH FROM THE MELT

Contents

List of Figures v

List of Photographs vi

List of Tables vii

Abstract viii

I. Introduction 1

II. Background Theories 3

A. Absolute Rate Theory 4

1. Crystal Growth from the Pure Melt 5

2. Crystal Grwoth from the Binary Melt without Solid Solutions 7

B. Liquid Inclusion Theory 10

III. Description of Experiment 15

A. Description of Experimental Apparatus 17

B. Sample Preparation 23

C. Experimental Procedures 24

1. Data Analysis 25

a. Interfacial Temperature 27

b. Interfacial Liquid Concentration 28

c. Interfacial Solid Concentration 29

IV. Results and Discussion 32

A. Interfacial Temperature Rise 32

B. Interferograms 33

C. Application of the Absolute Rate Theory. 43

1. Pure Salol and Thymol. 43

2. Binary Mixtures of Salol-Thymol System 50

D. Application of the Liquid Inclusion Theory 63

V. Conclusions. 76

Acknowledgements 78

Nomenclature 79

References 82

Appendix I

A. Physical Properties. 85

1. Phase Diagram. 85

2. Refractive Index 86

3. Viscostiy. 86

4. Density. 86

5. Diffusivity. 88

Appendix II

A. Sample Calculations. 90

1. Measured Data for Salol-Thymol Systems 90

2. Calculation of the Interfacial Liquid Composition. . 90

3. Calculation of the Interfacial Solid Composition . . 91

4. Theoretical Prediction of the Interfacial Solid Composition from the Absolute Rate Theory. 92

5. Theoretical Prediction of the Interfacial Solid Composition from the Liquid Inclusion Theory 93

Appendix III.

A. Infrared Absorption Analysis 95

Appendix IV. Fortran IV Computer Program Listing. 99

0 0 0 0 3 8 0 0 7 2 4

LIST OF FIGURES

Fig. 1. Dendrite Growth at the Interface. 12

Fig. 2. Microinterferometric Setup. 16

Fig. 3. Optical Wedge 22

Fig. 4. Phase Diagram of Salol-Thymol System. 26

Fig. 5. Fringe Pattern at Interface during Crystal Growth 30

Fig. 6. Interfacial Temperature Rise during the Growth of Pure Salol at 20 °C/cm 34

Fig. 7. Interfacial Temperature Rise during the Growth of Pure Thymol at 20 °C/cm. 35

Fig. 8. Growth Rates of Pure Salol Crystals in Undercooled Liquid . 44

Fig. 9. Growth Rates of Pure Thymol Crystals in Undercooled Liquid. 45

Fig. 10. Interfacial Compositions of Thymol-rich Mixtures. 60

Fig. 11. Interfacial Composition of Salol-rich Mixtures. 61

Fig. 12. Comparison of Interfacial Solid Compositions (Absolute Rate Theory). 64

Fig. 13. Experimental Data Plotted in the Form of Eq. (28) 65

Fig. 14. Comparison of Interfacial Solid Compositions (Liquid Inclusion Theory) 70

Fig. 15. Experimental Data Plotted in the Form of Eq. (31) 71

Fig. 16. Qualitative Temperature Profiles in the Optical Wedge . . . 73

LIST OF PHOTOGRAPHS

Photo. 1. Overall-view of Experimental Apparatus. 18

Photo. 2. Temperature-Gradient Microscope Stage 20

Photo. 3. Crystal Growing from Pure Thymol. 36

Photo. 4. Crystal Growing from Pure Salol 37

Photo. 5. Crystal Growing from Salol-Thymol Melt in 5 mole % Salol. 38

Photo. 6. Crystal Growing from Salol-Thymol Melt in 10 mole % Salol 39

Photo. 7. Crystal Growing from Salol-Thymol Melt in 15 mole % Salol 40

Photo. 8. Crystal Growing from Salol-Thymol Melt in 90 mole % Salol 41

Photo. 9. Crystal Growing from Salol-Thymol Melt in 95 mole % Salol 42

0 0 0 0 3 8 0 0 9 2 3

LIST OF TABLES

Table I. Melting Temperatures of Pure Salol and Thymol. 25

Table II. Observed Interfacial Temperature Rise Above Extrapolated Straight Lines 32

Table III. Experiment Results, Pure Salol 46

Table IV. Experiment Results, Pure Thymol. 47

Table V. Comparison of the Kinetic Relations for Pure Salol 49

Table VI. Growth Velocities, Interfacial Conditions and Predicted Interfacial Solid Compositions 51

Table VII. Experimental Measurements, Salol-Thymol System 55

Table VIII. Theoretical Derived Values of Radii of Dendritic Projections Growing from Crystal Surfaces. 67

Table IX. Comparison of Solid Compositions Computed from Flux Balance with Values from Infrared Absorption and Liquid Inclusion Theory 69

Table X. The Melting Temperatures for the Salol-Thymol System . . . 85

Table XI. Viscosities and Densities of Pure Salol and Thymol 87

Table XII. Calculated Diffusivities of the Salol-Thymol System. . . . 88

Table XIII. Physical Properties of the Pure Substances 89

Table XIV. The Infrared Absorption of Pure Thymol 98

Table XV. The Infrared Absorption of Pure Salol. 98

THE QUESTION OF EQUILIBRIUM AT A PHASE BOUNDARY DURING CRYSTAL GROWTH

Tsung-Shen Thomas Shih

Lawrence Berkeley Laboratory
University of California
Berkeley, California 94720

September 1972

ABSTRACT

The rates of crystal growth from undercooled binary organic melts were studied using a simple eutectic system of salol and thymol.

A temperature-gradient microinterferometric method was used to determine the interfacial liquid and solid concentrations and temperatures as well as the liquid concentration gradients near the growing faces of the crystals.

The experimental results indicated that considerable departure of the interfacial compositions and temperatures from equilibrium can occur, depending on the growth rate and the interface conditions. It was found that, even at small crystal growth rates, equilibrium at the phase boundary did not exist at all.

Both the absolute rate theory and the liquid inclusion theory were discussed and compared with the experimental data. It was found that the Eyring-type of kinetic rate expression predicted the growth rate of crystallization for pure substances within an order of magnitude.

No liquid inclusions were observed in this sytem. The criterion for breakdown of planar interfaces was found not to be valid in the

eutectic organic system used. The presence of a stabilizing temperature gradient applied to the interfacial liquid had no effect on the concentration of impurity in the crystal but did affect interfacial shape and stability.

I. INTRODUCTION

Crystallization is a powerful separation process involving phase transformation at relative low temperature which provides several unique advantages over other separation processes. For example, crystallization can be used to purify thermally unstable materials, to separate close-boiling chemically similar isomers, and to obtain ultrapure materials. In addition, crystals can be produced in a form convenient for processing, packing, storage and marketing.

Crystallization from solution is the most common method at present. However, crystal growth from a melt, known as fractional solidification, is often much faster than that from aqueous solution. Furthermore, a solvent for the substances to be purified is not required and this avoids difficulties with solvent occlusion. Sometimes fractional solidification is attractive in terms of cost and convenience of operations.

The growth of a crystal from its melt is a complicated problem involving mass and heat transfer in the bulk phases and a kinetic process at the solid-liquid interface. The transport mechanism in the bulk phases is fairly well understood. However, the interfacial rate phenomena are still obscure.

The optical, electrical and mechanical properties of crystals depend not only upon the structure of the crystal lattice but also on the growth mechanism. The rapid growth of the solid-state industry and the high demands of the semiconductor and electronic industries for uniform and stable ultrapure crystals have placed heavy demands for extensive understanding on the kinetics of crystallization.

Although artificial crystal growth has had much effect on various sciences and industries, the process itself has retained more of the flavor of art than of science.

Crystallization, unlike most mass transfer processes, has a rather high interface transfer resistance. To define better the actual interface kinetic effect on crystallization, an experimental project was initiated. The object was to investigate the interfacial kinetics for crystal growth from a binary melt, i.e., the relations between non-equilibrium distribution, interfacial conditions, and growth velocity.

The experimental method was selected to enable measurement of the interfacial quantities such as the interfacial liquid and solid concentrations and temperatures.

II. BACKGROUND THEORIES

Crystallization can be considered to occur in two consecutive steps: 1) the initial nucleation of crystals, and 2) the growth of these nuclei by the accretion of atoms from the melt. Much has been written on nucleation (1,2,3). The main concern of this work, however, is with the growth of a crystal once it has been formed, irrespective of its origin.

Numerous studies of crystal growth phenomena have been conducted. Several crystal growth mechanisms have been proposed. In this chapter the Absolute Rate Theory and the Liquid Inclusion Theory for crystal growth from the liquid melt are presented. It has become apparent that the concentration of impurities in a crystal solidified from its melt is often different from that expected from the equilibrium distribution coefficient. The deviations are associated with the interface rate phenomena that are the main concern of this thesis.

In the past few years, the field of non-equilibrium impurity distribution has become extensive. Some investigators (4,5) have suggested that the solid composition does not have its equilibrium value because of the requirement for a kinetic driving force at the interface. Some have considered the interface region of crystal growth as an open thermodynamic system undergoing irreversible change (6). Others have noted that small particles of liquid are sometimes occluded during crystal growth (7,8), giving an apparent composition to the crystal that lies between those of the pure solid phase and the interface liquid. Impurity concentrations exceeding the solid solubility limit were also noted at higher crystal growth rates (9,10). Therefore impurity mechanical capture has been proposed (12) to be the cause of the apparent non-equilibrium distribution.

A. Absolute Rate Theory

The atomic mechanisms for the growth of a solid into a supercooled liquid have been suggested (13,14) but are only slightly understood. In crystal growth there is probably an atomic flux transfer back and forth from the ordered crystal face into the disordered liquid, more atoms joining the growing crystal than leaving it.

Originally it was thought that a crystal surface must be atomically rough (15) and that molecules attach themselves freely and independently on any surface orientation that is presented. This view was criticized later by Jackson et al. (16). Evidence from the direct observation of a great many crystal growth studies has shown that the crystal grows from the melt by attachment of molecules to the steps of screw dislocations (17,18,19).

Hillig and Turnbull (19) suggested that the rate of addition of molecules to an advancing step can be expressed using Eyring's concept (20) of "absolute rate theory". This theory was further developed by Kirwan and Pigford (4) and critically tested recently by Cheng (30) using certain complex pure organic compounds. The theory was found to be within an order of magnitude of the observations.

The absolute rate theory for cyrstallization was derived (4) based on the assumption that the difference of the chemical potential between solid and liquid phase is the driving force for the phase transformation, and that the crystal surface is imperfect. Therefore, the rate of growth of an advancing face is governed by the rate of addition of molecules to the screw dislocation steps on the solid surface as well as the density of

the steps on the crystal surface. It is also based on the hypothesis that there exists an intermediate activated state for crystallization; the liquid molecules at the interface need not only have a certain orientation but must have a certain amount of energy in order to overcome an energy barrier when they attach themselves to the crystal.

1. Crystal Growth from the Pure Melt

The net flux of material onto the crystal interface may be written as

$$N = f(\lambda_L \rho_L k^F - \lambda_s \rho_s k^R) = f\lambda_s \rho_s (k^F - k^R) \qquad (1)$$

where k^F, k^R, represent the forward and reverse rate coefficients respectively. λ is the distance the interface advances when a monomolecular layer is added to the solid or liquid. It is also assumed that the molecular spacings are inversely proportional to the densities. The factor "f" is the fraction of the crystal surface which is available for attachment of a molecule.

Both the forward and reverse rate coefficients can be expressed by the Eyring concept (20) of reaction rate theory. The forward rate coefficient is given by the equation,

$$k^F = \chi(\frac{kT}{h}) \exp(-\frac{\Delta H_C^{\ddagger}}{RT}) \exp(\frac{\Delta S_C^{\ddagger}}{R}) \qquad (2)$$

where kT/h is a universal frequency factor, $\Delta S_C^{\ddagger}$ and $\Delta H_C^{\ddagger}$ represent the entropy and enthalpy excess of the activated state of the crystallization. χ is the transmission coefficient, representing the probability that each activated complex is converted into the product. A similar equation can be written for the reverse coefficient, k^R. It is related to k^F by the equation

$$k^R = k^F \exp(\frac{-\Delta\mu^{\circ}}{RT}) \qquad (3)$$

where $\Delta\mu^\circ$ is the difference of chemical potentials at the standard state between the liquid and solid phases.

The density of active sites on the crystal surface depends on the nature of the solid-liquid interface. For an atomically rough interface all sites on the surface are available for attachment and f equals to one. For a screw dislocation mechanism suggested by Frank (21), the step density is given in terms of the intermolecular spacing and the radius of the two-dimensional critical embryo, r_c,

$$f = \frac{\lambda_s}{4\pi r_c} \tag{4}$$

where,

$$r_c = \frac{\sigma}{\rho_s \Delta G} \tag{5}$$

σ is the surface free energy in the interface per unit of surface area. Without considering the dependence of surface energy on the shapes of the interface, the surface energy can be obtained from Turnbull's correlation (1),

$$\sigma = 0.3 \left(\frac{\Delta H_f}{N^{1/3} V_s^{2/3}}\right) \tag{6}$$

where ΔH_f is the entropy of fusion, N is Avogadro's number, and V_s is the molar volume of the solid.

If we introduce $V_s = 1/\rho_s$, and $\lambda_s = (V_s/N)^{1/3}$, the absolute rate theory of crystallization from the pure melt predicts a freezing velocity of

$$V = \left(\frac{\Delta T}{1.2\pi T_m}\right)\left(\chi \frac{kT}{h}\right)\lambda_s\left[1 - \exp\left(\frac{-\Delta\mu^\circ}{RT}\right)\right] \exp\left(\frac{-\Delta H_C^{\ddagger} + T\Delta S_C^{\ddagger}}{RT}\right) \tag{7}$$

where $\Delta\mu^\circ$ can be approximated by $\Delta S_f \Delta T$ for pure substances. Taking the first term in the Taylor expansion for the exponential term the final form

for the absolute rate theory yields for pure materials,

$$V = \left(\frac{1}{1.2\pi}\right)\left(\chi \frac{kT}{h}\right)\left(\frac{\Delta S_f}{R}\right)\lambda_s\left(\frac{\Delta T}{T_m}\right)^2 \exp\left(\frac{-\Delta H_C^{\ddagger} + T\Delta S_C^{\ddagger}}{RT}\right) \quad . \tag{8}$$

2. Crystal Growth from the Binary Melt Without Solid Solutions

If A represents the impurity component in the binary system, the rate at which B molecules leave a phase and traverse the interface is proportional to the mole fraction of the B specie in that phase. The net flux of component B toward the surface of the crystal is

$$N_B = f(\lambda_L k_B^F \rho_L y_B - \lambda_s k_B^R \rho_s x_B) \tag{9}$$

where x_B and y_B are the concentrations in the solid and liquid phases. If we assume that the lattice dimensions are inversely proportional to the molar densities, i.e., $\rho_s\lambda_s = \rho_L\lambda_L$, we may write Eq. (9) as

$$N_B = f\lambda_s\rho_s k_B^F\left(y_B - \frac{k_B^R}{k_B^F} x_B\right) \quad . \tag{10}$$

At equilibrium between the phases the net crystallization flux must be zero. Then the ratio of two rate coefficients can be expressed in terms of the equilibrium phase compositions, for a simple eutectic system with negligible solid solubility,

$$\frac{k_B^F}{k_B^R} = \frac{x_{Be}}{y_{Be}} = \frac{1}{y_{Be}} \tag{11}$$

which at a constant pressure is a function of interface temperature only.

In order to apply the theory to the laboratory coordinate system in which experimental observation are made we define u_B as the average velocity of B molecules as they more toward the surface. We obtain

$$u_B = \frac{N_B}{\rho_L y_B} \quad . \tag{12}$$

Similarly, an equation can be written for A molecules,

$$u_A = \frac{N_A}{\rho_L y_A} \quad . \tag{13}$$

The average of the velocities for all molecules is given by

$$u = y_A u_A + y_B u_B \tag{14}$$

where u can be positive, zero, or negative. Since A is the impurity component the term $y_A u_A$ may be very small compared to $y_B u_B$ of the major component. Combining Eqs. (10) and (12), we obtain

$$u \simeq u_B y_B = f\lambda_s k_B^F (y_B - x_B y_{Be}) \quad . \tag{15}$$

The equation for the flux of B component in the laboratory coordinates can be obtained by adding terms to Eq. (10) representing the convective transport of the component B,

$$N_B = f\lambda_s \rho_s k_B^F (y_B - x_B y_{Be}) + (V \frac{\rho_s}{\rho_L} - u) y_B \rho_L \quad . \tag{16}$$

By substituting u from Eq. (15), we obtain

$$N_B \simeq f\lambda_s \rho_s k_B^F y_A (y_B - x_B y_{Be}) + V\rho_s y_B \quad . \tag{17}$$

If diffusion in the solid phase is neglected, the ratio of the mole fraction of the component is equal to the ratio of the molar flux to the interface, i.e., $x_B = N_B/V\rho_s$, and Eq. (17) gives

$$x_B \cong \frac{f\lambda_s k_B^F}{V} y_A (y_B - x_B y_{Be}) + y_B \quad . \tag{18}$$

If we define an effective distribution coefficient, K_B, for component B as the ratio of actual solid mole fraction to the mole fraction of liquid

at the interface, and introduce the growth rate parameter, $g_B = f\lambda k_B^F/V$, into Eq. (17) and rearrange, we obtain an equation similar to one developed by Cheng and Pigford (5),

$$K_B = \frac{x_B}{y_B} \cong \frac{g_B y_A + 1}{1 + g_B y_A / K_{Be}} \tag{19}$$

where K_{Be} is the equilibrium distribution coefficient. According to this equation K_B approaches unity as the growth velocity increases or the forward rate coefficient decreases. Moreover, K_B approaches the equilibrium value as the growth velocity reaches zero. The numerical value of K_B lies between unity and the equilibrium value K_e and depends on the temperature, the interfacial liquid concentration, and the growth velocity.

Again the factors f, λ, and k^F have the same meanings as described before. For a binary system the step density f must be estimated by the evaluation of the Gibbs free energy change ΔG. ΔG represents the difference of the Gibbs free energy of a mole of solid and a mole of liquid of the same composition. If we have a pure melt from which the crystal is growing the free energy difference is approximately equal to the entropy of fusion multiplied by the degree of undercooling. However, when the crystal is growing from a binary melt, the free energy change depends on both the temperature and the liquid composition. This has been given by Kirwan and Pigford (4) for B molecules as

$$\Delta G = \mu_B^L - \mu_B^s = [\Delta S_f - \Delta C_{PB}(1 - \frac{T}{T_{Bm}}) - R\ell n(\gamma_B y_B]\Delta T \tag{20}$$

where γ_B is the activity coefficient of B in the interface liquid.

The absolute rate theory is of little use unless the quantities of the thermodynamic properties of the activated state for crystallization

are known. It was first suggested by Hillig and Turnbull (19) that the activated states for crystallization and viscous flow are identical. However, Kirwan and Pigford pointed out that the activation energy for crystallization should be smaller than that for viscous flow. After all, the liquid molecules only require a specific orientation in order to join the crystal. The difference between the entropies of the two states is given by

$$\Delta S^{\ddagger} = \Delta S_V^{\ddagger} - (\Delta S_f - R) \tag{21}$$

where R is the gas constant. The enthalpy of the activated state of crystallization is more difficult to predict. It may be approximated by the activation enthalpy needed to cause a molecule to jump away from its surroundings in viscous flow. This latter activation enthalpy is smaller than the total activation enthalpy in viscous flow. Therefore, we can assume that

$$\Delta H_C^{\ddagger} = c\Delta H_V^{\ddagger} \tag{22}$$

where c is less than one.

B. Liquid Inclusion Theory

Edie and Kirwan (12) and Edie (44) suggested that the cause of apparent non-equilibrium during crystal growth is the purely mechanical entrapment of liquid between dendritic projections of solid that form on the interface as it advances. They assumed that the initial solid phase has the thermodynamic equilibrium composition. After trapped liquid inclusions freeze, the crystals, they assumed, are actually composed of two solid phases. The average composition of such a finely divided structure will of course lie between those of the original interfacial liquid and

the equilibrium solid. Fig. 1 shows the growth model proposed by these workers. The cells and dendrites at the interface represent the breakdown of the planar interface and its distortion into a columnar structure.

The spacing R of the cells is a characteristic of the breakdown of the planar front and is determined by the variables G, m, K_e, D, and μ (the kinetic growth coefficient for the particular crystal growth plane). Studies in metal systems (22) indicate empirically that the radius of a dendrite, r, growing out from each cell is proportional to $(Vy_o)^{-1/2}$,

$$r = \frac{k_1}{(Vy_o)^{1/2}} + k_2 \tag{23}$$

where k_1, k_2 are assumed to be functions of G, m, K_e, D and μ but not of growth velocity or liquid composition. Therefore, the fraction of the growing interface which is actually crystalline is approximately equal to the ratio of the projected area of the solid columns to that of the entire base,

$$\psi = \frac{\pi r^2}{\pi R^2} = \frac{1}{R^2}\left[\frac{k_1}{(Vy_o)^{1/2}} + k_2\right]^2 \quad . \tag{24}$$

It was assumed that the crystalline portion of the interface was in equilibrium with the interface liquid,

$$x_c = K_e y_i \quad . \tag{25}$$

Therefore, the interfacial solid concentration is

$$x_i = x_c\psi + (1 - \psi)y_i \quad . \tag{26}$$

The effective distribution coefficient at the interface is given by the equation,

$$K = \frac{x_i}{y_i} = \psi(K_e - 1) + 1 \quad . \tag{27}$$

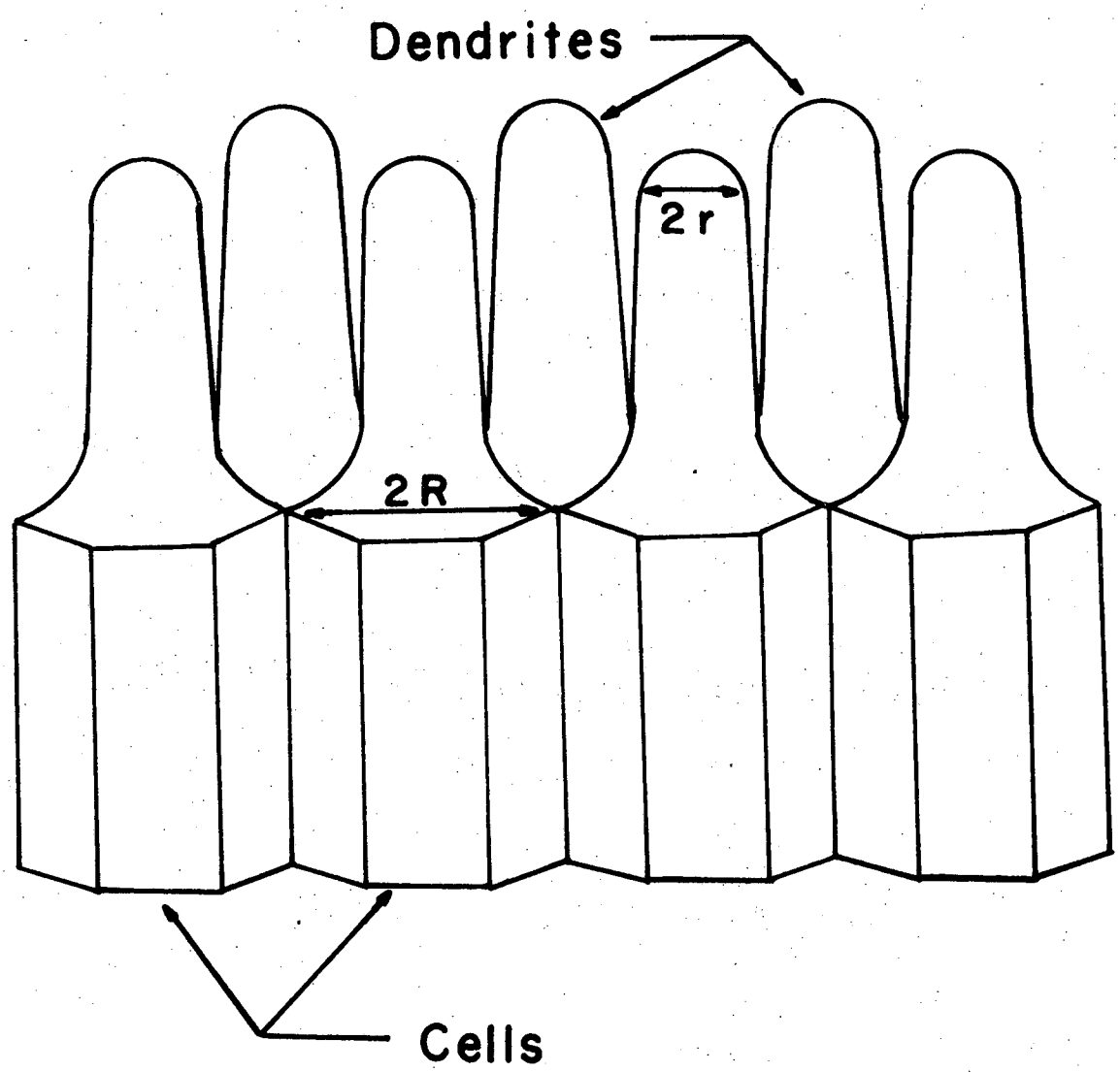

Dendrite growth at the interface.

XBL 725-868

Fig. 1

Rearrangement of Eq. (27) and substitution for ψ yields,

$$\sqrt{\frac{K-1}{K_e-1}} = \frac{k_1}{R} \cdot \frac{1}{\sqrt{Vy_o}} + \frac{k_2}{R} \tag{28}$$

for a binary system forming an equilibrium solid solution.

In order for liquid to be occluded in the growing crystal, the planar growth front must break down. Rutter and Chalmers (23) explained the conditions under which a planar interface would break down into a cellular structure. The breakdown of the interface is caused by the interaction of temperature and diffusion fields. Chalmers (14) also stated the criterion for stable planar growth at steady state as:

$$\frac{G}{V} \geq \frac{my_i(1 - K_e)}{D} \tag{29}$$

where $G = \frac{dT}{dx}$, the imposed temperature gradient,

m, slope of the liquidus line, and

D, diffusion coefficient in the liquid phase.

This criterion has been verified on metal systems (11,24,25). Kirwan and Edie suggested normalizing the first term of the right hand side in Eq. (28) by applying this criterion. For a simple eutectic system without solid solution ($K_e = 0$), the criterion of the planar interface breakdown is approximately:

$$(Vy_o)_{crit} = \frac{GD}{m} \quad . \tag{30}$$

This is not quite the critical velocity above which the planar interface would break down but differs by a factor of y_o/y_i. This ratio is expected to be a little different from unity at the break point. The final equation

of the Liquid Inclusion Theory is given by:

$$\sqrt{\frac{K-1}{K_e-1}} = \frac{k_1'}{R}\sqrt{\frac{(Vy_o)_{crit}}{(Vy_o)}} + \frac{k_2}{R} \tag{31}$$

where $k_1' = k_1/(Vy_o)$ is a function of G, m, K, D, and μ.

III. DESCRIPTION OF EXPERIMENT

The experimental method was selected to be able directly to observe interface phenomena during the growth of a solid from its melt. For many years people tried to find a method with which they could determine the interfacial concentration and temperature, but none of them was very successful until Berg (26) and Bann (27) employed an optical interference method for the observation of concentration patterns around crystals as they grew in a supersaturated solution under a microscope. Consequently, Kirwan and Pigford (4) applied this method to observe the crystal growth from organic melts. In isothermal growth, however, the irregularity of the interface shape makes the experimental measurement very difficult. Jackson et al. (28) designed a temperature-gradient microscope stage (T.G.M.S.) to overcome this problem. Recently, Cheng and Pigford (5) modified Jackson's T.G.M.S. and investigated the interfacial rate phenomena of crystal growth quite successfully.

Similar methods have been used (29,30) for the determination of the diffusion coefficients from the curvatures of the fringes observed during the mixing of two liquids.

The principle of the interferometric method can be explained from Fig. 2. The liquid melt is held in an optical wedge, formed by two partially coated slides, set on the temperature-gradient stage. A parallel monochromatic light beam passes through the optical wedge, which is partially reflective. Whenever the optical path length difference between the reflected ray and the original ray is an integral multiple of the wavelength of the light, reinforcement occurred and bright fringes appear.

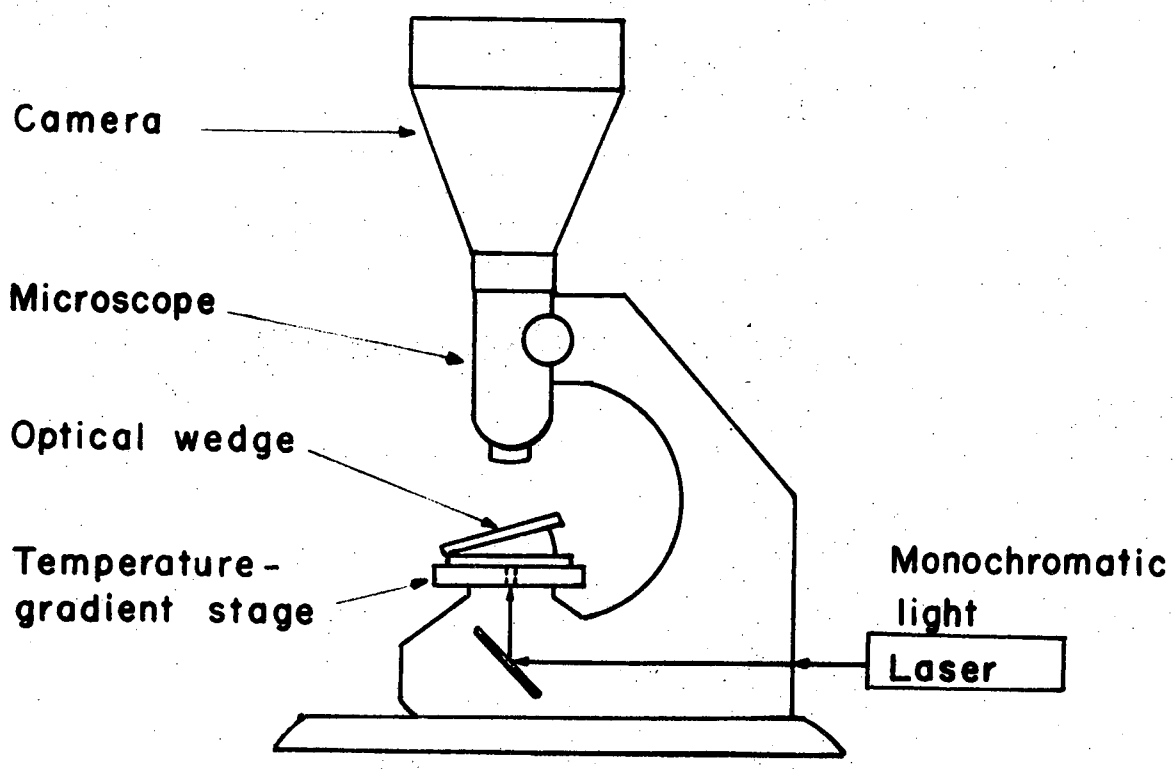

Microinterferometric setup

XBL 725-876

Fig. 2

Dark areas result from the destructive interference . The fringe patterns were observed under the microscope and photographed. The condition of reinforcement is given by the equation,

$$tn = \frac{\lambda_o N}{2} \tag{32}$$

where λ_o is the wavelength of monochromatic light, n is the refractive index of the liquid in the wedge, t is the thickness of the optical wedge, and N is an integer. The product of wedge thickness and refractive index is constant along a fringe. The spacing between two straight fringes is $d = \lambda_o/2n\theta$, where θ is the angle of the wedge in radians. The larger the wedge angle the narrower is the spacing between two fringes. As long as it provides a clear and readable fringe pattern, the angle of the wedge is not very critical.

A. Description of Experimental Apparatus

An overall view of the apparatus is shown in Photograph 1. The major items consist of:

A,B-6	Constant temperature ice bath for cold junction of thermocouples.
B-4	"Batt-Sub" constant voltage supply for K-2 potentiometer with output 3.0 VDC at 24.4 m.a. by Dynage, Inc., Hartford, Connecticut.
B-5	Standard cell for K-2 potentiometer, the Eppley Laboratory, Inc., Newport, Rhode Island.
B,C-2,3	E.M.F. recorder, Type G, Leeds and Northrup Company.

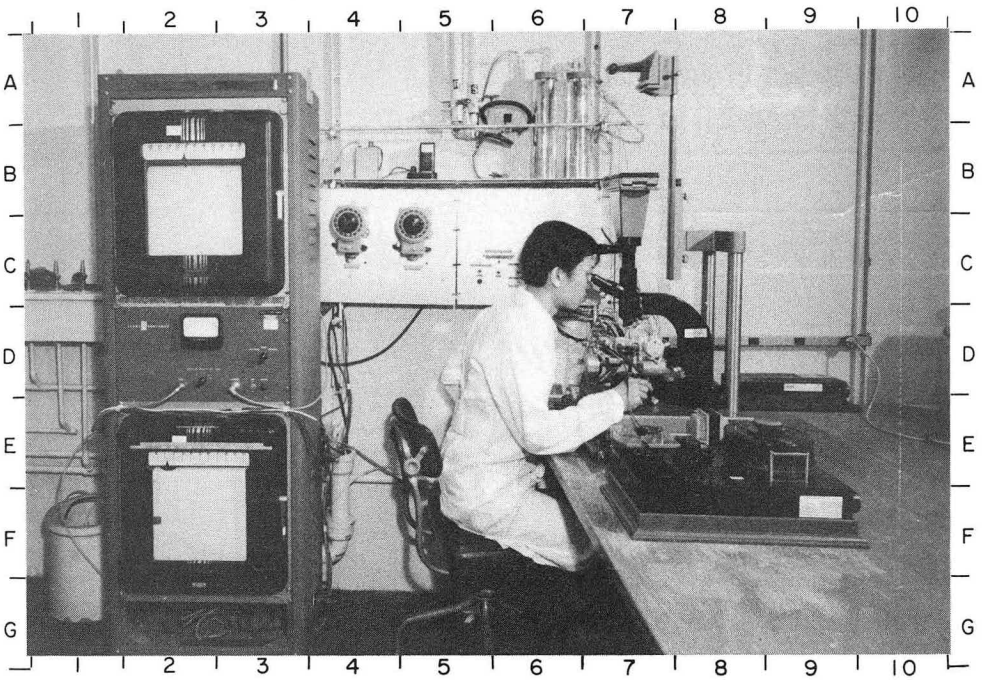

Overall-view of experimental apparatus.
Photo I.

C,D-7	Leitz Research Microscope Ortholux and Leitz Arisophot stand for photography consisting of large base plate, vertical camera carrier on twin columns with adjustable prismatic bar, Leitz focusing attachment with horizontal telescope, Letiz holder for Polaroid camera back, Model CB 100.
D-2,3	Microvolt Amplifier 935B, Leeds and Northrup Company.
D-7	Temperature gradient microscope stage. A detailed description of this stage is given in Photo. 2.
D-9	Quantum Physics Model LS-30 He-Ne gas laser with integral power supply. Unit provides a standard wavelength of 6328 Å coherent, monochromatic light.
E,F-2,3	Multichannel E.M.F. Recorder. Leeds and Northrup Co.
E,F-7,8,9	Leeds and Northrup K-2 Potentiometer.
F-1	Constant temperature ice bath for cold stage.

Detailed description of the temperature gradient microscope stage in Photo. 2:

1) Teflon boat with optical wedge.
2) Cold stage.
3) Hot stage.
4) D.C. power supply for the adjustment of D.C. clock motor.
5) Quantum Physics Model LS-30 He-Ne gas laser.
6) Polaroid camera Model CB 100.
7) Ice bath for thermocouple junctions.
8) Leitz Research Microscope.

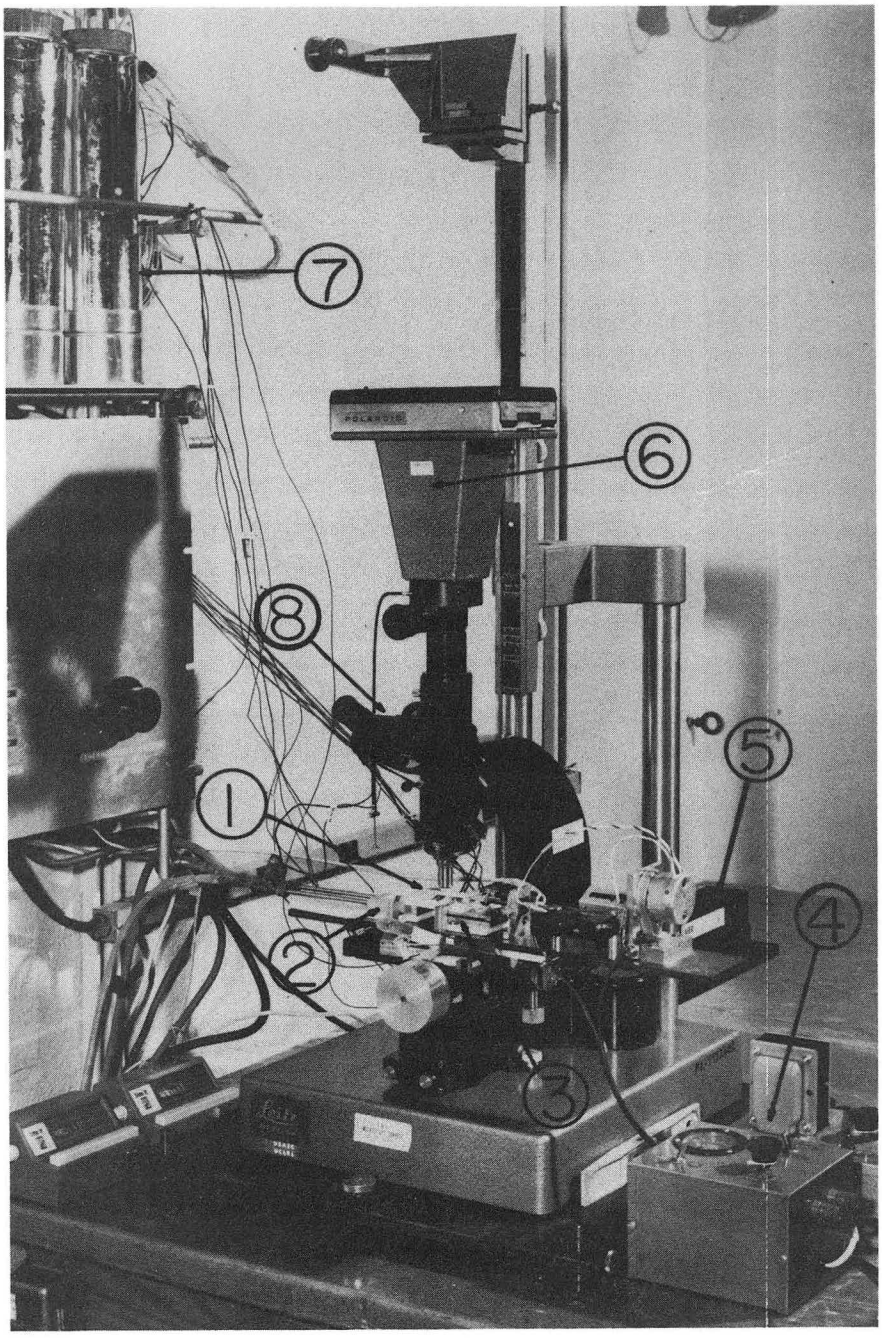

Temperature-gradient microscope stage.

Photo. 2.

XBB 725-2899

The T.G.M.S. is shown in Photo. 2. The thin optical wedge containing the material under investigation was set on a Teflon boat and moved by a motor over adjustable plates which were held at different temperatures. The wedge or boat speed was adjusted so that the interface was stationary with respect to the microscope objective lens even though the wedge or boat and interface were moving.

The cold and hot plates were made from aluminum blocks 3/8 inches thick. They were placed at the left and right of the stationary mount, which could be adjusted in position with the microscope's mechanical stage.

The hot plate had a small heater (nichrome wire wound on a mica sheet) inside the aluminum block. The cold plate contained a U-type hole connected to a cooling coil set inside the ice bath.

Water flow into the cold plate was first cooled in an ice bath to maintain the stage at a constant temperature. The minimum temperature of 5°C could be obtained.

The open slide optical wedge used by Cheng (31) was modified to prevent evaporation and air contamination of specimens. It consisted of two partially aluminized slides glued on a fixed-angle Teflon boat as shown in Fig. 3. One slide was fitted and fastened with epoxy resin into the frame of the boat from below. It formed the bottom of the wedge. The other fitted on the top of the boat at a fixed angle to the bottom slide. There were two small holes in the front of the Teflon boat. One was used to inject the melt into the wedge. A very fine, calibrated copperconstantan thermocouple made from wire 0.002 inches in diameter was inserted from the other hole into the wedge, perpendicular to the direction

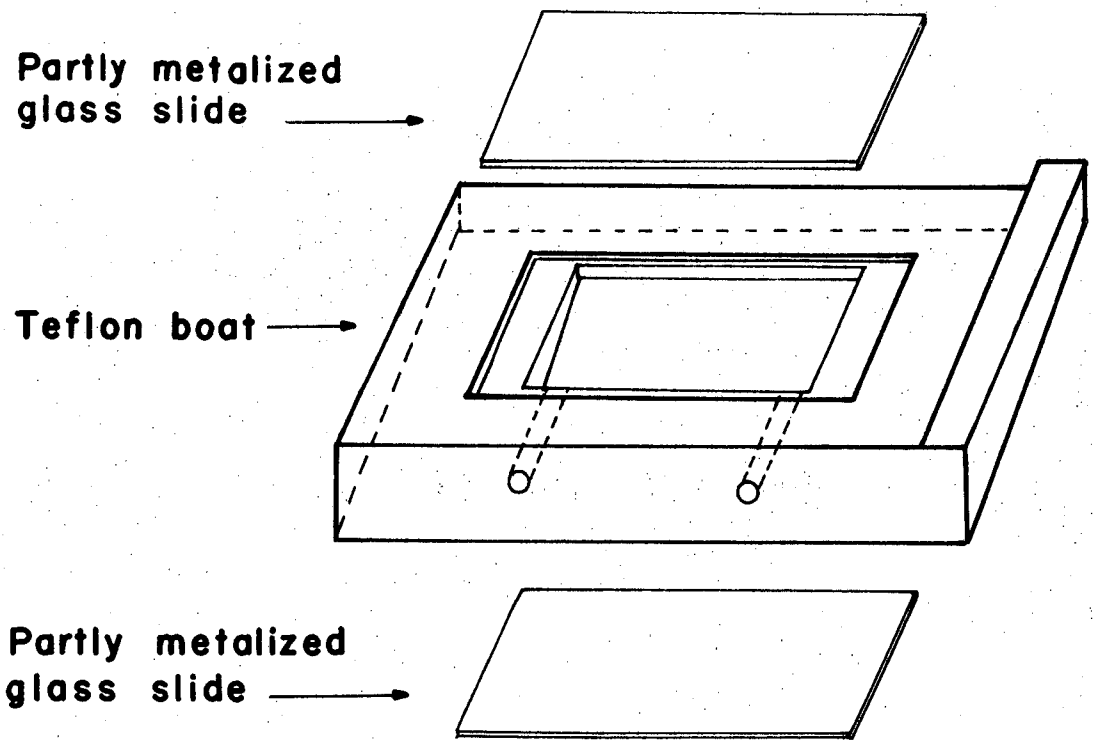

Optical wedge

XBL 725-874

Fig. 3

of motion. A lead screw connected to a digital counter turned by a small motor was fitted into the yoke at the right end of the boat. As the screw advanced, the boat moved horizontally toward the cold plate under the microscope objective. The growth rate was determined by the reading of the digital counter, which was driven by the motor.

Different growth rates were obtained by moving the wedge at different constant speeds. The temperature gradients in the vicinity of the solid-liquid interface could be varied either by changing the distances between the plates or by altering their temperatures.

If the crystal interface was not perpendicular to the direction of the movement of the optical wedge, the growth velocity of the interface was calculated from the motor moving speed by considering the angle between the two directions.

B. Sample Preparation

The molecular structures of salol (phenyl salicylate) and thymol (3-p cymenol) are shown below:

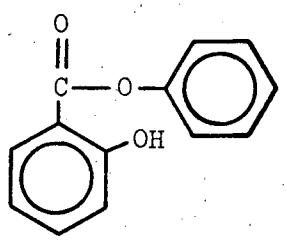

salol

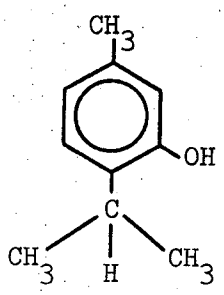

thymol

They form a single eutectic system and were selected for the growth rate experiments for three reasons. First, the refractive indices of the pure materials differ substantially and provide a sensitive fringe shift for small changes in concentration of the mixture. Second, the

melting or freezing points of the mixtures lie above room temperature, avoiding refrigeration requirements. Third, the phase diagram is available (32).

The salol and thymol were obtained from the Eastman Kodak Organic Chemical and DuPont Companies, respectively. The salol was purified first by repeated crystallization from methanol and then by zone-refining using a Fisher zone refiner. Finally it was degassed in a vacuum jar. The thymol was purified first by repeated crystallization from spectro-grade acetone, then a procedure was applied similar to that used for salol.

C. Experimental Procedures

The cold and hot stages were first brought to the steady temperatures needed for any desired temperature gradient. The measurement of the wedge angle was carried out by focusing on the scratches on the facing surfaces of both slides. The measured angle checked with the known angle of the Teflon boat.

The melt had been previously prepared by weighing samples of each pure component into a vial, melted and agitated until well mixed. A small portion of the melt was injected into the wedge from a small heated syringe. Several minutes were allowed to reach thermal equilibrium with the glass slides. Crystallization was initiated by introducing a small seed crystal into the hole at the cold side of the Teflon boat. Then the motor was turned on to push the Teflon boat farther toward the cold plate. The moving crystal was kept steadily in view through the microscope by adjusting the motor setting until a constant rate was obtained. Temperatures were measured at different positions of the optical wedge and

positions of the solid-liquid interface. Pictures of the fringe pattern at the interface were taken for further analysis.

Sometimes trouble was encountered owing to the instability of the interface speed. In some experiments the interface moved somtimes fast and sometimes slow. When this occurred the average velocity was used.

1. Data Analysis

The melting points of pure salol and thymol measured by the author agree well with the literature (Table I).

Table I

Melting Temperatures of Pure Salol and Thymol

Substance	Measured °C	Literature °C
Salol	42.20 ± 0.05	42.5 (28)
Thymol	49.80 ± 0.05	49.7 (28), 51.0 (29)

The phase diagram of salol-thymol system as given by Timmermans (32) is shown by the solid line in Fig. 4. The dashed line gives our carefully measured values, which are a little different. Our values were used in the subsequent calculations.

Since the liquid in the optical wedge was of uniform refractive index before the crystallizaton, the fringes were straight and parallel. The composition of the solid freezing out was different from that of the original liquid owing to the finite diffusion rate in the liquid phase. The liquid composition at the solid-liquid interface was different from that of the original liquid far from the interface.

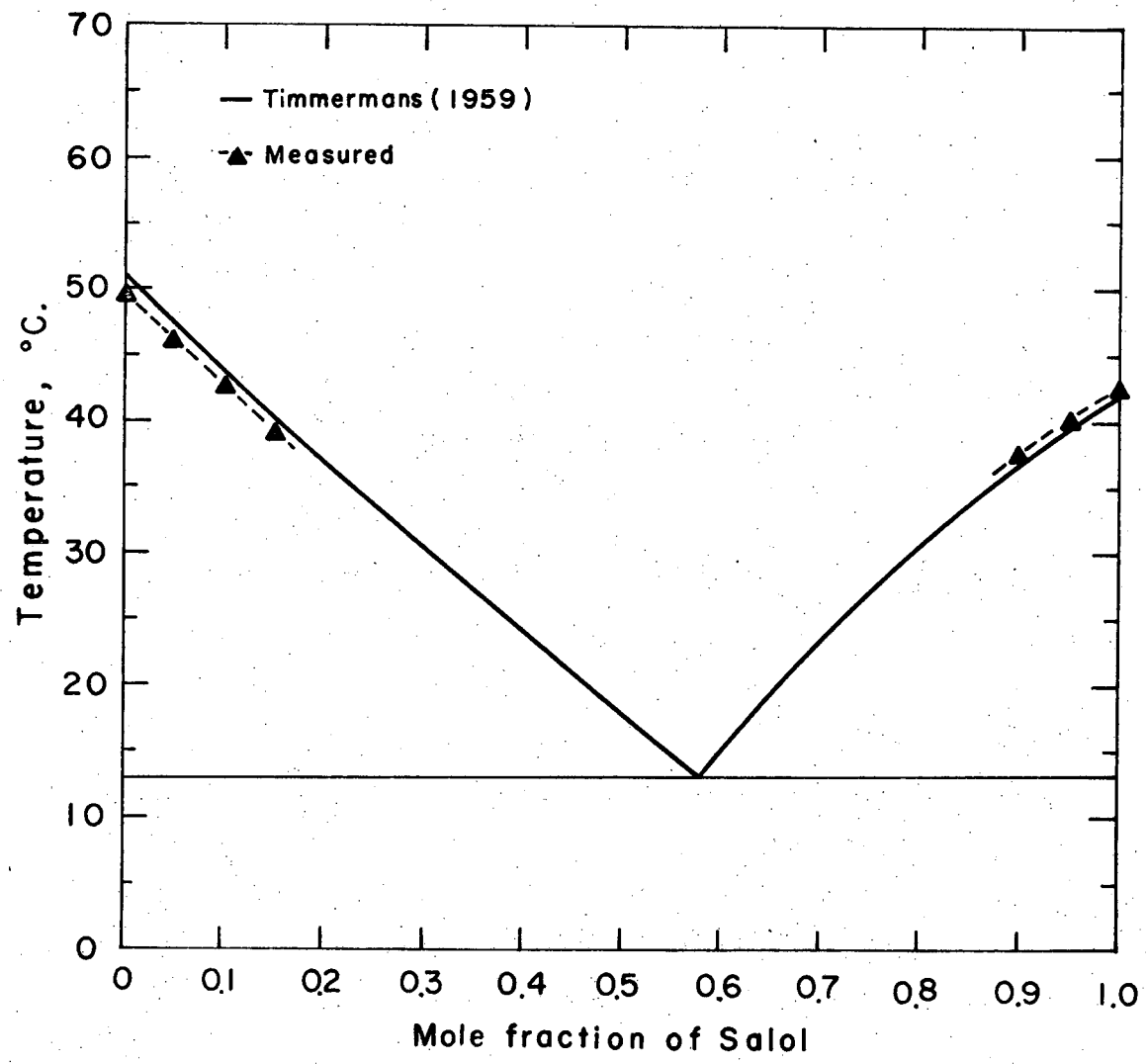

Phase diagram of Salol-Thymol system

XBL 725-869

Fig. 4

The refractive index will therefore vary from the interface to the bulk liquid, resulting in a corresponding fringe bending near the interface. This difference in the refractive index can be calculated by measuring the fraction of deviated fringe displacement at the interface, ΔN, along a fringe, as given in the equation,

$$\Delta n = \frac{\lambda_o}{2t} \Delta N \quad . \tag{33}$$

Part of this ΔN may be contributed by the temperature rise at the interface due to the latent heat release caused by freezing. The residual part is due to the concentration change. The variation of refractive index with temperature could be measured by crystallizing the pure substance on the T.G.M.S. The refractive index of the pure material is a linear function of temperature in the range we are interested in,

$$n = a + bT \tag{34}$$

where a, b are constants. The refractive index change was due to the effect of temperature

$$\Delta n = b\Delta T \quad . \tag{35}$$

Substituting Eq. (35) into Eq. (33), at the interface,

$$\Delta T_i = \frac{2t}{b\lambda_o} \Delta N \quad . \tag{36}$$

a. <u>Interfacial Temperature</u>. Liquid temperatures near the advancing interface were measured using the thermocouple which was inserted into the optical wedge as described before. The junction of thermocouple moved with the wedge, but at steady state the crystal interface was fixed relative to the microscope objective. The temperatures measured at different times therefore correspond to different distances from the interface. The

interface temperature was found by extrapolating the best-fit line to the interface. A correlation was applied to compute the actual temperature at the interface, based on the observed fringe shift of pure materials under the T.G.M.S.

b. Interfacial Liquid Concentration. For the binary melt the liquid refractive index is a function of concentration and temperature, $n = f(T,y)$,

$$dn = \left.\frac{\partial n}{\partial y}\right)_T dy + \left.\frac{\partial n}{\partial T}\right)_y dT \quad . \tag{37}$$

At the solid-liquid interface the refractive index change is given,

$$\Delta n = \left.\frac{\partial n}{\partial y}\right)_{T_i} \Delta y_i + \left.\frac{\partial n}{\partial T}\right)_{y_i} \Delta T_i \quad . \tag{38}$$

Substituting Eq. (33) into Eq. (38) and rearranging the interfacial liquid concentration is given by the equation,

$$y_i = y_o - \frac{\frac{\lambda_o}{2t}\Delta N - \left.\frac{\partial n}{\partial T}\right)_{y_i} \Delta T_i}{\left.\frac{\partial n}{\partial y}\right)_{T_i}} \tag{39}$$

where ΔN and ΔT_i are measurable quantities from the experiment and the two partial derivatives can be determined for the solutions.

At this point, it may be well to emphasize that the fringe shift, ΔN, at the interface was measured by a very precise "microscope" machine original designed for the tracing of the tracks of elementary particles in cloud chambers at Lawrence Berkeley Radiation Laboratory. The accuracy of the measured ΔN depended only on the resolution of the picture taken from the Polaroid film.

In some measurement, trouble was encountered due to the obscurity of the fringes at the interface and the uncertainty of the interface

position. This may be improved by using high resolution film or by employing a thinner optical wedge, with which it would be easier to focus simultaneously on the crystal face and the fringe patterns.

c. Interfacial Solid Concentration. The concentration of the solid at the interface is difficult, if not impossible, to measure directly during the experiment. But it can be computed from the concentration gradient in the liquid phase near the interface. This was done by using a mass flux balance equation at the interface. Choosing the freezing interface as stationary, if V is the freezing rate of the crystal, the velocity of the melt caused by freezing is $V(\rho_s/\rho_L)$.

Assuming that solid-phase diffusion is negligible, the only diffusion flux is the one in the melt, $D\rho_L(\frac{dy}{dz})_{z=0}$. The convective flux into the interface is $V\rho_s y_i$; the flux outward from the interface is $V\rho_S x_i$. This leads to the equation,

$$-D\left.\frac{dy}{dz}\right)_{z=0} = V\left(\frac{\rho_s}{\rho_L}\right)(y_i - x_i) \qquad (40)$$

where D is the binary liquid diffusion coefficient, V is the measured growth velocity, z is the coordinate perpendicular to the interface, and ρ's are densities of liquid and solid phases. All terms are evaluated at the interface temperature.

The interfacial concentration gradient $(\frac{dy}{dz})_{z=0}$ in the liquid phase was computed by considering the geometry involved in the interferograms, as shown in Fig. 5. This was derived by Cheng and Pigford (30) who obtained the equation,

$$\left.\frac{dy}{dz}\right)_{z=0} = \frac{\lambda_o\left(\frac{dw}{dv}\right)_{v=0}}{2st_i\cos\alpha[\sin\beta + \left.\frac{dw}{dv}\right)_{v=0}\cos\beta]\left(\frac{\partial n}{\partial y}\right)_T} \qquad (41)$$

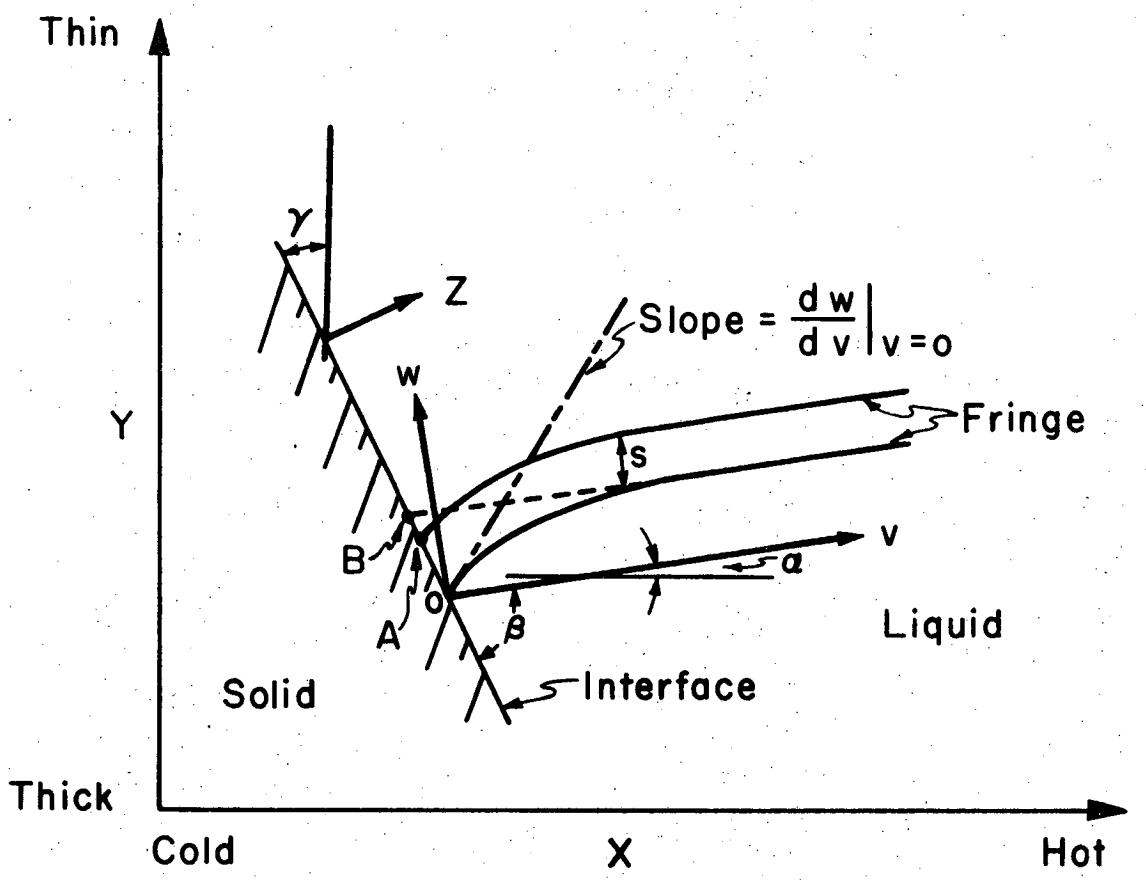

Fringe pattern at interface during crystal growth

XBL6910-3998

Fig. 5

where s is the fringe spacing measured in the Y direction. The v-w coordinate system has its origin in the interface. The v-axis is parallel to the fringe at $v = \infty$. All the quantities s, α, β, $\left.\frac{dw}{dv}\right)_{v=0}$ were measured using the precise instrument mentioned previously. It may be well to emphasize that the slope of the fringe line at the interface $\left.\frac{dw}{dv}\right)_{v=0}$ was computed by measuring at least seven different points along one fringe near the interface in v-w coordinates. A polynomial curve-fitting program was used to find the fringe-curve equation and its slope at the interface. Four fringes were measured. The average value of $\left.\frac{dw}{dv}\right)_{v=0}$ was used to calculate the concentration gradient.

IV. RESULTS AND DISCUSSION

The crystals solidified from the liquid mixtures in the salol and thymol system were observed using the interferometric technique described in Chapter III. More than 300 Polaroid Type-107 pictures were taken. At least 50 experimental runs were carefully carried out.

In this chapter, typical fringe patterns and experimental results for the salol-thymol system are presented. The heat and mass transfer phenomena as well as interfacial stability of crystallization will be discussed. The validity of the experimental results will be discussed with regard to the possible error in the experiments. A quantitative comparison of the results with the Absolute Rate Theory and Liquid Inclusion Theory will be made.

A. Interfacial Temperature Rise

The temperature rise at the interface is a function of the growth velocity, the local thickness of the wedge, and the applied temperature gradient. The interfacial temperature rises observed at various temperature gradients are listed in Table II.

Table II

Observed Interfacial Temperature Rises Above Extrapolated Straight Lines

Substance	Growth Velocity cm/sec	Temperature Rise, °C		
		Isothermal Stage (30)	$\frac{dT}{dx}$ = 20 °C/cm	$\frac{dT}{dx}$ = 40 °C/cm
Thymol	1.0×10^{-3}	1.5	1.6	1.7
Salol	1.5×10^{-3}	2.0	2.1	2.3

The relation of the temperature rise, wedge thickness, and growth velocity are presented in Fig. 6 for pure salol and in Fig. 7 for pure thymol at a moderate temperature gradient (20 °C/cm). These two figures were used to estimate the interface temperatures occurring with mixtures.

B. Interferograms

Typical observed interferograms of pure salol and thymol are shown in Photos. 3 and 4. Fringe patterns observed with binary melts are presented in Photos. 5-9 for different compositions at various growth velocities and temperature gradients.

Since the refractive index of the pure salol melt is higher than that of the thymol melt, growing a crystal from a melt richer in salol results in decreasing the interfacial concentration of salol, consequently decreasing the refractive index of the binary melt at the interface. The fringe shift will move toward the thicker side of the wedge. For a thymol-rich mixture the fringe shift will be in the opposite direction, as we can see from the photographs.

Nucleation of gas bubbles on the interface occurred during the freezing of melts containing dissolved gases. The gas bubbles inhibited the growth of the solid crystal beneath the caps of the bubbles and voids were left in the solid as the interface advanced. At rapid freezing rates an array of bubbles was formed. This is shown in Photo. 4 for salol growth from the pure melt. This defect was prevented by degassing the samples before crystallization.

According to Jackson et al. (16), the roughness of an interface depends on the entropy of the transformation and on the crystal face type.

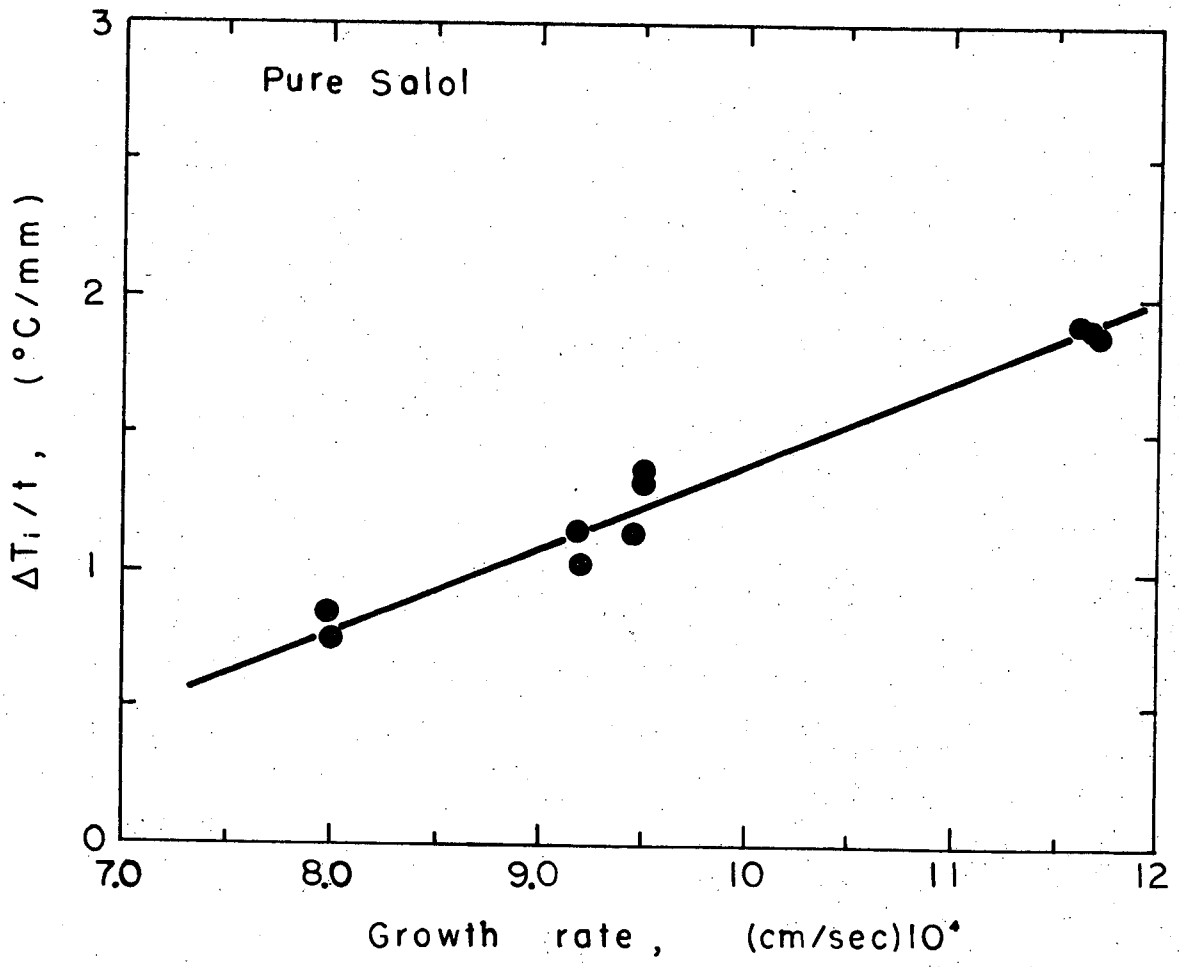

XBL 725-836

Fig. 6. Interfacial Temperature Rise During the Growth of Pure Salol at 20 °C/cm.

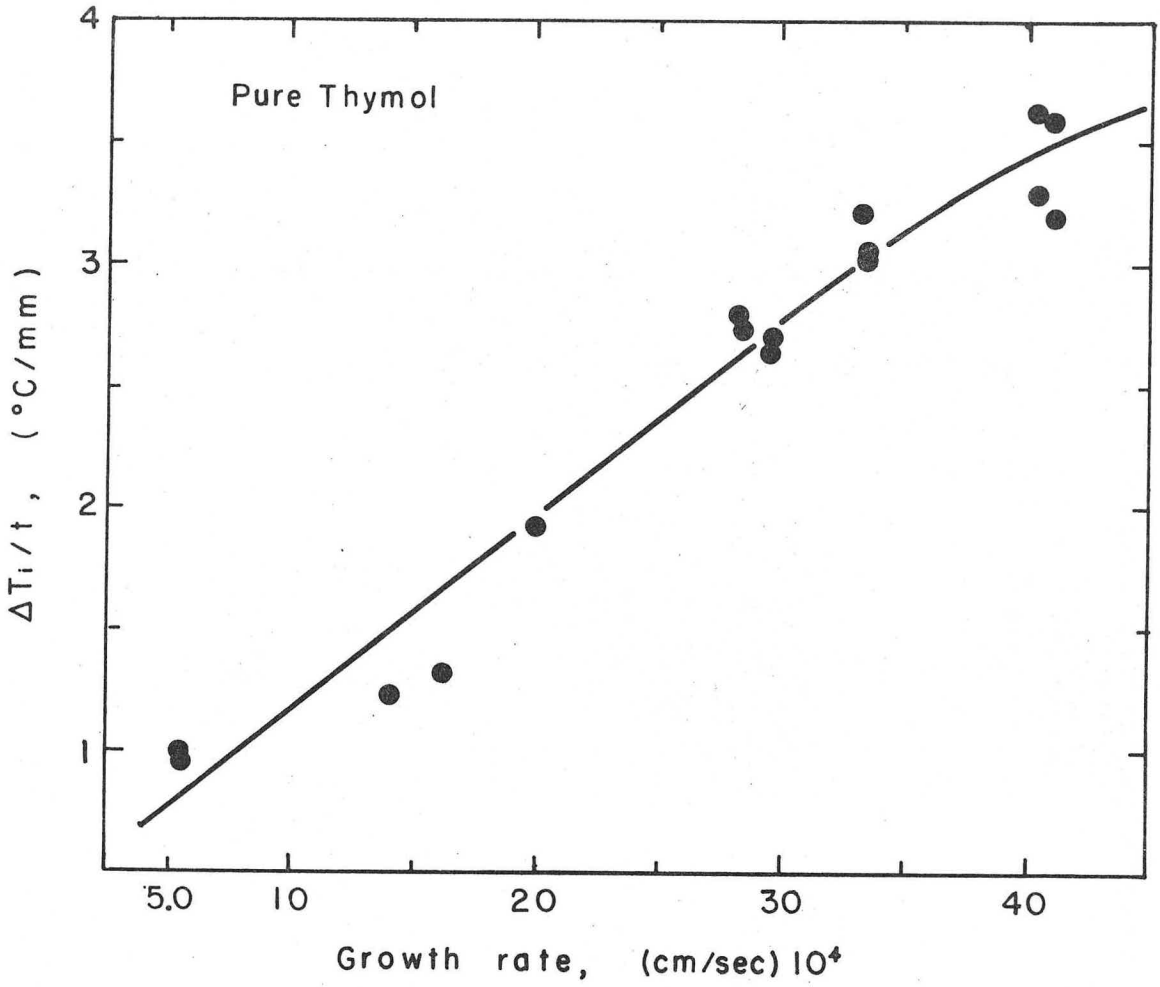

XBL 725-835

Fig. 7. Interfacial Temperature Rise During the Growth of Pure Thymol at 20 °C/cm.

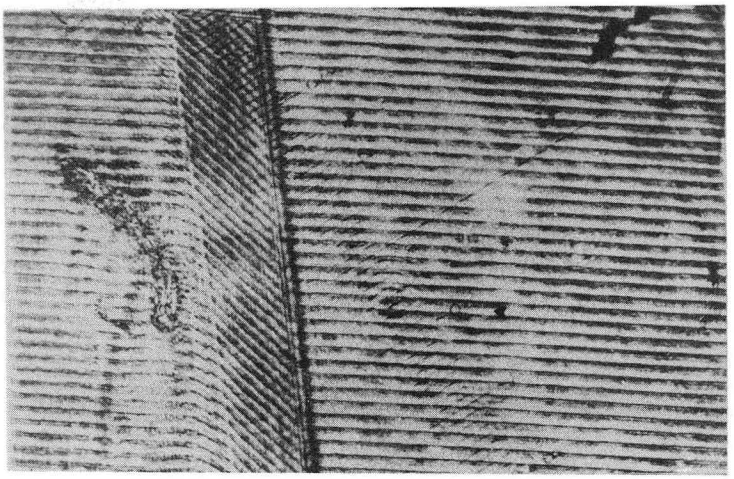

(a) $V = 1.43 \times 10^{-4}$ cm/sec, T.G. = 42.5 °C/cm

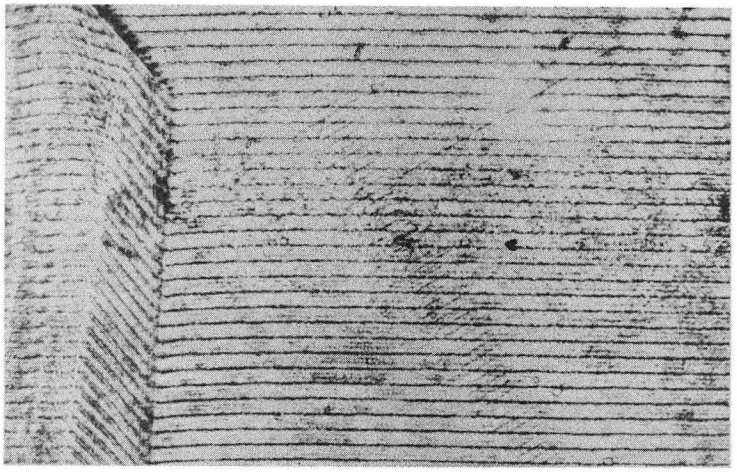

(b) $V = 2.81 \times 10^{-4}$ cm/sec, T.G. = 42.5 °C/cm

Crystal growing from pure Thymol.

Photo 3.

XBB 725-2433

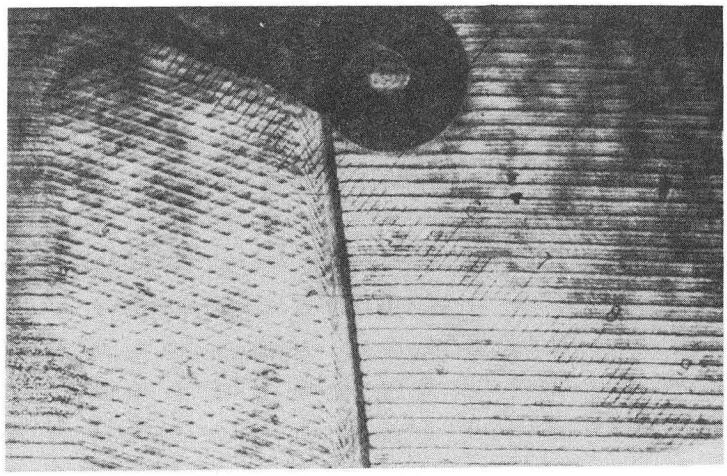

(a) $V = 9.51 \times 10^{-4}$ cm/sec, T.G. = 41.5 °C/cm

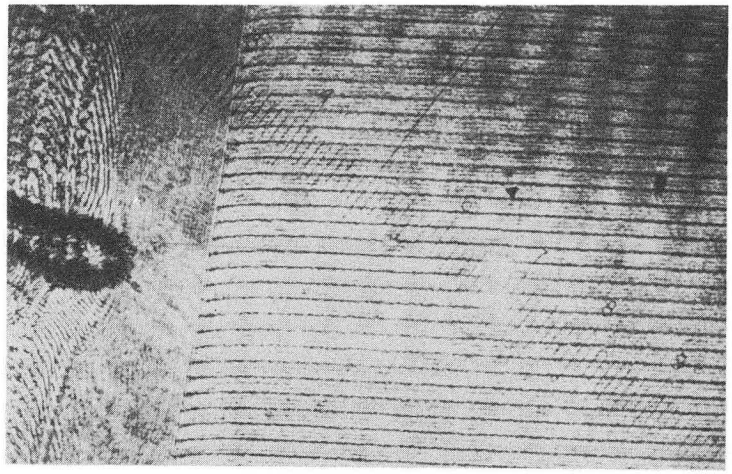

(b) $V = 1.03 \times 10^{-3}$ cm/sec, T.G. = 41.5 °C/cm

Crystal growing from pure Salol.

Photo 4.

XBB 725-2435

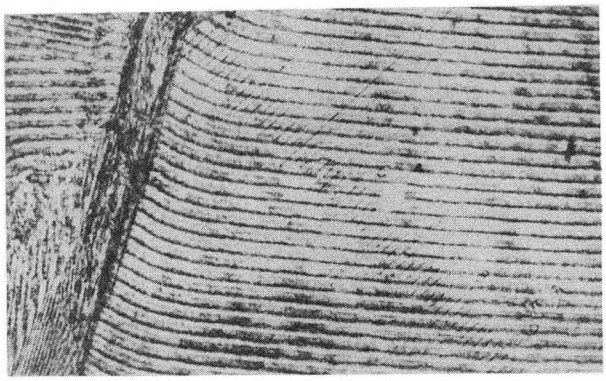

(a) $V=5.88\times10^{-5}$ cm/sec, T.G.=29.3 °C/cm

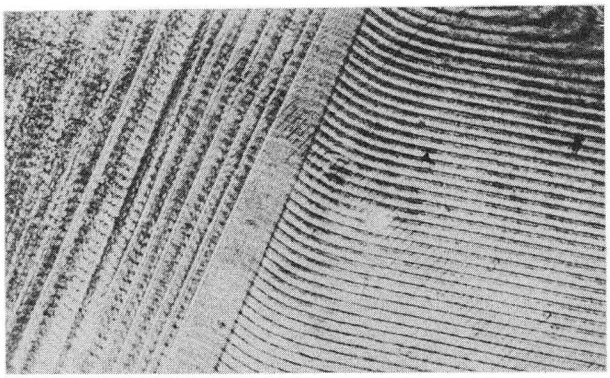

(b) $V=2.34\times10^{-4}$ cm/sec, T.G.=38.8 °C/cm

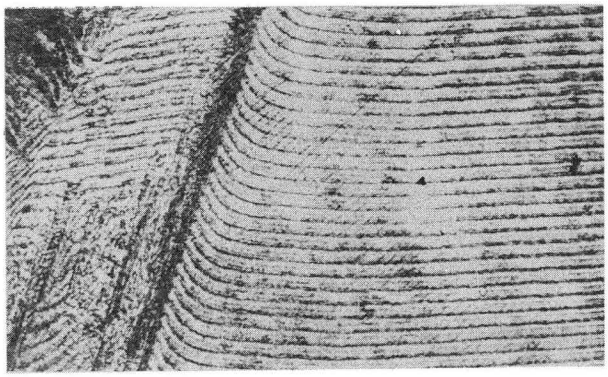

(c) $V=4.94\times10^{-4}$ cm/sec, T.G.=27.4 °C/cm

Crystal growing from Salol-Thymol melt in 5 mole % Salol.
Photo 5.

XBB 725-2434

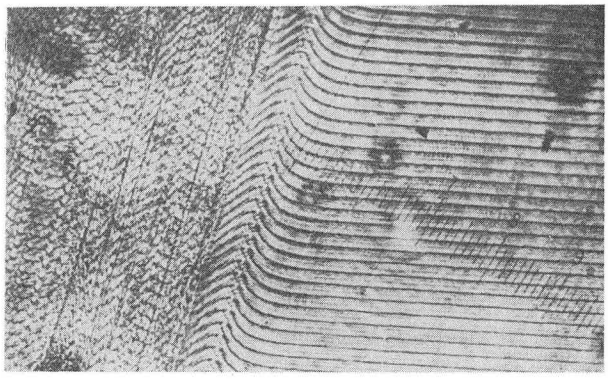

(a) $V = 3.60 \times 10^{-4}$ cm/sec, T.G. = 20.9 °C/cm

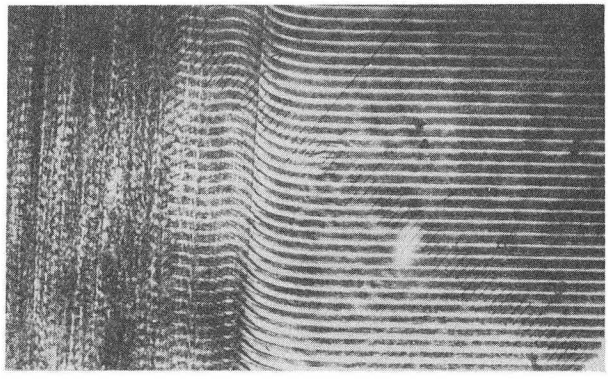

(b) $V = 4.45 \times 10^{-4}$ cm/sec, T.G. = 26.5 °C/cm

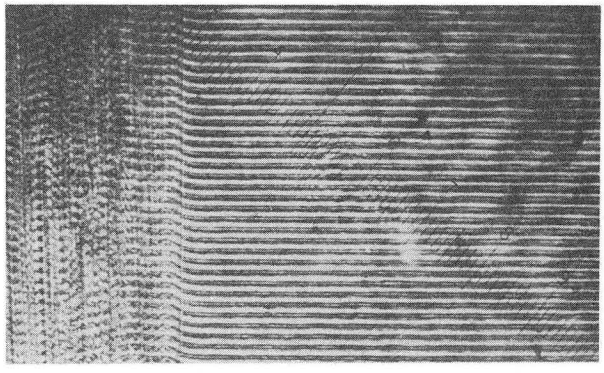

(c) $V = 9.12 \times 10^{-4}$ cm/sec, T.G. = 13.9 °C/cm

Crystal growing from Salol-Thymol melt in 10 mole % Salol.

Photo 6.

XBB 725-2438

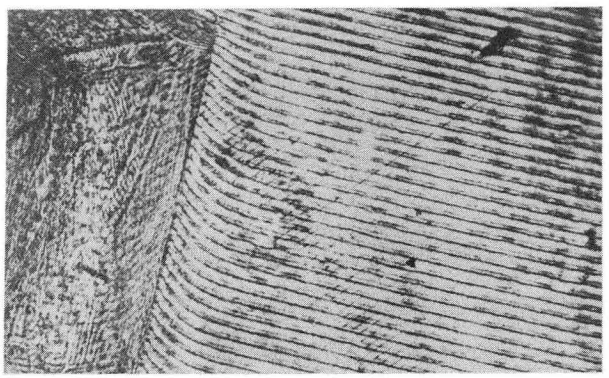

(a) $V = 4.81 \times 10^{-5}$ cm/sec, T.G. = 31.3 °C/cm

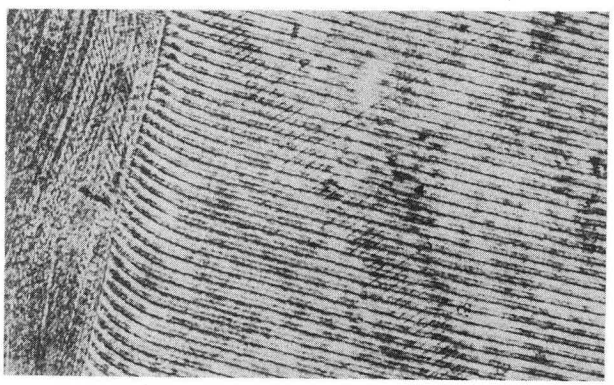

(b) $V = 8.61 \times 10^{-5}$ cm/sec, T.G. = 14.4 °C/cm

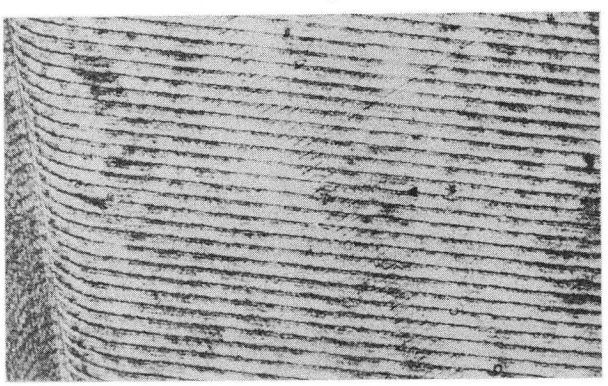

(c) V = 3.23x10 cm/sec, T.G. = 16.7 °C/cm

Crystal growing from Salol-Thymol melt in 15 mole % Salol.

Photo 7.

XBB 725-2432

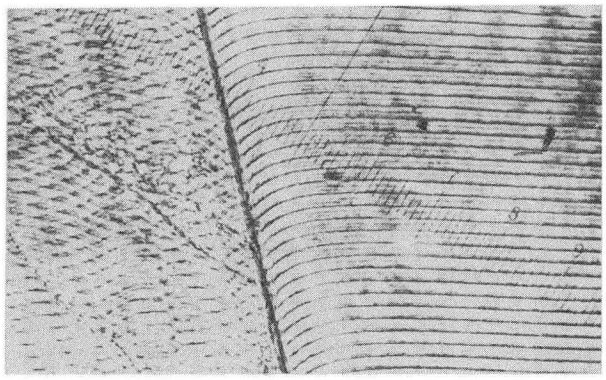

(a) $V = 1.19 \times 10^{-4}$ cm/sec, T.G. = 12.0 °C/cm

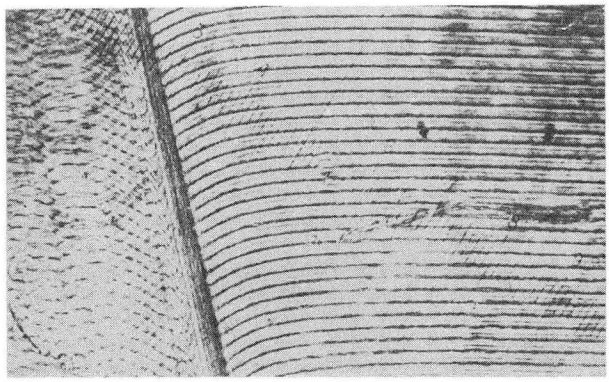

(b) $V = 3.12 \times 10^{-4}$ cm/sec, T.G. = 21.4 °C/cm

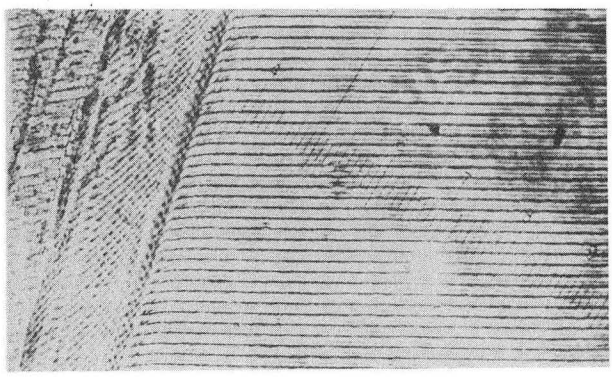

(c) $V = 6.67 \times 10^{-4}$ cm/sec, T.G. = 15.1 °C/cm

Crystal growing from Salol-Thymol melt in 90 mole % Salol.

Photo 8.

XBB 725-2436

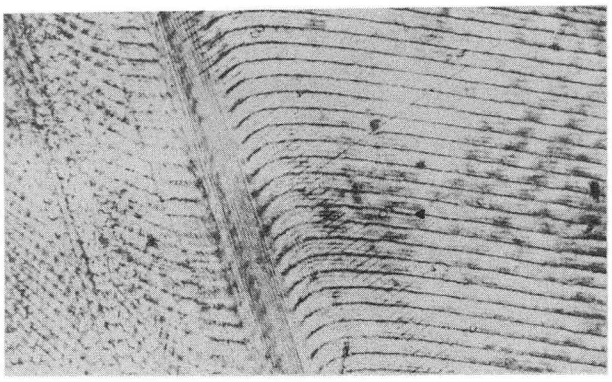

(a) $V=3.11\times10^{-5}$ cm/sec, T.G.= 17.5 °C/cm

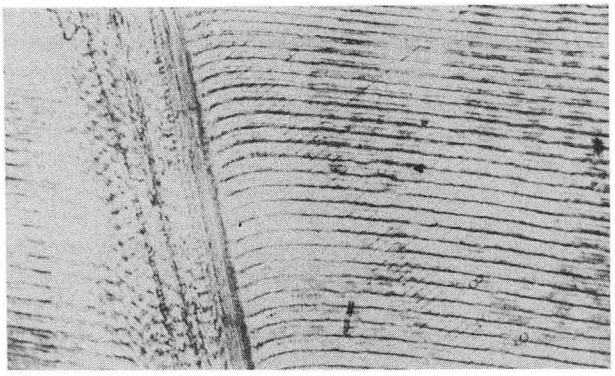

(b) $V=1.16\times10^{-4}$ cm/sec, T.G.= 22.9 °C/cm

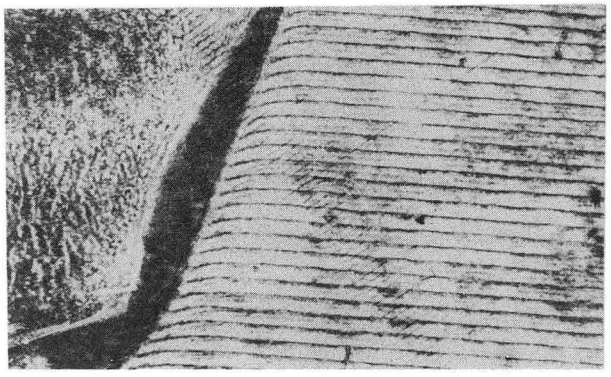

(c) $V=6.71\times10^{-4}$ cm/sec, T.G.= 29.7 °C/cm

Crystal growing from Salol-Thymol melt in 95 mole % Salol.

Photo 9.

XBB 725-2437

Close-packed faces, having smaller entropies of fusion, are smooth. Other faces are rough. It was not clear which crystallographic faces were growing during the experiments. In general, at low supercoolings the crystals grew with well-defined faces. As the supercooling increased, the growth front became more irregular and faceted.

C. Application of the Absolute Rate Theory

1. Pure Salol and Thymol

The Absolute Rate Theory for crystal growth from a pure melt with a screw dislocation mechanism on the surface was expressed in Eq. (8) of Chapter II,

$$V = \left(\frac{1}{1.2\pi}\right)\left(\chi \frac{kT}{h}\right)\left(\frac{\Delta S_f}{R}\right)\lambda_s\left(\frac{\Delta T}{T_m}\right)^2 \exp\left(\frac{-\Delta H_C^{\ddagger} + T\Delta S_C^{\ddagger}}{RT}\right) \qquad (8)$$

showing that the growth velocity is approximately proportional to the square of the undercooling. It is often used as a test of the postulate that growth occurs by the screw dislocation mechanism. Fig. 8 and Fig. 9 show the experimentally observed growth velocities for pure salol and thymol, respectively. The data of these pure materials are listed in Tables III and IV and plotted in the form of growth velocity vs. the square of the undercooling. The short lines through some of the data points represent the spread of measured interfacial temperatures when more than one value was obtained at very nearly the same growth velocities; the data points themselves represent the average value of the square of the undercooling. The scatter of the data on these figures is primarily because of the uncertainties in the measurement of the interfacial temperatures.

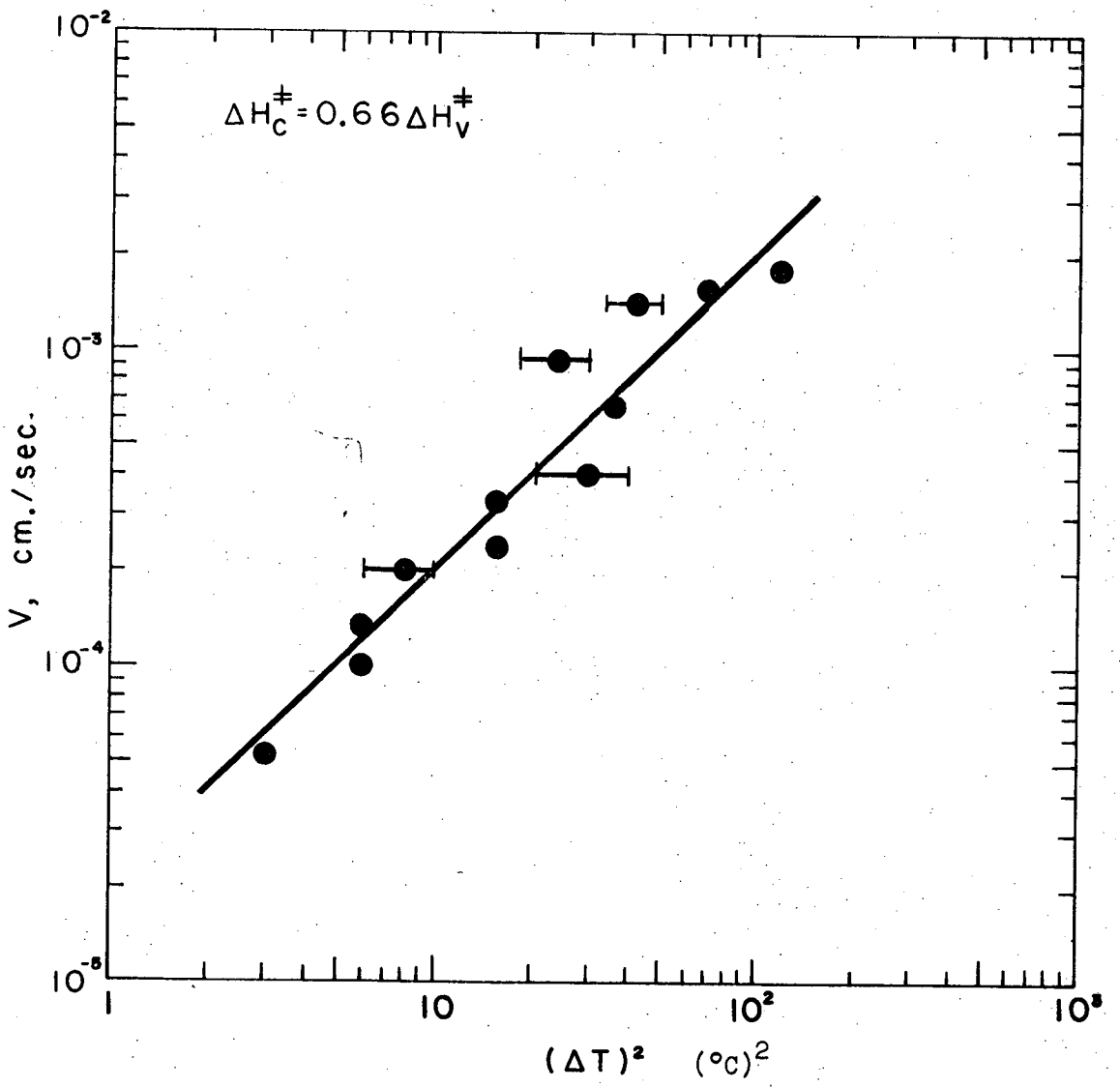

Growth rates of pure Salol crystals in undercooled liquid

XBL 725-870

Fig. 8

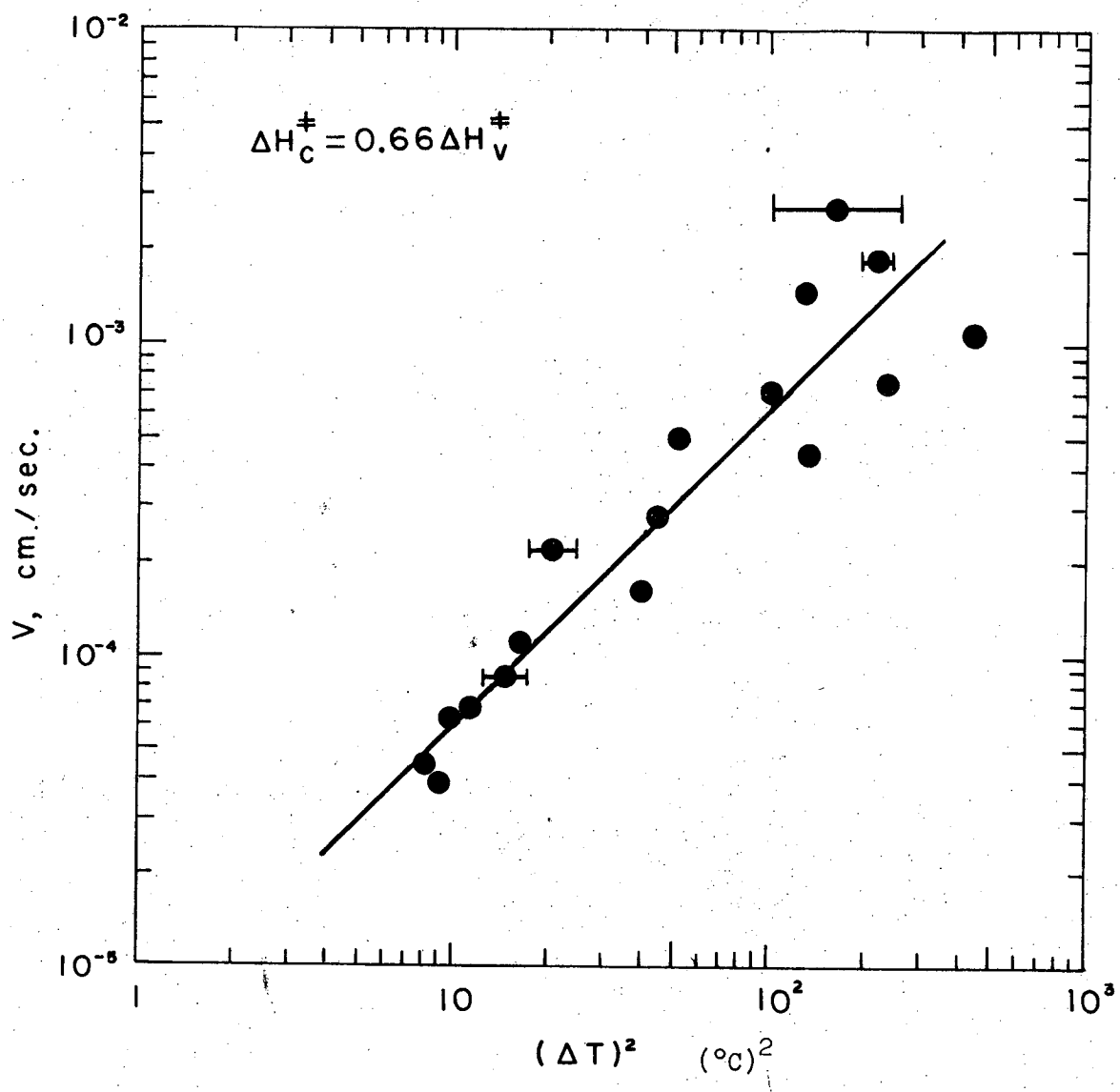

Growth rates of pure Thymol crystals in undercooled liquid

XBL 725-877

Fig. 9

Table III. Experiment Results, Pure Salol

Run No.	$V \times 10^4$ (cm/sec)	$(T_i)_1$ [a] °C	$(T_i)_2$ [a] °C	T_e [b] °C	$(\Delta T)_1$ °C	$(\Delta T)_2$ °C	$(\Delta T)_1^2$ $(°C)^2$	$(\Delta T)_2^2$ $(°C)^2$	G [c] (°C/cm)
7-3	0.52	40.47		42.2	1.73		2.99		25.4
8-4	1.35	39.7		42.2	2.50		6.25		23.3
8-9	2.00	39.01	39.74	42.2	3.19	2.46	10.2	6.05	27.4
8-7	1.10	39.74		42.2	2.46		6.05		24.1
8-6	2.40	38.3		42.2	3.9		15.21		20.8
8-3	3.3	38.26		42.2	3.94		15.5		19.6
8-2	4.1	37.6	35.86	42.2	4.6	6.34	21.2	40.2	17.3
9-3	14.1	36.37	35.09	42.2	5.83	7.11	34.0	50.6	23.2
9-2	15.4	33.81		42.2	8.39		70.4		24.3
9-4	9.4	37.95	36.72	42.2	4.25	5.46	18.1	29.8	25.1

a) Interfacial temperature corrected with interfacial temperature rise measured at 20 °C/cm.

b) Melting point measured using Buchi apparatus.

c) Slopes of best-fitting lines representing temperature-vs.-distance data.

Table IV. Experiment Results, Pure Thymol

Run No.	$V \times 10^4$ (cm/sec)	$(T_i)_1$ [a] °C	$(T_i)_2$ [a] °C	T_e [b] °C	$(\Delta T)_1$ °C	$(\Delta T)_2$ °C	$(\Delta T)_1^2$ $(°C)^2$	$(\Delta T)_2^2$ $(°C)^2$	G [c] (°C/cm)
13-4	0.4	46.77		49.8	3.03		9.2		22.4
13-7	0.45	46.96		49.8	2.84		8.2		22.4
12-2	0.65	46.72		49.8	3.08		9.5		20.8
12-3	0.69	46.34		49.8	3.46		12.0		20.8
14-7	0.86	46.22	45.65	49.8	3.58	4.15	13.1	17.5	23.1
11-2	1.10	45.79		49.8	4.01		16.1		19.7
13-2	1.70	43.45		49.8	6.35		40.3		18.3
11-6	2.23	45.65	44.78	49.8	4.15	5.02	17.2	25.4	20.3
11-1	2.81	44.76		49.8	5.04		44.3		23.3
14-2	4.54	38.2		49.8	11.6		135.0		23.4
14-4	5.01	42.6		49.8	7.2		52.0		21.2
15-3	7.05	39.66		49.8	10.14		100.3		21.2
15-7	7.51	34.6		49.8	15.2		230.4		25.4
15-4	11.0	28.9		49.8	20.9		440.8		25.4
16-3	14.5	38.3		49.8	11.5		131.2		24.2
16-6	18.34	35.85	34.3	49.8	13.95	15.5	195.1	240.0	23.1
16-4	27.2	39.78	33.63	49.8	10.02	16.17	100.4	261.3	24.3

0 0 0 0 3 8 0 0 7 4 2

Table IV. (continued)

[a]) Interfacial temperature corrected with interfacial temperature rise measured at 20 °C/cm.

[b]) Melting point measured using Buchi apparatus.

[c]) Slopes of the best-fitting line representing temperature-vs.-distance data.

In order to test the theory that velocity is proportional to the square of undercooling, we evaluated the forward rate coefficient k^F, using Kirwan and Pigford's equation for entropy of activation,

$$\Delta S_C^{\ddagger} = \Delta S_V^{\ddagger} - (\Delta S_f - R) \quad . \tag{21}$$

We approximated the enthalpy of activation by,

$$\Delta H_C^{\ddagger} = c\Delta H_V^{\ddagger} \quad . \tag{22}$$

By choosing c = 0.66 for salol and c = 0.66 for thymol, we can obtain straight lines passing through the data points. For salol crystallization the theoretical curve is in reasonable agreement with the experimental data. It seems likely, therefore, that the pure salol crystals grew by the screw dislocation mechanism. The comparison of the experimental kinetic relations representing pure salol data available from the literature are listed in Table V.

Table V

Comparison of the Kinetic Relations for Pure Salol

Author(s)	Empirical Relation Observed
Pollatschek (33)	$8 \times 10^{-6}\ \Delta T^{2.6}$
Neuman and Micus (34)	$1.56 \times 10^{-5}\ \Delta T^{2.3}$
Danilov and Malkin (35)	$5.2 \times 10^{-2}\ \exp(-7020/T\Delta T)$
Ovsienko and Alfintsev (36)	$4.6 \times 10^{-5}\ \Delta T^{2}$
De Leeuw den Bouter and Heertjes (37)	$2.28 \times 10^{-4}\ \Delta T^{0.98}$
Hillig and Turnbull (19)	$4 \times 10^{-4}\ \Delta T^{1.7}$
This work	$2 \times 10^{-5}\ \Delta T^{2}$

The theoretical prediction of the crystallization rates for pure thymol freezing from the melt agree well with the experimental data at low undercooling, at higher undercooling the data are somewhat scattered. Again this is due to the uncertainties in the interfacial temperatures and possibly because screw dislocations may no longer exist at the higher undercooling due to a change of the surface morphology. Evidence in support of the screw dislocation growth mechanism for salol and thymol has been obtained by Amelinckx (38,39) from direct observation of spirals on the face of thymol and salol which were growing from the melt and from various solutions.

The degree of undercooling for a given growth rate for salol is smaller than that for thymol. This disagrees with the conclusion of Sharp (11) that, for materials having a large entropy of fusion, the undercooling at a given growth velocity is greater than that for materials having a small value of ΔS_f. This disagreement is probably because the assumption of equal atomic mobility is not valid for this system. Although salol has a greater entropy of fusion (14.8 cal/mole-°K) than thymol (12.8 cal/mole-°K); thymol molecules apparently have higher mobility than salol molecules do.

2. <u>Binary Mixtures of Salol and Thymol</u>

In Table VI are presented the growth velocities and interfacial conditions for five constant values of the liquid mole fraction of salol at a great distance from the crystal interface. Measured and calculated quantities necessary for the computation of the interfacial concentrations are listed in Table VII. The mole fraction of salol in the liquid at the

Table VI. Growth Velocities, Interfacial Conditions and Predicted Interfacial Solid Compositions

Run No.	$V \times 10^4$ (cm/sec)	x_{Bi} mole fraction	y_{Bi} mole fraction	y_e mole fraction	T_i °C	T_e °C	$(x_{Bi})_{th}$* mole fraction
y_o = 0.95 mole fraction of salol							
35-3	1.16	.938	.921	.792	29.61	37.11	.921
35-4	1.16	.942	.923	.792	29.61	37.20	.923
35-6	1.16	.938	.931	.785	29.20	37.66	.931
35-7	1.17	.942	.931	.785	29.20	37.68	.931
35-8	1.16	.934	.926	.785	29.20	37.40	.926
35-9	1.16	.937	.925	.707	24.23	37.35	.926
35-10	1.16	.941	.929	.707	24.23	37.59	.929
35-13	0.31	.966	.939	.683	22.56	38.16	.939
35-14	0.31	.974	.945	.683	22.56	38.55	.946
35-15	0.31	.971	.944	.683	22.56	38.49	.945
35-16	0.34	.965	.936	.768	28.17	37.98	.936
35-17	0.34	.964	.940	.768	28.17	38.24	.940
35-18	0.34	.968	.938	.768	28.17	38.12	.938
35-19	0.31	.979	.935	.688	22.97	37.95	.936
35-20	0.31	.976	.938	.688	22.97	38.11	.938
35-21	0.31	.973	.941	.688	22.97	38.28	.941
35-24	0.58	.957	.938	.765	27.97	38.09	.938
35-25	0.58	.950	.936	.765	27.97	38.00	.936
35-26	0.58	.951	.935	.765	27.97	37.80	.935
35-27	0.58	.922	.911	.860	33.70	36.50	.911
35-28	3.57	.923	.916	.860	33.70	36.79	.916
35-29	3.58	.922	.914	.860	33.70	36.72	.914
35-30	3.60	.917	.906	.861	33.71	36.21	.906
35-31	6.69	.924	.920	.879	34.79	37.07	.920
35-32	6.71	.926	.923	.879	34.80	37.20	.923
35-33	6.72	.924	.921	.879	34.80	37.00	.921
y_o = 0.90 mole fraction of salol							
20-01	9.17	.880	.877	.761	27.71	34.57	.877
20-02	9.10	.880	.874	.761	27.71	34.41	.874
20-03	6.67	.882	.873	.743	26.62	34.34	.873
20-04	8.79	.873	.868	.749	27.00	34.09	.869

(continued)

Table VI. (continued)

Run No.	$V \times 10^4$ (cm/sec)	x_{Bi} mole fraction	y_{Bi} mole fraction	y_e mole fraction	T_i °C	T_e °C	$(x_{Bi})_{th}$* mole fraction
20-05	7.89	.876	.872	.627	18.26	34.57	.873
20-06	0.62	.901	.882	.652	20.32	34.87	.898
20-07	1.46	.887	.871	.791	29.58	34.26	.873
20-08	1.19	.897	.867	.807	30.54	33.74	.864
20-09	1.19	.895	.867	.807	30.54	34.03	.869
20-10	3.12	.866	.856	.646	19.87	33.39	.859
20-11	1.08	.890	.876	.786	29.29	34.51	.879
20-12	2.94	.884	.876	.781	28.94	34.55	.878
20-13	1.51	.877	.859	.652	20.28	33.56	.866
20-14	8.73	.901	.872	.744	26.68	34.30	.878
20-15	1.63	.881	.870	.806	34.02	34.17	.870

Run No.	$V \times 10^4$ (cm/sec)	x_{Ai} mole fraction	y_{Ai} mole fraction	y_e mole fraction	T_i °C	T_e °C	x_{Bi} mole fraction	$(x_{Bi})_{th}$* mole fraction
y_o = 0.15 mole fraction salol								
36-01	0.71	0.058	0.178	0.52	16.15	36.77	0.952	0.931
36-02	0.71	0.040	0.183	0.52	16.15	36.41	0.960	0.927
36-04	0.71	0.077	0.165	0.528	16.15	37.66	0.923	0.942
36-07	0.48	0.010	0.175	0.579	13.07	36.96	0.990	0.999
36-09	0.48	0.044	0.166	0.579	13.07	37.50	0.956	1.006
36-27	0.86	0.125	0.171	0.377	25.38	37.25	0.875	0.876
36-28	0.86	0.122	0.171	0.377	25.38	37.27	0.878	0.878
36-29	0.86	0.877	0.173	0.373	25.61	37.17	0.912	0.896
36-31	1.03	0.092	0.169	0.559	14.25	37.37	0.908	0.915
36-32	1.03	0.086	0.177	0.559	14.25	36.86	0.914	0.909
36-36	1.92	0.120	0.190	0.320	28.91	35.95	0.880	0.883
36-37	1.92	0.117	0.179	0.320	28.91	36.69	0.884	0.884
36-38	3.22	0.129	0.161	0.459	20.34	37.93	0.871	0.860
36-39	3.22	0.143	0.162	0.459	20.34	37.89	0.857	0.859
36-40	3.23	0.142	0.160	0.459	20.34	38.01	0.858	0.861
36-41	2.67	0.127	0.163	0.479	19.13	37.81	0.873	0.864
36-42	2.67	0.133	0.163	0.479	19.13	37.79	0.867	0.864

(continued)

Table VI. (continued)

Run No.	$V \times 10^4$ (cm/sec)	x_{Ai} mole fraction	y_{Ai} mole fraction	y_e mole fraction	T_i °C	T_e °C	x_{Bi} mole fraction	$(x_{Bi})_{th}$* mole fraction
y_o = 0.10 mole fraction of salol								
4-04	2.07	0.010	0.120	0.528	16.18	39.43	0.905	0.898
4-05	2.06	0.087	0.114	0.528	16.18	41.25	0.913	0.910
4-06	5.02	0.100	0.122	0.347	27.19	40.69	0.900	0.886
4-07	4.45	0.096	0.114	0.428	22.26	41.26	0.904	0.898
4-08	4.46	0.100	0.118	0.428	22.26	40.93	0.900	0.894
4-09	4.47	0.108	0.123	0.428	22.26	40.63	0.893	0.890
4-10	6.61	0.099	0.109	0.303	30.01	41.59	0.901	0.895
4-11	6.61	0.108	0.115	0.303	30.01	41.17	0.893	0.889
4-12	9.12	0.098	0.104	0.275	31.78	41.93	0.902	0.892
4-13	9.12	0.097	0.103	0.275	31.78	41.99	0.903	0.899
4-14	3.37	0.099	0.111	0.392	24.44	41.44	0.902	0.902
4-15	3.37	0.101	0.117	0.392	24.44	41.04	0.899	0.897
4-16	3.37	0.104	0.121	0.392	24.44	40.76	0.896	0.893
4-17	10.60	0.109	0.115	0.345	27.36	41.14	0.892	0.889
4-18	10.40	0.103	0.107	0.345	27.36	41.72	0.897	0.896
4-19	10.50	0.106	0.110	0.345	27.36	41.49	0.894	0.893
25-03	2.86	0.098	0.116	0.447	21.07	41.12	0.902	0.904
25-04	2.86	0.105	0.122	0.447	21.07	40.67	0.895	0.898
25-08	2.85	0.098	0.111	0.366	26.06	41.42	0.902	0.903
25-09	2.94	0.097	0.112	0.366	26.06	41.37	0.903	0.902
20-17	1.01	0.070	0.112	0.518	16.77	40.43	0.896	0.895
20-20	1.01	0.060	0.108	0.500	17.83	40.56	0.912	0.896
20-23	0.51	0.044	0.105	0.263	32.57	41.91	0.562	0.552
20-24	0.51	0.040	0.123	0.420	22.67	40.58	0.599	0.594
y_o = 0.05 mole fraction of salol								
31-02	4.89	0.061	0.071	0.309	29.60	44.40	0.939	0.930
31-03	2.34	0.047	0.066	0.378	25.33	44.76	0.953	0.935
31-04	2.33	0.048	0.065	0.378	25.33	44.82	0.952	0.936
31-05	2.33	0.048	0.064	0.378	25.33	44.90	0.952	0.937
31-06	2.34	0.047	0.059	0.378	25.33	45.24	0.953	0.941

(continued)

Table VI. (continued)

Run No.	$V \times 10^4$ (cm/sec)	x_{Ai} mole fraction	y_{Ai} mole fraction	y_e mole fraction	T_i °C	T_e °C	x_{Bi} mole fraction	$(x_{Bi})_{th}$* mole fraction
32-06	3.40	0.038	0.063	0.573	13.41	44.96	0.962	0.937
32-07	3.41	0.052	0.075	0.573	13.41	44.05	0.948	0.925
32-08	3.38	0.063	0.081	0.573	13.41	43.63	0.937	0.920
33-10	0.45	0.026	0.065	0.288	30.92	44.78	0.974	0.936
33-13	0.45	0.024	0.060	0.288	30.92	45.19	0.976	0.941
33-14	0.59	0.016	0.059	0.392	24.44	45.23	0.984	0.942
33-15	0.59	0.021	0.058	0.392	24.44	45.30	0.979	0.943
33-16	0.59	0.021	0.058	0.392	24.44	45.33	0.979	0.943
35-22	4.67	0.046	0.055	0.295	30.50	45.56	0.954	0.945
35-23	4.63	0.046	0.058	0.295	30.50	45.34	0.955	0.942
34-06	0.82	0.020	0.071	0.416	22.95	44.39	0.980	0.931
34-07	0.82	0.018	0.074	0.416	22.95	44.16	0.982	0.928
34-08	0.82	0.015	0.075	0.416	22.95	44.07	0.985	0.926

*Theoretical prediction of the interfacial solid composition from the absolute rate theory with $\chi \simeq 10^{-8}$, $\Delta H_C^{\ddagger} = 0.66\Delta H_V^{\ddagger}$ and $\Delta S_C^{\ddagger} = \Delta S_V^{\ddagger} - (\Delta S_f - R)$.

Table VII. Experimental Measurements, Salol-Thymol System

Run No.	$V \times 10^4$ (cm/sec)	t_i (mm)	$s \times 10^2$ (mm)	α	β	γ	ΔN (mf/mm)	$\left.\frac{dw}{dv}\right)_{v=0}$ (mf/mm)	$\left.\frac{dy}{dz}\right)_{z=0}$ (mf/mm)	G (°C/cm)
				Angle, Degree						
y_o = 0.95 mole fraction salol										
35-3	1.16	0.700	1.71	7.58	71.15	11.24	1.7197	0.607	0.249	22.93
35-4	1.16	0.700	1.72	6.55	72.34	11.03	1.5285	0.734	0.291	22.93
35-6	1.16	0.567	1.87	6.32	69.20	14.45	0.7298	0.218	0.117	24.07
35-7	1.17	0.567	1.90	5.26	71.97	12.73	0.6924	0.347	0.170	24.07
35-8	1.16	0.567	1.89	8.95	67.74	13.27	1.1757	0.233	0.120	24.07
35-9	1.16	0.671	1.92	7.63	63.35	18.99	1.1766	0.455	0.174	25.79
35-10	1.16	0.671	1.93	6.70	63.60	19.67	0.6883	0.442	0.168	25.79
35-13	0.309	0.573	1.88	4.94	80.52	14.38	0.8846	0.215	0.109	26.28
35-14	0.309	0.573	1.72	4.25	79.75	14.47	0.2329	0.205	0.114	26.28
35-15	0.308	0.573	1.64	5.42	80.14	15.25	0.3345	0.182	0.106	26.28
35-16	0.339	0.592	1.86	6.52	60.60	22.95	1.2078	0.264	0.127	21.49
35-17	0.341	0.592	1.86	5.76	62.01	22.20	0.7585	0.209	0.103	21.49
35-18	0.342	0.592	1.81	6.16	62.05	21.75	0.9678	0.258	0.128	21.49
35-19	0.307	0.674	1.94	7.44	60.16	22.36	1.3959	0.457	0.171	33.21
35-20	0.311	0.674	1.95	7.85	61.75	20.37	1.0814	0.395	0.153	33.21
35-21	0.310	0.674	1.97	6.50	62.77	20.69	0.7389	0.328	0.128	33.21
35-24	0.580	0.573	1.87	5.73	82.83	12.86	0.8936	0.283	0.144	23.27
35-25	0.578	0.573	1.89	5.59	81.83	13.72	1.0484	0.199	0.101	23.27
35-26	0.580	0.573	1.90	6.95	84.25	12.67	1.2046	0.244	0.123	23.27
35-27	3.58	0.668	1.86	7.51	64.37	18.08	2.5598	1.902	0.479	17.53
35-28	3.57	0.668	1.91	8.31	63.44	18.22	1.9625	0.955	0.306	17.53
35-29	3.58	0.668	1.94	9.47	62.85	17.65	2.1060	1.020	0.317	17.53
35-30	3.60	0.668	1.94	8.88	64.40	16.70	3.1680	2.472	0.527	17.53
35-31	6.69	0.538	1.88	5.14	73.41	21.70	0.8996	0.597	0.276	9.16
35-32	6.71	0.538	1.91	4.23	72.99	21.21	0.6782	0.571	0.262	9.16
35-33	6.72	0.538	1.90	4.18	73.17	20.97	0.8580	0.478	0.226	9.16

Table VII. (continued)

Run No.	$V \times 10^4$ (cm/sec)	t_i (mm)	$s \times 10^2$ (mm)	α	β	γ	ΔN (mf/mm)	$\left.\frac{dw}{dv}\right)_{v=0}$ (mf/mm)	$\left.\frac{dy}{dz}\right)_{z=0}$ (mf/mm)	G (°C/cm)
				Angle, Degree						
y_o = 0.90 mole fraction salol										
20-01	9.17	0.426	1.33	1.96	85.01	2.99	0.2429	0.334	0.319	13.57
20-02	9.18	0.426	1.33	2.25	86.19	1.52	0.4659	0.702	0.658	13.57
20-03	6.64	0.443	1.33	1.03	73.04	17.95	0.9104	1.045	0.739	15.11
20-04	8.79	0.423	1.33	0.51	72.18	18.29	0.9654	0.718	0.574	15.11
20-05	7.89	0.428	1.30	2.51	69.89	17.57	0.7703	0.576	0.482	31.62
20-06	0.63	0.313	1.35	3.96	33.68	60.24	0.8891	0.160	0.152	41.71
20-07	1.46	0.423	1.27	3.75	48.80	37.42	1.5310	0.337	0.284	27.86
20-08	1.19	0.452	1.54	2.96	74.11	12.89	2.3887	0.770	0.508	12.03
20-09	1.19	0.452	1.56	2.16	75.35	12.46	1.9620	0.588	0.402	12.03
20-10	3.12	0.469	1.56	2.17	75.68	12.12	2.7593	0.625	0.409	21.38
20-11	1.08	0.323	1.69	1.16	54.01	34.80	1.0442	0.218	0.194	12.54
20-12	2.94	0.493	1.53	0.95	71.01	19.90	1.0445	0.437	0.278	17.63
20-13	1.51	0.445	1.58	4.34	53.07	41.23	2.5636	0.759	0.357	40.62
20-14	0.87	0.498	1.55	4.10	78.52	15.54	2.1909	0.480	0.309	26.13
20-15	1.63	0.477	1.58	6.07	66.99	29.05	1.7902	0.390	0.233	11.19
y_o = 0.15 mole fraction of salol										
36-01	0.71	0.457	1.51	8.43	84.58	13.84	3.085	1.121	0.755	27.43
36-02	0.71	0.457	1.51	8.13	84.33	13.75	3.651	1.310	0.903	27.43
36-04	0.71	0.457	1.49	13.57	88.76	12.37	1.673	0.884	0.559	27.43
36-07	0.48	0.448	1.52	13.11	89.83	12.98	2.7196	1.156	0.715	31.26
36-09	0.48	0.448	1.56	12.75	89.42	12.21	1.757	0.874	0.531	31.26
36-27	0.86	0.441	1.53	13.70	89.18	12.92	2.247	0.548	0.345	14.39
36-28	0.86	0.441	1.53	13.63	88.90	12.57	2.214	0.575	0.362	14.39
36-29	0.86	0.441	1.55	14.45	89.76	14.25	2.2369	1.010	0.624	14.20

(continued)

Table VII. (continued)

Run No.	$V \times 10^4$ (cm/sec)	t_i (mm)	$s \times 10^2$ (mm)	α	β	γ	ΔN (mf/mm)	$\left(\frac{dw}{dv}\right)_{v=0}$ (mf/mm)	$\left(\frac{dy}{dz}\right)_{z=0}$ (mf/mm)	G (°C/cm)
				Angle, Degree						
36-31	1.03	0.414	1.59	15.07	69.91	4.97	2.003	0.739	0.708	21.96
36-32	1.03	0.414	1.50	14.34	70.91	4.70	2.734	0.815	0.840	21.96
36-36	1.92	0.397	1.66	7.05	78.48	4.42	3.879	1.298	1.153	5.23
36-37	1.91	0.397	1.75	6.50	77.95	5.50	2.859	1.224	1.024	5.23
36-38	3.22	0.398	1.73	6.73	73.59	9.63	1.192	1.022	0.919	16.72
36-39	3.22	0.398	1.73	6.95	73.51	9.59	1.226	0.690	0.539	16.72
36-40	3.23	0.399	1.76	7.70	73.80	8.45	1.0652	0.664	0.508	16.72
36-41	2.67	0.392	1.80	7.54	73.64	8.77	1.312	0.077	0.844	20.49
36-42	2.67	0.392	1.83	7.97	72.84	9.14	1.338	0.864	0.716	20.49
y_o = 0.10 mole fraction of salol										
4-04	2.07	0.474	1.52	0.23	63.76	25.96	4.6179	0.512	0.396	26.73
4-05	2.06	0.474	1.53	0.07	63.42	26.60	1.6828	0.591	0.475	26.73
4-06	5.02	0.467	1.53	0.59	68.81	20.55	2.5709	0.968	0.895	21.08
4-07	4.45	0.501	1.48	1.08	86.50	4.53	1.8059	1.110	0.659	26.53
4-08	4.46	0.501	1.45	3.64	89.03	2.71	2.3635	1.172	0.680	26.53
4-09	4.47	0.501	1.39	3.26	88.32	1.61	2.8761	0.933	0.570	26.53
4-10	6.61	0.530	1.45	0.52	88.72	0.80	1.3658	0.969	0.528	17.25
4-11	6.62	0.530	1.42	0.82	87.80	1.35	2.1130	0.713	0.400	17.25
4-12	9.12	0.536	1.36	0.35	89.73	0.12	0.8355	0.815	0.457	13.90
4-13	9.12	0.536	1.37	0.52	89.29	1.18	0.7180	0.839	0.472	13.90
4-14	3.37	0.522	1.32	1.06	85.78	3.10	1.5588	0.580	0.360	20.60
4-15	3.37	0.522	1.34	0.73	86.67	2.55	2.3072	0.745	0.459	20.60
4-16	3.37	0.522	1.48	1.11	87.92	3.14	2.7469	0.866	0.476	20.60
4-17	10.60	0.477	1.36	0.55	86.77	2.63	2.0162	0.892	0.593	15.88
4-18	10.40	0.477	1.35	0.70	80.32	8.93	1.0849	0.559	0.393	15.88
4-19	10.50	0.477	1.36	0.56	82.79	6.61	1.4522	0.583	0.398	15.88

(continued)

Table VII. (continued)

Run No.	$V \times 10^4$ (cm/sec)	t_i (mm)	$s \times 10^2$ (mm)	α	β	γ	ΔN (mf/mm)	$\left.\frac{dw}{dv}\right)_{v=0}$ (mf/mm)	$\left.\frac{dy}{dz}\right)_{z=0}$ (mf/mm)	G (°C/cm)
				Angle, Degree						
25-03	2.86	0.440	2.00	6.19	77.20	6.56	1.7661	0.711	0.406	26.64
25-04	2.86	0.440	2.03	6.84	76.85	6.26	2.4332	0.734	0.420	26.64
25-08	2.85	0.461	2.05	6.56	76.93	6.47	1.3806	0.609	0.316	21.74
25-09	2.84	0.461	2.06	6.77	75.76	7.42	1.4531	0.679	0.365	21.74
20-17	1.01	0.458	1.41	5.05	62.02	33.00	2.9151	0.686	0.658	22.49
20-20	1.01	0.369	1.56	4.13	78.16	15.92	2.1658	1.168	0.092	20.94
20-23	0.51	0.462	1.42	3.67	73.31	12.97	0.6319	0.760	0.624	10.07
20-24	0.51	0.454	1.44	2.94	74.59	12.42	2.6820	0.754	0.608	26.74
y_o = 0.05 mole fraction of salol										
31-02	4.89	0.484	1.25	11.14	80.18	20.91	2.5181	0.512	0.363	30.44
31-03	2.34	0.500	1.30	11.52	78.45	23.03	1.9903	0.539	0.362	38.82
31-04	2.33	0.500	1.29	11.74	78.32	23.36	1.8966	0.500	0.333	38.82
31-05	2.33	0.500	1.30	11.06	77.83	23.18	1.7566	0.468	0.310	38.82
31-06	2.34	0.500	1.29	11.47	0.28	23.14	1.1997	0.374	0.243	38.82
32-06	3.40	0.355	1.64	1.99	74.45	12.51	1.1754	0.818	0.728	42.94
32-07	3.41	0.355	1.64	0.17	78.45	11.67	2.2343	0.798	0.667	42.94
32-08	3.38	0.355	1.64	0.52	76.06	13.36	2.7279	0.623	0.518	42.94
33-10	0.45	0.459	1.76	0.44	71.66	17.85	1.7608	0.263	0.145	25.11
33-13	0.45	0.459	1.76	3.57	69.06	17.32	1.1405	0.234	0.132	25.11
33-14	0.59	0.538	1.79	6.98	82.47	14.46	1.2625	0.483	0.213	29.29
33-15	0.59	0.538	1.75	6.51	82.00	14.47	1.1329	0.408	0.182	29.29
33-16	0.59	0.538	1.75	6.45	82.05	14.36	1.0884	0.401	0.179	29.29
33-22	4.67	0.466	1.53	3.31	64.07	22.47	0.6377	0.466	0.349	18.11
33-23	4.63	0.466	1.56	3.18	63.09	23.70	0.9787	0.579	0.466	18.11
34-06	0.82	0.317	1.94	1.82	83.69	8.08	1.6204	0.495	0.344	28.56
34-07	0.82	0.317	1.92	2.58	85.07	7.47	1.8630	0.545	0.380	28.56
34-08	0.82	0.317	1.87	4.48	87.02	7.42	1.9516	0.578	0.407	28.56

interface was obtained from the fringe shift at the interface and the original composition of melt, as expressed in Eq. (39) of Chapter III.

Some auxiliary experiments were performed to test an assumption implied in Eq. (39), that the original liquid concentration was constant throughout the experiment even though solids with different concentrations were continuously freezing out of the liquid. Samples of the solid phase were measured with an infrared absorption spectrometer. The concentration of the solid after crystallization was measured at different positions parallel to the growing direction. (It was found that the concentration gradient across the solid phase was not appreciable.) The change of bulk liquid concentration during the experiment was negligible. Therefore, using the constant bulk-liquid concentration in Eq. (39) was quite reasonable. The solid composition at the interface was calculated from Eq. (40) using measured velocity, the observed liquid mole fraction at the interface, and the mole fraction gradient.

The observed liquid and solid interfacial concentrations are plotted in Fig. 10 for thymol-rich mixtures and in Fig. 11 for salol-rich mixtures. For thymol-rich mixtures the interfacial liquid mole fraction of thymol fell slightly below the original liquid concentration. At the lowest growth rate the solid interfacial concentration tended toward the equilibrium value. As growth rate increased the deviation from equilibrium became considerable. At very higher growth rates the solid composition differed only very slightly from that of the original liquid. This observation agrees well with theory.

The figure also indicates that for thymol-rich mixtures the mass transfer resistance in the liquid phase is not the main cause of the

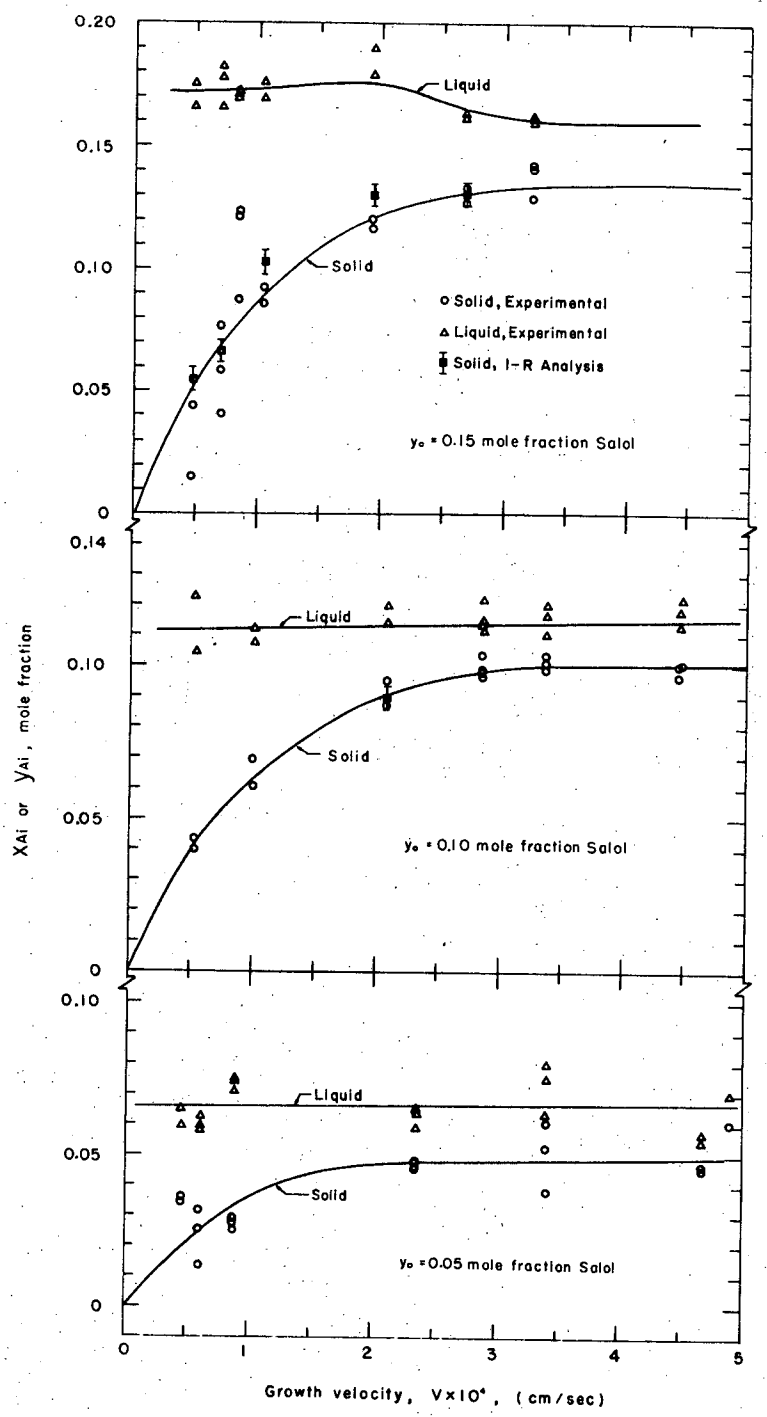

Interfacial compositions of Thymol-rich mixtures

XBL 725-879

Fig. 10

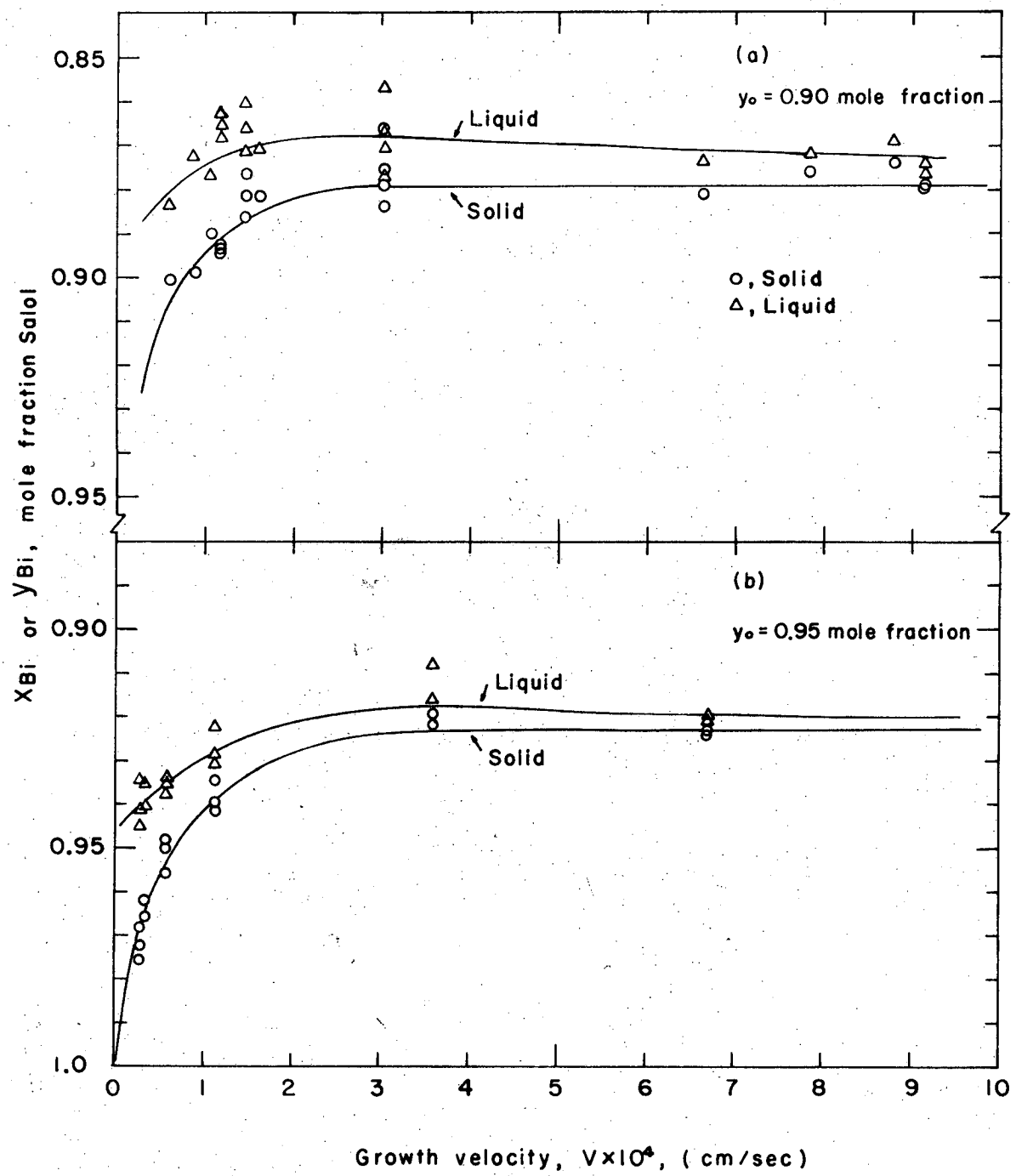

Interfacial compositions of Salol-rich mixtures

XBL 725-880

Fig. 11

failure to reach equilibrium. The observed salol-rich mixtures exhibit a similar phenomenon, except there is an appreciable mass transfer resistance in the liquid phase, resulting in a larger difference of the concentration between the interfacial and bulk liquid. No doubt this liquid phase resistance could be minimized by mechanical stirring.

Due to experimental difficulties, crystal growth could not be executed at very slow rates. However, the equilibrium solid concentration was not inconsistent with the data, which could be extrapolated to V = 0. This suggests that in order to get very pure material from a simple eutectic melt by crystallization, a very slow growth velocity is needed. This growth rate limitation is a most serious disadvantage for the crystallization process as a separation tool.

Although the measurements were carried out with great care, it is possible that the solid compositions obtained from the diffusion equation were in error. This will be critically discussed later in this chapter.

It is possible to compute the product of $f\lambda_s k^F$ from Eq. (18), using the observed solid and liquid interfacial concentrations and temperatures and the growth velocities. The step density, f, for the screw dislocation model can be computed using Eqs. (4), (5), and (6),

$$f = \frac{1}{1.2\pi} \left(\frac{\Delta G}{T_m \Delta S_f}\right) \tag{42}$$

where ΔG is computed from the liquid compositions and temperatures at the interface and the physical properties of the pure materials, using Eq. (20), and assuming ideal solution behavior in the liquid phase. The intermolecular spacing λ_s is estimated from $\lambda_s = \left(\frac{V_s}{N}\right)^{1/3}$, where N is Avogadro's number. Therefore, k^F follows directly. Theoretical values of k^F can be

calculated from Eyring's theory, Eq. (2), and $\Delta S_C^{\ddagger}$ and $\Delta H_C^{\ddagger}$ from Eq. (21) and Eq. (22) with c = 0.66, provided χ is known. Assuming $\chi = 1$ yields $k^F \simeq 10^5$, which is about eight orders of magnitude smaller than the values obtained from the data for both pure salol and thymol. Thus, in order to reconcile the data for the pure crystals with those for the solution one may assume $\chi = 10^{-8}$.

From Eq. (42), the estimated step density, f, for the screw dislocation model is about 5×10^{-3} for thymol and 7.9×10^{-3} for salol at 10 °C of supercooling. Thus, the active sites on the crystal face at 10 °C of supercooling correspond to less than one percent of the total surface. It is believed, therefore, that the roughness of the interface may not affect the surface energy appreciably.

Fig. 12 compares the experimentally observed solid composition and the composition predicted from Eq. (19) using c = 0.66 ($\Delta H_C^{\ddagger} = c\Delta H_V^{\ddagger}$) and assuming $\chi = 10^{-8}$. The absolute rate theory is employed. The predicted values are given in Table VI. Although the validity of the assumption that the velocities of the molecules of the minor constituent contributed very little to the overall system velocity is uncertain at this point, the agreement of the prediction from the absolute rate theory with experiment is satisfactory.

D. Applications of Liquid Inclusion Theory

In order to test the liquid-inclusion theory, extensive interfacial data are required. At each growth velocity one must know the liquid and solid interfacial concentrations and temperatures. Data for the salol-thymol system taken during the T.G.M.S. experiments were plotted in the form of Eq. (28), suggested by the theory (see Fig. 13).

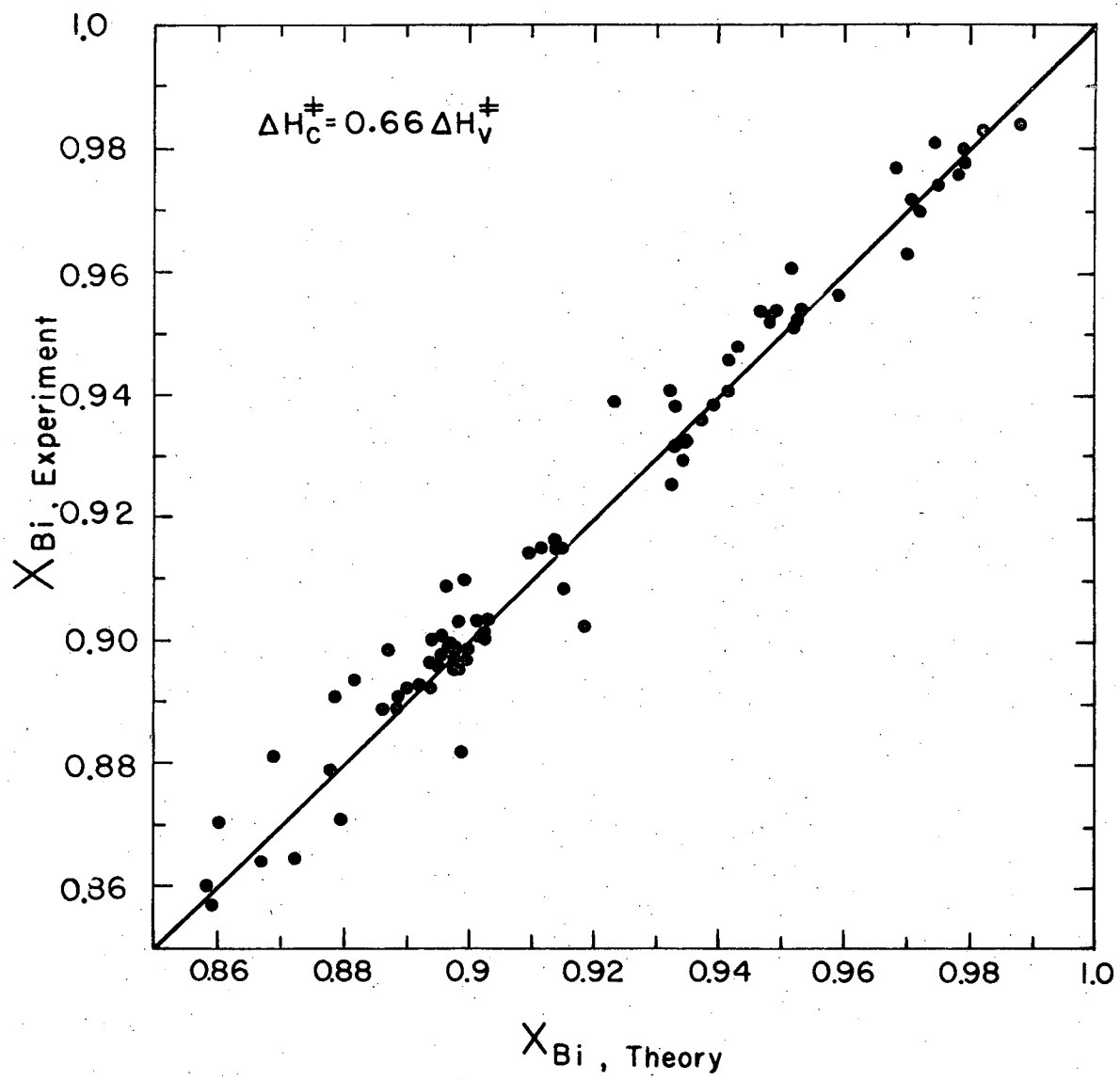

Comparison of interfacial solid compositions

(Absolute rate theory)

XBL 725-872

Fig. 12

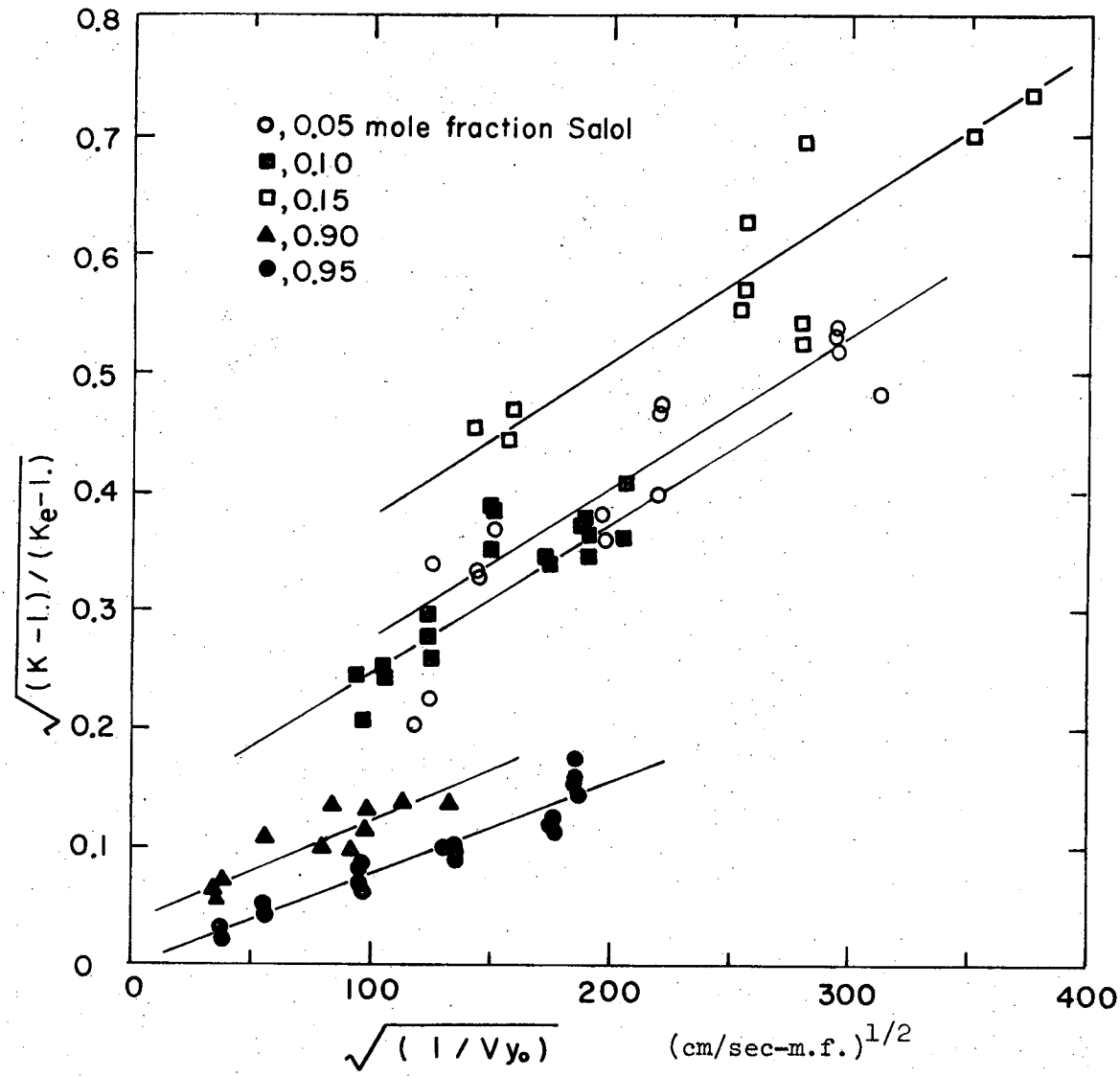

XBL 725-875

Fig. 13. Experimental Data Plotted in the Form of Eq. (28).

The figure shows that the dependency of $(\frac{K-1}{K_e-1})^{1/2}$ on $(\frac{1}{Vy_o})^{1/2}$ is about right qualitatively. However, the temperature gradients applied to the liquid phase near the interface had no effect on the distribution coefficient, in contrast with the theoretical expectation. With the same original liquid concentrations the data fall on one line, regardless of the temperature gradient. The slopes of these lines are nearly the same, which suggests that (k_1/R) is neither a function of concentration nor of temperature gradient. The different intercepts of these lines suggest that (k_2/R) depends on the liquid concentration but not on the temperature gradient. This is inconsistent with the theory.

The values of the slopes and intercepts of these straight lines were used to calculate the radius of the dendrites growing out from the interface. The calculated radii and the approximate radii observed directly from the microscope at the same growth velocity, temperature gradient and liquid composition are listed in Table VIII.

For 0.95 mole fraction of salol at 30 °C/cm, the calculated radius was about 160μ at 10^{-4} cm/sec and 340μ at 10^{-5} cm/sec growth rate, yet there was no interface breakdown discernible through the microscope. The resolution of the microscope is about 1μ. Also from the slope and intercept of the line at 0.9 mole fraction of salol, we obtain the fraction of the interface that is crystalline, $\psi = 0.09$, for a 10^{-4}cm/sec growth rate; i.e., only 9% of the interface is solid. This is inconsistent with our observation.

The values of the slopes and intercepts of the straight lines in Fig. 13, along with the observed growth velocities, interfacial liquid concentrations and temperatures, were used to calculate the solid compositions

Table VIII

Theoretical Derived Values of Radii of Dendritic Projections Growing from Crystal Surfaces

Growth Velocity cm/sec	Dendrite Radius, r, microns	
	Calculated from Eq. (23)	Observed in Microscope*
10^{-5}	340	< 1
10^{-4}	160	< 1
10^{-3}	---	100

*One micron was the limit of resolution of the microscope. "< 1" means that no dendritic features were seen.

using Eqs. (23), (24), and (26). The results of these calculations are compared with the solid compositions measured from infrared absorption in Table IX. The theoretical values are much higher than those observed, as shown in Fig. 14. This is probably because the theory overestimates the radius of the dendrites, and the amount of trapped liquid--if either phenomenon actually occurs at all.

The visual appearance of the crystals just behind the interface during the freezing experiments indicated that the crystals did not contain included liquid. The imposed temperature gradient tended to make all the crystal grains on the interface grow at the same rate. Thus, it was very difficult for liquid inclusions to be trapped behind the interface, even in the small indentations between adjacent crystals. Just behind the interface a continuous interference pattern could be seen in the solid as well as liquid.

Data were also plotted in the linear form suggested by Eq. (31), which is normalized based on the criterion of interface breakdown. If the theory and the planar interface breakdown criterion are correct all the data points should fall onto one straight line. Fig. 15 shows that the data are scattered. Although the data for each bulk liquid composition fall near one straight line, the theory fails to bring all the data together as it should.

There are other important factors, such as heat transfer and mass transfer, which may affect the stability of an interface during crystallization. These need some discussion.

The important function of heat transfer on the process of crystal growth from melts may be categorized as follows:

Table IX

Comparison of Solid Compositions Computed from Flux Balance with Values from Infrared Absorption and Liquid Inclusion Theory

Run No.	$V \times 10^4$ (cm/sec)	x_{Ai}* from Equation (40)	x_A from I.R. Analysis	x_{Ai}* from Liquid Inclusion Theory
y_o = 0.15 mole fraction salol				
36-01	0.71	0.0585	0.065 ± 0.021	0.1040
36-09	0.48	0.0440	0.055 ± 0.032	0.0767
36-31	1.03	0.0924	0.103 ± 0.024	0.1110
36-36	1.92	0.1197	0.130 ± 0.012	0.1450
36-38	3.23	0.1287	0.131 ± 0.023	0.1330
y_o = 0.10 mole fraction of salol				
4-05	2.06	0.0875	0.0910 ± 0.011	0.0927
4-13	9.12	0.0971	0.096 ± 0.005	0.0975
4-19	10.40	0.1027	0.103 ± 0.012	0.1043

*A sample calculation is shown in Appendix II.

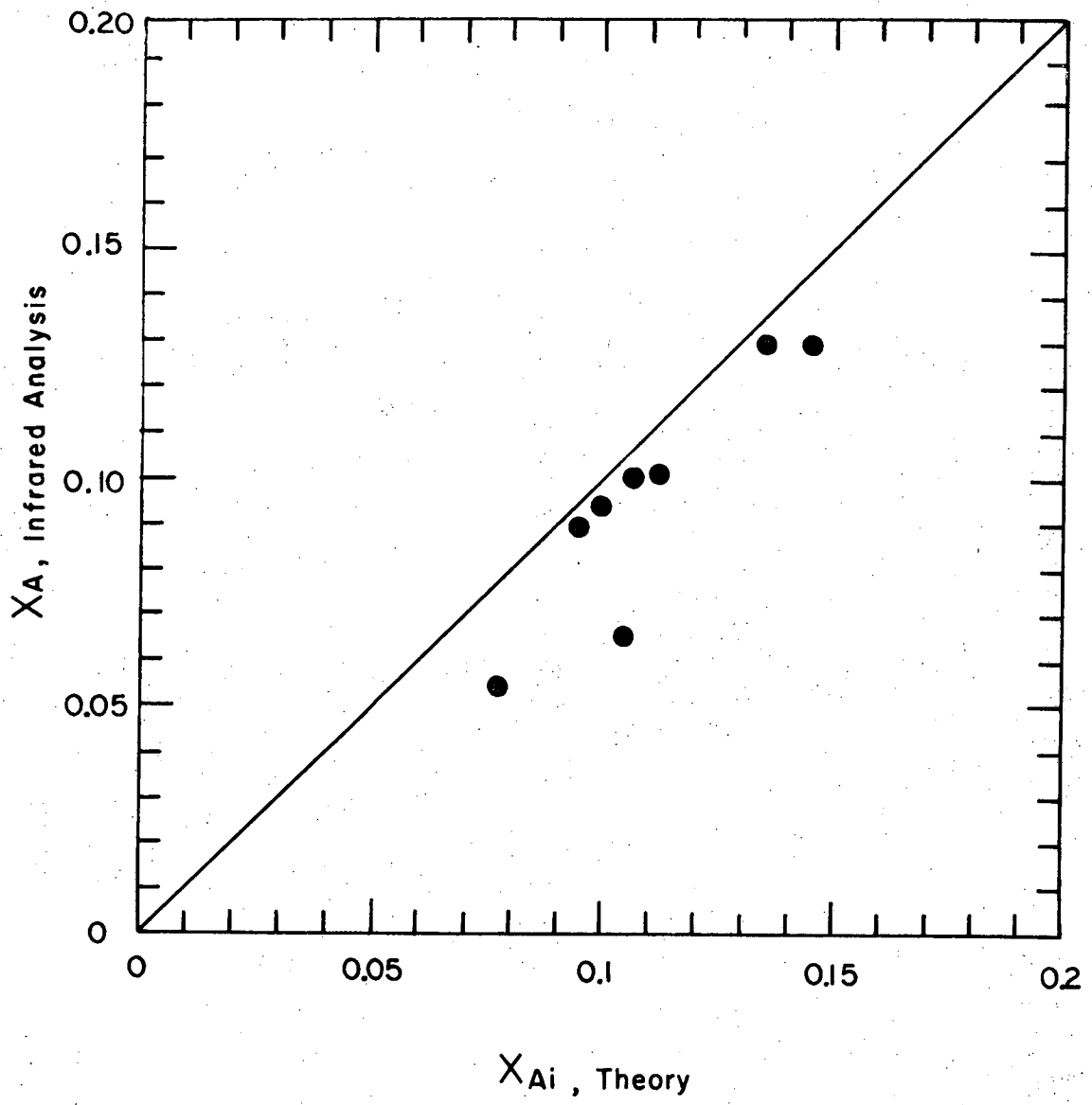

Comparison of interfacial solid compositions

(Liquid inclusion theory)

XBL 725-873

Fig. 14

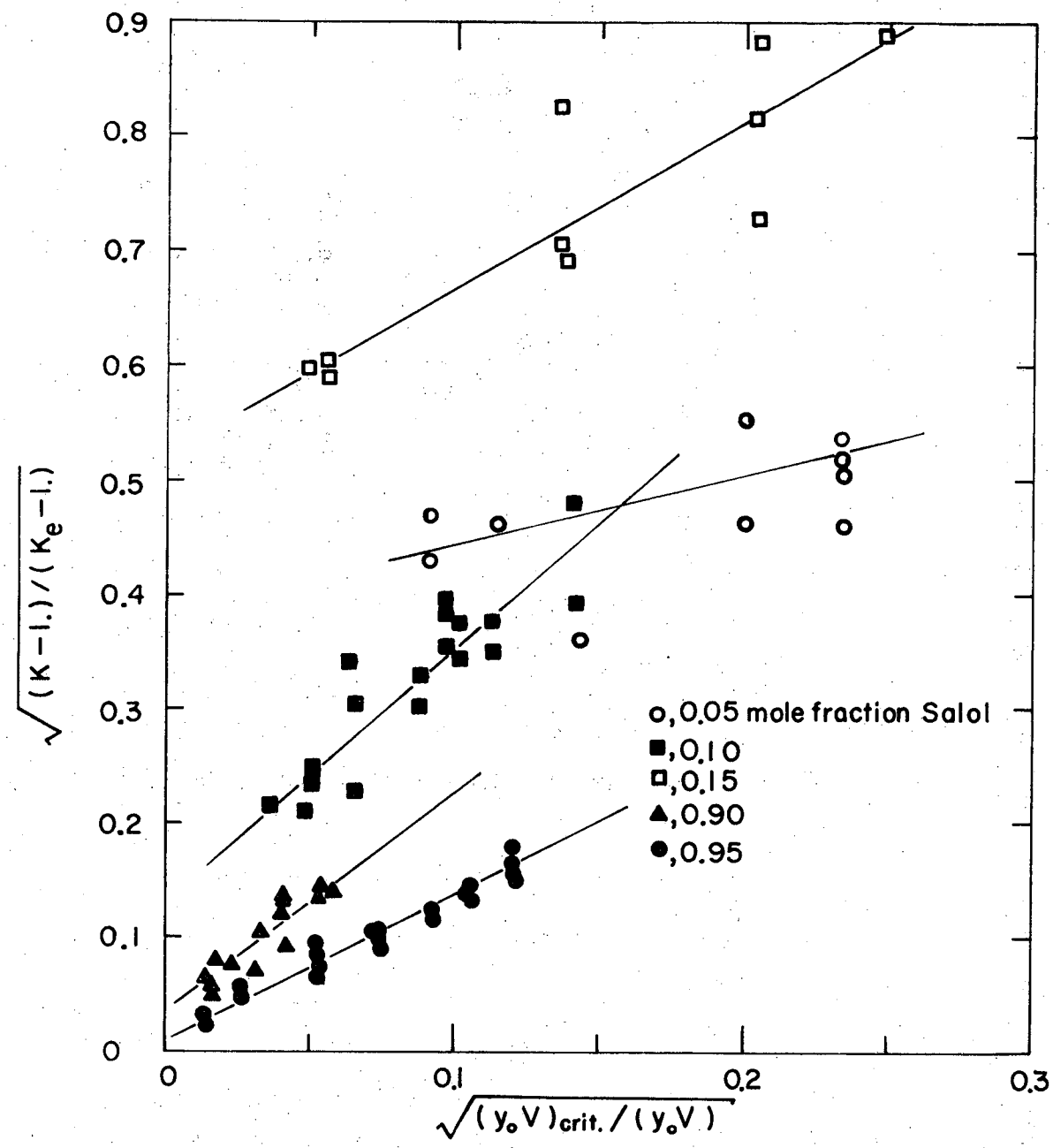

XBL 725-871

Fig. 15. Experimental Data Plotted in the Form of Eq. (31).

1) To remove the latent heat of fusion at the interface,

2) To control the shape of the interface by applying a substantial temperature gradient across the interface.

The latent heat released by freezing is removed by heat conduction through the solid phase and by convective transport in the liquid phase at the interface. The heat transfer pattern may affect growth kinetics and therefore the impurity distribution.

The interface of a growing crystal tends to be irregular without a substantial temperature gradient across it. The presence of the dendritic substructure at the interface would alter the situation, thus altering the impurity distribution.

Since the optical wedge made from glass slides moved slowly toward the cold stage, as described in Chapter III, there is possibly a small temperature difference between the glass and the liquid melt, even at the steady state growth velocity. The lag of heat conduction from the aluminum stages to the slides and from the slides to the melt depends on the slide's velocity and the heat capacity, heat conductivity and density differences between slide and melt. The temperature distribution is shown qualitatively in Fig. 16. At zero slide velocity the temperature gradient in the wedge is equal to the difference between T_h and T_c divided by the spacing between the stages. As velocity becomes larger the temperature profile becomes curved. A crystal growing near the cold stage at very high velocity experiences a larger temperature gradient than the nominal value; near the hot stage the opposite is true.

Computing the thermal displacement is a difficult mathematical problem involving the differential heat transfer equation with a moving

0 0 0 0 3 8 0 0 9 5 5

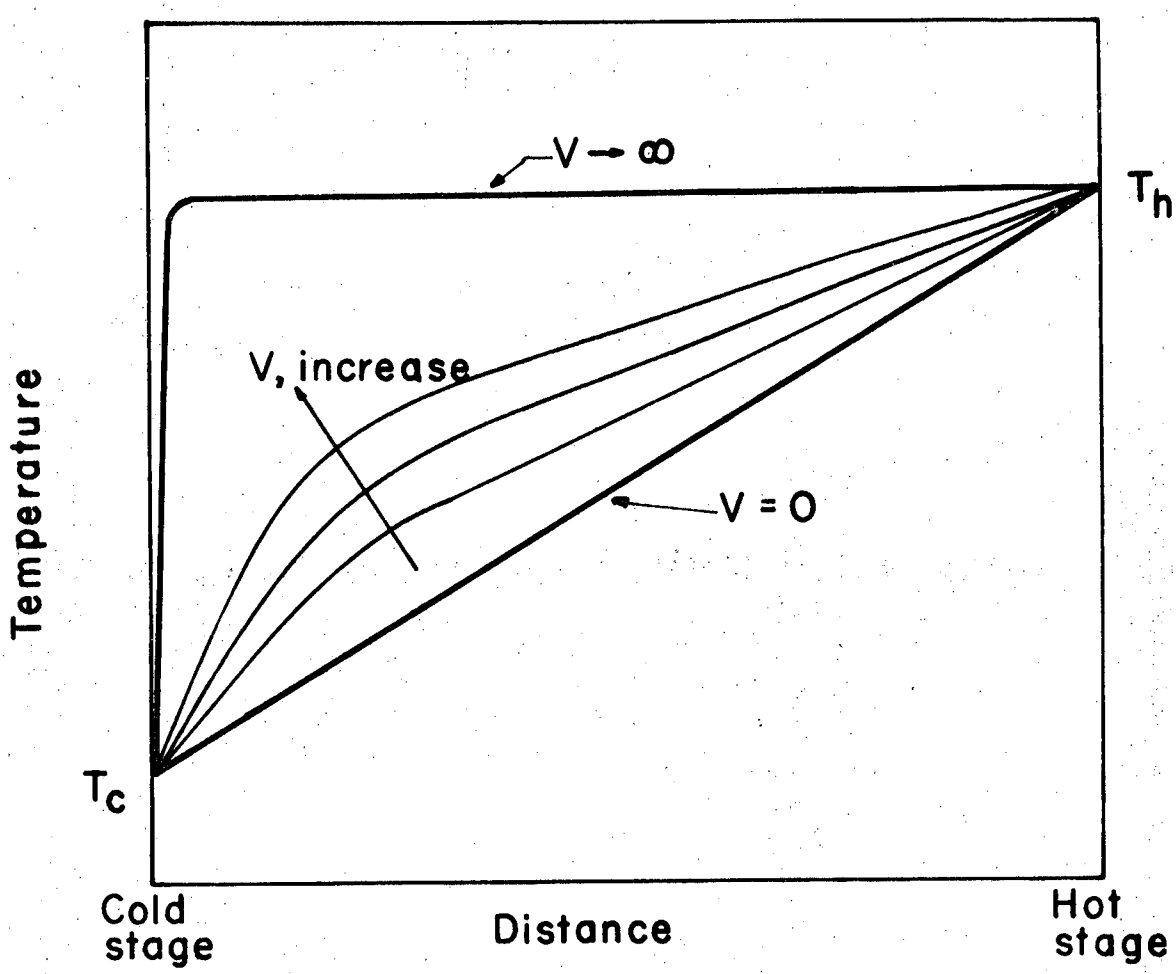

Qualitative temperature profiles in the optical wedge

XBL 725-878

Fig. 16

boundary. Fortunately, the growth velocity of the salol and thymol system was slow enough that the thermal displacement was not of critical importance in this experiment, especially as temperatures of the liquid were measured directly with the fine thermocouple. The temperature gradients listed in the tables of data were computed from such measurements.

The degree of separation attainable in crystallization from melts depends on a variety of parameters. The most basic of these are thermodynamic, expressed in the form of a phase diagram. The phase diagram of the salol and thymol systems, Fig. 4, indicates that the solid freezing out from the binary melt should be either pure salol or pure thymol. However, the ideal equilibrium condition does not occur at practical rates. The concentration of impurity in the crystal becomes considerable as the growth velocity increases.

Since one of the objectives of crystallization is to purify materials, the composition of the solid is of practical importance. Therefore, the values of the interfacial solid concentration (obtained by applying the interface flux balance to measured velocity, liquid concentration, and concentration gradient in the liquid phase) must be carefully examined. The solid concentrations were obtained in this study primarily from the flux balance equation,

$$x_i = y_i + \frac{D}{V\left(\frac{\rho_s}{\rho_L}\right)} \left(\frac{dy}{dz}\right)_{z=0} \quad . \tag{43}$$

The solid concentrations calculated from this equation fell far from the equilibrium concentrations, as shown in Figs. 10 and 11. The accuracy of the computed compositions depends on the accuracy of the fringe measurements and on the validity of this equation.

The "microscope" machine used to measure the fringe is believed to be very accurate. At most, 10 percent error is expected when fringes were somewhat obscure. In some cases the calculated solid composition lay rather close to the original liquid composition. This is probably because the true gradient at the interface could not be observed because the region near the interface was obscure and the position of the interface uncertain.

The liquid diffusivity and the densities used in Eq. (40) may be somewhat in error. They were not measured in this study. The diffusion coefficient was estimated from the empirical correlation of Wilke and Chang (40). The densities were taken from Timmermans (41). It is believed that the probable errors in these properties can account for a 10 percent uncertainty in the difference between liquid and solid mole fractions.

V. CONCLUSIONS

There was non-equilibrium at the phase boundary during crystal growth from the melts at any practical growth rate.

The absolute rate theory developed by Kirwan and Pigford, using the screw dislocation mechanism to compute the density of active sites on the crystal face and assuming the energy of activation for viscous flow to approximate the activation energy of crystallization, was applied to predict the growth rates of pure salol and thymol. The predicted values agreed well with the experimental data for salol and thymol when $\Delta H^{\ddagger} = 0.66\Delta H_V^{\ddagger}$ was used for both substances. The results confirmed that both pure salol and thymol apparently grew from their melts according to the screw dislocation mechanism.

A theory based on Eyring's concept was applied to a simple binary eutectic system without a solid solution and approximately accounted for the observed crystallization phenomena. The predicted solid compositions agreed well with the experimental data provided that the activation energy for crystallization was estimated from viscosities. The solid concentration depended upon the growth velocity, the interfacial liquid concentration, and the temperature.

The temperature gradients which were applied to the interface were found to have no effect on the distribution coefficient. They did however affect interfacial shape and stability. The criterion of planar interface breakdown used for metal alloys was found to be not suitable for the salol-thymol system.

No microscopic inclusions of liquid between adjacent crystals were observed during the epxeriments, and dendritic projections from the faces

of individual crystals were not seen. The variation of solid composition with the temperature gradient expected from the theory of liquid inclusions was not observed.

It is concluded that, in all probability, the observed deviations of the solid compositions from their equilibrium values are owing to the presence of foreign molecules in the crystal lattice, rather than their entrapment between pure crystals in the solid phase. Thus, it was found that because no microscopic inclusions were observed, the liquid inclusion theory could not successfully be applied. It is believed that the absolute rate theory is the most accurate in explaining the experimental data.

ACKNOWLEDGEMENTS

The author wishes to express his deep appreciation to Professor Robert L. Pigford for his encouragement and guidance, and to both him and his wife for their warm personal concern during the course of this work.

The suggestions, discussion and help of my fellow graduate students, Robert A. Freet and James A. Latty, are also greatly appreciated.

Above all, the author is grateful to his wife, Feng Ying, who performed most of the infrared absorption analyses for the determination of the mixed crystal compositions. Her understanding and encouragement throughout the course of the work has been invaluable.

Financial support from the Atomic Energy Commission Contract No. W-7405-eng-48 is gratefully acknowledged.

NOMENCLATURE

c = constant, less than 1.

C_p = molar heat capacity, cal/g mole °C.

D = diffusion coefficient, square cm/sec.

f = surface step density, dimensionless

g_B = dimensionless growth rate parameter, $\lambda_s f k_B^F/V$.

G = molar free energy, cal/g-mole or temperature gradient °C/cm.

h = Planck's constant, 6.6252×10^{-27} erg/sec.

H = molar enthalpy, cal/g-mole.

k = interfacial rate constant, sec^{-1}, or Boltzmann's constant, 1.38045×10^{-16} erg/°K.

K = distribution coefficient, dimensionless.

m = liquidus slope in the phase diagram.

M = molecular weight.

n = refractive index of liquid.

N = crystallization flux, mole/sq.cm-sec, or Avogadro's number, 6.0232×10^{23} $mole^{-1}$, or integer in Eqs. (32) and (33).

r = radius of dendrite, cm.

r_c = critical radius of two-dimensional nucleus, cm.

R = gas constant, cal/g-mole-°K, or radius of cell, cm.

s = interference fringe spacing, mm.

S = molar entropy, cal/g-mole-°K.

t = thickness of optical wedge at observation point, mm.

T = temperature, °C or °K.

u = average molecular velocity, cm/sec.

V = freezing velocity, cm/sec, or molar volume, cc/g-mole.

v,w = coordinates for interference fringe.

x = mole fraction in solid phase.

y = mole fraction in liquid phase.

X,Y = coordinates for optical wedge.

z = distance perpendicular to growing crystal face.

GREEK LETTERS

α = angle, degree.

β = angle, degree.

γ = liquid phase activity coefficient or angle, degree.

η = viscosity, poise.

λ = interatomic spacing, cm.

λ_o = wavelength, 6328 Å, for He-Ne gas laser.

μ = chemical potential, cal/g-mole, or kinetic growth coefficient.

ρ = molar density, g-mole/cc.

σ = interfacial surface free energy, cal/sq-cm.

χ = transmission coefficient.

ψ = solid fraction at the interface, dimensionless.

SUPERSCRIPTS

F = forward process.

L = liquid state property.

o = standard state property.

R = reverse process.

‡ = activated state property.

* = equilibrium condition.

SUBSCRIPTS

A = component A, minor component.

B = component B, major component, either thymol or salol.

C = crystallization activated state property.

c = crystalline portion at the interface, or cold stage condition.

e = equilibrium condition.

ex = experimental condition.

f = fusion process.
h = hot stage condition.
i = interfacial condition.

L = liquid-state property.

m = melting process.

O = initial condition.

P = constant pressure condition.

s = solid state property.

T = constant temperature condition.

th = theoretical prediction.

V = viscous-flow, activated-state property, or constant-volume condition.

REFERENCES

1. D. Turnbull, Solid State Physics, Vol. III (Academic Press, New York, 1958).
2. J. Burke, The Kinetics of Phase Transformation in Metal (Pergammon Press, Ltd., Oxford, 1956), p. 99.
3. M. E. Fine, Introduction to Phase Transformations in Condensed Systems (MacMillan, New York, 1965), p. 1 - 43.
4. D. J. Kirwan and R. L. Pigford, A. I. Ch. E. J. 15, 442 (1969).
5. C. T. Cheng and R. L. Pigford, I. E. C. Fund. 10, 220 (1971).
6. B. K. Jindal and W. A. Tiller, J. Chem. Phys. 49, 4632 (1968).
7. R. Brook, A. T. Houton and J. L. Torgesen, J. of Crystal Growth 2, 739 (1966).
8. K. G. Denbigh and E. T. White, Chem. Engr. Sci. 21, 739 (1966).
9. J. C. Baker and J. W. Cahn, Acta. Met. 17, 575 (1969).
10. C. S. Cheng, D. A. Irvin and B. G. Kyle, A. I. Ch. E. J. 13, 739 (1967).
11. R. M. Sharp and A. Hellawell, J. of Crystal Growth 6, 253 (1970).
12. D. D. Edie and D. J. Kirwan, paper presented at San Francisco A. I. Ch. E. Meeting, December 1971.
13. A. Van Hook, Crystallization (Rheinhold Publishing Co., New York, 1963).
14. B. Chalmers, Principles of Solidification (John Wiley and Sons, New York, 1964).
15. H. Wilson, Phil. Mag. 50, 238 (1900).
16. K. A. Jackson, D. R. Uhlman and J. Hunt, J. Crystal Growth 1, 1 (1967).
17. J. W. Cahn, B. Hillig and G. W. Sears, Acta Meta. 12, 1421 (1964).
18. M. I. Kozlovskii, Growth of Crystals, Vol. III (Consultant Bureau, New York, 1962), p. 101.

19. W. Hillig and D. Turnbull, J. Chem. Phys. 24, 914 (1956).

20. S. Glasstone, K. J. Laidler and H. Eyring, The Theory of Rate Processes, 1st Edition (McGraw-Hill, New York, 1941).

21. F. C. Frank, Disc. Frad. Soc. 5, 48 (1948).

22. T. S. Plaskett and W. C. Winegard, Can. J. of Physics 34, 96 (1956).

23. R. W. Rutter and B. Chalmers, J. Phys. 31, 15 (1953).

24. W. A. Tiller, J. W. Rutter and B. Chalmers, ACTA. 1, 428 (1953).

25. W. A. Tiller and J. W. Rutter, Can. J. Phys. 34, 96 (1956).

26. W. Berg, Proc. Roy. Sco. 164A, (London, 1938), p. 79.

27. C. W. Bunn, Disc. Frad. Sco. 5, 132 (1949).

28. J. D. Hunt, K. A. Jackson and H. Brown, Review of Scientific Instruments 37, 805 (1966).

29. R. Secor, A. I. Ch. E. J. 11, 452 (1965).

30. Y. Nishijima and G. Oster, J. Polymer Science 19, 337 (1956).

31. C. T. Cheng, (Ph. D. Thesis), University of California, Berkeley, 1969.

32. J. Timmermans, Physico-chemical Constants of Binary Systems in Concentrated Solution (Interscience Publishers, New York, 1959), p. 1169.

33. H. Pollatschek, Z. Physik. Chem. 142 (Leipzig, 1929), p. 289.

34. K. Neuman and G. Micus, Z. Physik. Chem. 2 (Leipzig, 1954), p. 25.

35. V. I. Danilov and V. I. Malkin, Zh. Fiz. Khim. 27, 1837 (1954).

36. D. E. Ovsienko and G. A. Alfintsev, Crystallization Processes (Consultants Bureau, New York, 1966), p. 25.

37. J. A. De Leeuw den Bouter and P. M. Heertjes, J. Crystal Growth 5, 19 (1969).

38. E. Votava, S. Amelinckx and W. Dekeysen, Naturwiss 39, 547 (1952).

39. E. Votava, S. Amelinckx and W. Dekeysen, Naturwiss, 40, 143 and 290 (1953).

40. C. R. Wilke and P. Chang, A. I. Ch. E. J. 1, 264 (1955).

41. J. Timmermans, Physico-chemical Constants of Pure Organic Compounds (Elsevier Publishing Company, New York, 1950).

42. I. Flachsbart, Naturwissenschaften 44, 348 (1957).

43. O. Jantsch, Zeit. fur Krist 108, 185 (1956).

44. W. Slavyanski, Zhur obschei Klim 18, 1259 (1948).

45. A. Vignes, Ind. Engr. Chem. Fund. 5, 189, (1966).

46. J. L. Gainer and A. B. Metzner, Proc. A. I. Ch. E.- I. Chem. E. 6 (London, Joint Meeting, 1965), p. 74.

47. D. D. Edie, (Ph. D. Thesis), University of Virginia, 1972.

APPENDIX I

A. Physical Properties

1. Phase Diagram

The phase diagram of the salol-thymol system was given in Fig. 4 of Chapter II from the data of Timmermans (32). The melting points of different concentrations were measured in this work by putting a small amount of the liquid mixture in a vacuum jacketed tube. The rate of the cooling was controlled by evacuating the jacket. The cooling curve was recorded from a small calibrated copper-constantan thermocouple inserted into the sample. The results are listed in Table X and plotted with the dashed line in Fig. 4. These results, rather than the data from Timmermans, were used as equilibrium values for the subsequent calculations.

Table X

The Melting Temperatures for the Salol-Thymol System

Mole Fraction Salol	Melting Point, °C	
	Measured	Timmermans (32)
0.05	45.9 ± 0.05	47.3
0.10	42.5 ± 0.05	43.7
0.15	39.1 ± 0.05	40.2
0.90	37.5 ± 0.05	36.6
0.95	39.9 ± 0.05	39.5

The crystal structures of both substances were given by Flachsbart (42). Pure salol is rhombic with 12 molecules per unit cell and lattice

parameters a = 11.25 Å, b = 23.5 Å, c = 8.10 Å. Pure thymol is rhombohedral with 6 molecules per unit cell and a = 11.45 Å, $\alpha = 79°44'$.

2. Refractive Index

The refractive indices of pure melts and binary mixture were directly measured by using a Bausch and Lomb precision Refractometer (Model ABBE-3L). The results agree well with the values obtained by Cheng (1969). By using a nonlinear polynomial curve-fitting subroutine program in the L.B.L. Computer Center, the refractive index of the salol-thymol melts, as a function of the mole fraction of salol and temperature, was fitted by the equation,

$$n(T,y) = 1.53428 - 5.56883 \times 10^{-4}T + 7.95434 \times 10^{-2}y + 1.71362 \times 10^{-5}yT + 1.1 \times 10^{-6}T^2 - 1.31182 \times 10^{-2}y^2$$

where T is in °C, and y is mole fraction of salol. The refractive indices of the pure substances were found to be linear functions of temperature,

$$\text{Salol:} \quad n = 1.5433 - 4.666 \times 10^{-4}T$$

$$\text{Thymol:} \quad n = 1.5273 - 4.2053 \times 10^{-4}T \quad .$$

3. Viscosity

The literature values of viscosity, μ, by Jantsch (43) for salol and by Slavyanski (44) for salol, thymol and their mixtures are listed in Table XI. These values were used for the necessary calculations of viscosity activation energies and entropies.

4. Density

The densities of the pure melts were taken from Timmermans (41). Values are listed in Table XI for the appropriate range.

Table XI

Viscosities and Densities of Pure Salol and Thymol

T °C	η_S [a] poise	η_S [b] poise	η_T [b] poise	d_S [c] g/cc	d_T [c] g/cc
9.6	---	---	---	---	0.9816 (S)
25.0	---	0.216	0.200	---	---
28.4	0.171	---	---	---	---
29.2	0.168	---	---	---	---
30.0	---	0.155	0.150	---	---
32.8	0.137	---	---	---	---
35.0	---	0.107	0.110	---	---
37.5	0.109	---	---	---	---
40.0	---	0.095	0.096	---	---
41.7	0.091	---	---	---	---
45.0	---	0.076	0.072	1.17858 (L)	---
45.10	0.079	---	---	---	---
50.0	---	---	0.058	---	---
51.4	---	---	---	---	0.9484 (L)
54.9	---	---	---	---	0.9461 (L)
55.0	---	---	0.049	1.16981 (L)	---

[a] Viscosity of salol melt by Jantsch (43); all values for liquid state.

[b] Viscosities of pure salol and pure thymol by Slavyansky (44); all values for the liquid state.

[c] Densities of salol and thymol given by Timmermans (41); values for the solid are indicated by (S), those for the liquid by (L).

5. Diffusivity

The Wilke-Chang correlation (40) was used for the prediction of the diffusivities at infinite dilution of salol in thymol and thymol in salol. The correlation suggested by Vignes (45) was applied to compute the diffusivities of binary mixtures,

$$D_{ST} = (D_{o_{ST}})^{y_T}(D_{o_{TS}})^{y_S} .$$

The relationship $(D\mu/T)$ = constant was used to correct the diffusivity for other temperatures. Table XII listed the calculated diffusivities in the salol-thymol system.

Table XII

Calculated Diffusivities of the Salol-Thymol System

Authors	Temperature °C	Diffusivity, $cm^2/sec \times 10^{-6}$	
		$D_{o_{ST}}$	$D_{o_{TS}}$
Wilke-Chang (40)	27	1.25	0.77
Gainer-Metzner (46)	27	0.80	0.67

Other physical properties of pure substances are listed in Table XIII.

Table XIII. Physical Properties of the Pure Substance

Substance	T_m [a]	ΔH_f [b]	ΔS_f [c]	C_p [d]	ρ_s [e]	ρ_L [e]	$\Delta H_V^{\ddagger}$ [b]	$\Delta S_V^{\ddagger}$ [c]	$\Delta H_C^{\ddagger}$ [b]	$\Delta S_C^{\ddagger}$ [c]	MW
Salol	42.2	4670	14.8	21.5	1.25	1.2	7860	27.8	5188	15.0	214.2
Thymol	49.8	4160	12.8	14.4	1.09	0.97	8140	26.4	5372	15.6	150.2

[a] Temperature, °C.

[b] Enthalpy change, cal/mole-°K.

[c] Entropy change, cal/mole-°K.

[d] Liquid heat capacity, cal/mole-°K.

[e] Density, gm/cm^3.

APPENDIX II

A. Sample Calculations

1. Measured Data for Salol-Thymol System

All measured quantities α, β, γ, s, t_i, ΔN, V, $(\frac{dw}{dv})_{v=0}$, for the computation of interfacial concentration gradients and concentrations are listed in Tables VI and VII of Chapter III. The fringe shift, ΔN, at the interface is equal to (OB/OA) in Fig. 5 of Chapter III. The measured refractive indices were given in the fitted equation in Appendix I.

Thus,

$$\frac{\partial n}{\partial T})_y = -5.56883 \times 10^{-4} + 1.71362 \times 10^{-5} y_o + 2.2 \times 10^{-6} T_i$$

$$\frac{\partial n}{\partial y})_T = 7.95434 \times 10^{-2} + 1.71362 \times 10^{-5} T - 2.62364 \times 10^{-2} y_o$$

where, T_i = interfacial temperature in °C,

y_o = original liquid concentration in mole fraction of salol.

2. Calculation of Interfacial Liquid Composition

For experimental run 36-1,

y_o = 0.15 mole fraction

λ_o = 6.328×10^{-4} mm

V = 0.71×10^{-4} cm/sec

t_i = 0.4572 mm

ΔT_i = 0.09 °C (from Figs. 6 and 7)

ΔN = -3.085

T_i = 16.15 °C

$\frac{\partial n}{\partial T})_{y_i} = -5.18 \times 10^{-4}$ °C^{-1}

$\frac{\partial n}{\partial y})_{T_i} = 7.52 \times 10^{-2}$

Eq. (39) of Chapter III,

$$y_i = 0.15 - \frac{\left(\frac{6.328 \times 10^{-4}}{2 \times 0.4572}\right)(-3.085) - (-5.18 \times 10^{-4})(0.09)}{7.52 \times 10^{-2}}$$

$$= 0.15 + 0.028$$

$$= 0.178 \text{ mole fraction of salol.}$$

3. <u>Calculation of Interfacial Solid Composition</u>

$y_i = 0.178$

$\frac{\rho_s}{\rho_L} \simeq 1$

$D = 1.123 \times 10^{-6}\ cm^2/sec$

$\alpha = 8.43$ degrees

$\beta = 84.58$ degrees

$\left.\frac{dw}{dv}\right)_{v=0} = -1.121$

$\Delta N = -3.085$

$s = 1.51 \times 10^{-2}$ mm

$t_i = 0.4572$ mm .

From Eq. (41) of Chapter III,

$$\left.\frac{dy}{dz}\right)_{z=0} = \frac{6.328 \times 10^{-4} \times (-1.121)}{2(1.51 \times 10^{-2})(0.4572)(\cos 8.43)[\sin 84.58 + (-1.121)\cos 84.58]}$$

$$\times \frac{}{(7.52 \times 10^{-2})}$$

$$= -0.7552\,(mm)^{-1}$$

$$= -7.552\,(cm)^{-1} .$$

From Eq. (40) of Chapter III,

$$x_i = 0.178 + \frac{1.123 \times 10^{-6}}{0.71 \times 10^{-4}} \times (-7.552)$$

$$= 0.0585 \text{ mole fraction of salol} \quad .$$

4. <u>Theoretical Prediction of the Interfacial Solid Composition from Absolute Rate Theory</u>

y_o = 0.15 mole fraction of salol

$\chi = 10^{-8}$

$\Delta H_C^{\ddagger} = c\Delta H_V^{\ddagger} = 0.66 \times 8140 = 5372$ cal/mole-°K

$\Delta S_C^{\ddagger} = \Delta S_V^{\ddagger} - (\Delta S_f - R) = 26.4 - 12.8 + 2 = 15.6$ cal/mole-°K

$h = 6.6252 \times 10^{-27}$ erg-sec

$k = 1.3805 \times 10^{-16}$ erg/°K

$T_i = 16.15$ °C = 289.3 °K .

Eq. (2) of Chapter II,

$$K_B^F = 10^{-8} \left(\frac{1.3805 \times 10^{-16}}{6.6252 \times 10^{-27}}\right)(289.3) \exp\left(\frac{-5372 + 289.3 \times 15.6}{2 \times 289.3}\right)$$

$$= 1.12 \times 10^5 \text{ (sec)}^{-1} \quad .$$

Eq. (20),

$$\Delta G = [\Delta S_f - \Delta C_p(1 - \frac{T}{T_{Bm}}) - r\ln(\gamma_B y_B)]\Delta T$$

$\Delta T = 20.62$ °K

$\Delta C_p(1 - \frac{T}{T_{Bm}}) \simeq 0$

$\gamma_B \approx 1$

$\Delta G = [12.8 - 2\ln(0.15)](20.62)$

$= 183.84$ cal/mole-°K .

Eq. (42),

$$f = \frac{1}{1.2\pi} \left(\frac{\Delta G}{T_{Bm}\Delta S_f}\right)$$

$$f = \frac{183.84}{1.2 \times 3.14 \times 309.9 \times 12.8} = 1.61 \times 10^{-2}$$

$$\lambda_s = \left(\frac{V_s}{N}\right)^{1/3} = \left(\frac{150.2}{0.98 \times 6.023 \times 10^{23}}\right)^{1/3}$$

$$= 6.34 \times 10^{-8} \text{ cm}$$

$$g_B = \frac{f\lambda_s K_B^F}{V}$$

$$= \frac{1.61 \times 10^{-2} \times 6.34 \times 10^{-8} \times 1.12 \times 10^{5}}{0.71 \times 10^{-4}}$$

$$= 1.61 \quad .$$

Eq. (19) of Chapter II,

$$x_B = \frac{g_B y_A y_B + y_B}{1 + g_B y_A y_{Be}}$$

$$y_A = 0.178$$

$$y_B = 0.822$$

$$y_{Be} = 0.528$$

$$x_B = \frac{1.61(0.178)(0.822) + 0.822}{1 + 1.61(0.178)(0.528)}$$

= 0.931 mole fraction thymol = 0.069 mole fraction of salol .

5. <u>Theoretical Prediction of Interfacial Solid Composition from Liquid Inclusion Theory</u>

From Fig. 13 of Chapter IV,

$$\frac{k_1}{R} = 0.00129 \text{ (cm/sec)}^{1/2}$$

$$\frac{k_2}{R} = 0.25 \quad .$$

Therefore, $\frac{k_1}{k_2} = \frac{0.00129}{0.25} = 0.00518\ (\text{cm/sec})^{1/2}$.

Eq. (23),

$$r = \frac{k_1}{(Vy_o)^{1/2}} + k_2$$

$$\frac{r}{k_2} = \frac{k_1}{k_2} \frac{1}{(0.71 \times 10^{-4} \times 0.15)^{1/2}} + 1$$

$$= 2.58$$

$$\frac{r}{R} = \frac{r}{k_2} \times \frac{k_2}{R} = 2.58 \times 0.25 = 0.645$$

$$\psi = \left(\frac{r}{R}\right)^2 = (0.645)^2 = 0.415 \quad .$$

Eq. (26),

$$x_i = x_c\psi + (1 - \psi)y_i$$

since $x_c = K_e y_i = 0$

$$x_i = (1 - 0.415) \times 0.178$$

$$= 0.104 \text{ mole fraction of salol} \quad .$$

APPENDIX III

A. Infrared Absorption Analyses

Crystals solidified from the binary mixture of salol and thymol under T.G.M.S. experiment were dissolved in the spectro-grade carbon-tetrachloride and then these solutions were analyzed by infrared absorption. The equation for analyzing binary mixtures dissolved in solution is based on the assumption that the absorbances of the individual species are additive. From Beer's Law,

$$A = \ell n \frac{I_o}{I} = a\ell c \qquad (1)$$

where, A = absorbance

I_o = input light intensity

I = output light intensity

a = absorbtivity

ℓ = path length

c = molar concentration .

Let,

A_1 = absorbance of salol and thymol mixture at wavelength 1

A_2 = absorbance of salol and thymol mixture at wavelength 2

S_1 = salol at wavelength 1

T_o = thymol at wavelength 1

S_2 = salol at wavelength 2

T_2 = thymol at wavelength 2 .

Therefore, at wavelength 1,

$$A_1 = A_{S_1} + A_{T_1} \qquad (2)$$

$$A_1 = a_{S_1} \ell c_S + a_{T_1} \ell c_T \quad . \qquad (3)$$

Also at wavelength 2,

$$A_2 = a_{S_2} \ell c_S + a_{T_2} \ell c_T \quad . \tag{4}$$

When Eq. (3) and Eq. (4) are solved simultaneously,

$$c_S = \frac{A_1 a_{T_2} - A_2 a_{T_1}}{\ell(a_{S_1} a_{T_2} - a_{S_2} a_{T_1})} \tag{5}$$

$$c_T = \frac{A_1 a_{S_2} - A_2 a_{S_1}}{\ell(a_{T_1} a_{S_2} - a_{T_2} a_{S_1})} \quad . \tag{6}$$

The Beckman Spectrophotometer, Model 227, and KCl liquid cells with 1 cm path length were used in this experiment. Pure salol and thymol spectra were calibrated to find a_{T_1} and a_{T_2} at known concentrations of pure thymol in carbon tetrachloride solutions, also a_{S_1} and a_{S_2} at known concentrations of pure salol.

The absorbance of pure thymol and salol at the characteristic wavelengths 2.8μ (OH group of thymol), 6.0μ (COO group of salol) and known concentrations are listed in Tables XIV and XV.

Let 2.8μ be wavelength 1 and 6.0μ be wavelength 2. The slopes of calibration lines for thymol are,

$$a_{T_1} = 2.11 \times 10^2$$

$$a_{T_2} = 0$$

and for salol, they are

$$a_{S_1} = 0$$

$$a_{S_2} = 8.58 \times 10^2 \quad .$$

Using run 36-01 (Table IX) as an example, the infrared absorption analysis of the solution of solid grown in the experiment gave,

$$\ell = 1 \text{ cm}$$

$$A_1 = 0.335$$

$$A_2 = 0.0591 \quad .$$

From Eq. (3) and Eq. (4),

$$c_S = \left(\frac{-0.0951 \times 2.11 \times 10^2}{-8.58 \times 2.11 \times 10^4}\right) = 1.108 \times 10^{-4} \text{ molar}$$

$$c_T = \left(\frac{8.58 \times 10^2 \times 0.335}{2.11 \times 8.58 \times 10^4}\right) = 1.59 \times 10^{-3} \text{ molar} \quad .$$

Therefore the mole fraction of salol in the solid is,

$$\frac{c_S}{c_S + c_T} = \frac{0.11 \times 10^{-4}}{(1.59 + 0.111) \times 10^{-4}} = 0.065 \quad .$$

Table XIV

The Infrared Absorption of Pure Thymol

Molar Concentration	Absorbance	
	2.8μ	6.0μ
0.0002	0.060	0
0.0005	0.109 ± 0.001	0
0.0010	0.210 ± 0.002	0
0.0020	0.440 ± 0.012	0

Table XV

The Infrared Absorption of Pure Salol

Molar Concentration	Absorbance	
	2.8μ	6.0μ
0.0001	0.037	0.0225 ± 0.0025
0.0002	0.038	0.1105 ± 0.0075
0.0003	0.040	0.02125± 0.0025
0.0005	0.038	0.3550 ± 0.005
0.00075	0.039	0.590 ± 0.005
0.001	0.038	0.785 ± 0.005

APPENDIX IV

FORTRAN IV PROGRAM LISTING

```
FRINGE,7,40,150000.468001,SHIH
*USERPR
RUN(S)
FRINGE.
EXIT.
DMP.
-
C     ***********
C
C      THIS PROGRAM WAS WRITTEN TO ANALYZE THE FRINGE SHIFT AT THE CRYSTAL
C      INTERFACE FOR THE THYMOL-SALOL SYSTEM AND CALCULATE ALL POSSIBLE VALUE
C      FROM THE TEMPERATURE-GRADIENTS MICROSCOPE STAGE EXPERIMENTS
C
C     N      = NUMBER OF THE DATA POINTS ( OR NUMBER OF THE PICTURES )
C     FACTOR = CONVERSION FACTOR FOR THE MAGNIFICATION OF MICROSCOPE
C     Y1,Y2  = Y DISTANCE OF THE WEDGE WHEN A,B AND C,D WERE MEASUREMED
C     Y3     = Y DISTANCE OF THE WEDGE WHEN PICTURE WAS TAKEN
C     CL1    = ORIGINAL LIQUID CONCENTRATION, MOLE FRACTION OF SALOL
C     DINT   = DISTANCE BETWEEN CRYSTAL FACE AND THERMOCOUPLE
C     DTH    = DISTANCE BETWEEN THERMOCOUPLE AND HOT STAGE
C     DMI    = MOTOR MOVEMENT READING WHEN THE DINT WAS MEASURED
C     DMR    = MOTOR MOVEMENT READING WHEN EACH PICTURE WAS TAKEN
C     S1     = MOTOR READING WHEN BEGIN TO MEASURE THE CRYSTAL GROWING RATE
C     S2     = MOTOR READING AT THE END OF GROWTH RATE MEASUREMENT
C                  ***S1 AND S2 MEASUREMENT HAS TO BE AT STEADY STATE GROWTH RATE
C     TIME   = TIME BETWEEN S1 AND S2 MEASUREMENTS
C     DELTI  = TEMPERATURE RISE AT THE INTERFACE DUE TO THE HEAT RELEASED
C     YO     = AVERAGE SLOPE OF THE FRINGE CURVE AT RHE INTERFACE
C     TG     = TEMPERATURE GRADIENT IN LIQUID PHASE (THE SLOPE OF EXTRRAOLATED
C              LINE.)
C     ST     = DEGREE OF SUPERCOOLING
C     TIEX   = EXTRAPOLATED INTERFACIAL TEMPERATURE
C     SR     = SLIDE MOVING SPEED, CM/SEC
C     ANGLE  = ANGLE BETWEEN THE INTERFACE AND VERTICAL LINE ON THE PICTURE
C     GR     = CRYSTAL GROWTH RATE ( SR*COS(ANGLE))
C     TIACT  = ACTUAL INTERFACIAL TEMPERATURE
C     DIF    = DIFFUSIVUTY OF THE LIQUID MIXTURE AT THE INTERFACIAL TEMPERATURE
C     DNDT   = REFRACTIVE INDEX CHANGE WITH RESPECT TO TEMPERATURE
C     DNDY   = REFRACTIVE INDEX CHANGE WITH RESPECT TO CONCENTRATION OF SALOL
C
C     DCDZ   = CONCENTRATION GRADIENT OF LIQUID AT THE INTERFACE
C     A,B,C,D = MEASUREMENTS OF WEDGE THICKNESS FROM THE FOCUS OF THE MICROSCOPE
C
C     TEMPCA = SUBROUTINE PROGRAM FOR THE TEMPERATURE MEASUREMENTS
C     LSQS   = SUBROUTINE FOR THE LINEAR LEAST SQUARE CURV FITTING
C     ***********************
C
      PROGRAM FRINGE (INPUT,OUTPUT)
C
C
      DIMENSION Z(500,20),Y(500,20),X(500,20),SX1(200),SX2(200),SX3(200)
     1,OB1(50),SYO(200),SXY(200),SX2Y(200),XX(200,10),YY(200,10),DENOTE(
     2200),A1(200),A2(200),A3(200),YO(60),SPAV(60),XL1(4),YL1(4),XL2(3),
     3YL2(3),OA(60),OB(60),CL(60),ANGLE(60),ANGL(60),BETA(60),BET(60),AL
     4PHA(60),ALPH(60),DCDZ(60),THETA(60),EMF(20),DMR(20),THICK(60),XI(2
     50),XT(20),TIEX(60),DELTI(60),SX4(200),DELN(60),TIACT(60),DNDCTI(60
     6),CYI(60),CXI(60),DIF(60),GRY(60)
      DIMENSION EK(60),AKI(60),TE(60),ST(60),ST2(60)
      DIMENSION GR(60),TGS(60),SR(60)
      DIMENSION X111(60)
```

```
      DIMENSION DSC(60),DHC(60)
      DIMENSION DN(60),T(30)
      DIMENSION DELNT(60)
      DIMENSION TD(60)
      DIMENSION DTT(60),DTS(60)
      DIMENSION SPA1(60)
      DIMENSION DNDT(60),DNDY(60)
      DIMENSION LIQM(60),PLANAR(60),PLANA1(60),HL7(60),HR7(60),YS(60)
      DIMENSION TG(60),CYETI(60)
      DIMENSION DN11(60)
      DIMENSION XIYI(60)
      DIMENSION CKF(60),DG(60)
      DIMENSION CO(60),HO(60)
      DIMENSION DCDZD(60)
      DIMENSION HR11(60)
      DIMENSION XXX(60),EKQB(60)
      DIMENSION GB3(60),TK3(60),FT3(60),EKQN3(60),EKQD3(60)
      DIMENSION TC(20)
      DIMENSION TRANS(60),FKT(60)
      DIMENSION FACT(20)
      DO 10000 NOR=1,5
      READ 1,N
    1 FORMAT(I3)
      READ 2,(FACT(I),I=1,14)
      FAC=0.
      DO 101 J=1,6
      FACI=ABS(FACT(J*2+1)-FACT(J*2-1))
  101 FAC=FAC+FACI
      FACTOR=0.01*6./FAC
      PRINT 555
    3 FORMAT(*  INPUT MICROSCOPE X-Y DATD FROM X-Y PLOTTER*)
    4 FORMAT(//,*     Y1       X1       Y2       X2       Y3       X3       Y4
     1     X4       Y5       X5       Y6       X6       Y7       X7*,/)
      N1=N*6
      DO 10 I=1,N1
C
C     INPUT MICROSCOPE X-Y DATA
C
      READ 2,(Z(I,J),J=1,14)
    2 FORMAT(10X,14F5.4)
    5 FORMAT(14F8.4)
   10 CONTINUE
      DO 30 I=1,N1
      DO 20 J=1,7
      J1=J*2-1
      Y(I,J)=Z(I,J1)
   20 X(I,J)=10.-Z(I,J*2)
   30 CONTINUE
C
C     ************************************
C
C     FOUR FRINGES WERE MEASURED ,EACH FRINGE HAS  7 POINTS IN X,Y, COORDINATE
C     THE 1ST POINT WAS ORIGIN
C
C
      IL=1
      N2=N1-N*2.
      LL=1
      DO 50 I=1,N2
```

```
      L=IL+2
      SX1(I)=0.
      SX2(I)=0.
      SX3(I)=0.
      SX4(I)=0.
      SYO(I)=0.
      SXY(I)=0.
      SX2Y(I)=0.
      DO 60 J=1,5
      Q1=Y(L,J+1)-Y(L,1)
      Q2=X(L,J+1)-X(L,1)
      YY(I,J+1)=Q1
   60 XX(I,J+1)=Q2
      XX(I,1)=0.
      YY(I,1)=0.
      IF(L.EQ.6.*LL) 61,62
   61 IL=IL+2
      LL=LL+1
   62 IL=IL+1
      DO 70 J=1,6
      SX1(I)=SX1(I)+XX(I,J)
      SX2(I)=SX2(I)+XX(I,J)**2
      SX3(I)=SX3(I)+XX(I,J)**3
      SX4(I)=SX4(I)+XX(I,J)**4
      SYO(I)=SYO(I)+YY(I,J)
      SXY(I)=SXY(I)+XX(I,J)*YY(I,J)
   70 SX2Y(I)=SX2Y(I)+(XX(I,J)**2)*YY(I,J)
      DENOTE(I)=6. *SX2(I)*SX4(I)+2.*SX1(I)*SX2(I)*SX3(I)-SX2(I)**3-6.*S
     1X3(I)*SX3(I)-SX4(I)*SX1(I)**2
      IF(DENOTE(I).EQ.0.) GO TO 50
      A1(I)=(SYO(I)*SX2(I)*SX4(I)+SX2Y(I)*SX1(I)*SX3(I)+SXY(I)*SX3(I)*SX
     12(I)-SX2Y(I)*SX2(I)**2-SXY(I)*SX1(I)*SX4(I)-SYO(I)*SX3(I)**2)/DENO
     2TE(I)
      A2(I)=(SXY(I)*6.*SX4(I)+SYO(I)*SX2(I)*SX3(I)+SX1(I)*SX2(I)*SX2Y(I)
     1-SX2(I)**2*SXY(I)-SYO(I)*SX1(I)*SX4(I)-6.*SX2Y(I)*SX3(I))/DENOTE(I
     2)
        A3(I)=(6.*SX2(I)*SX2Y(I)+SX1(I)*SX2(I)*SXY(I)+SYO(I)*SX1(I)*SX3(
     1I)-SYO(I)*SX2(I)**2-6.*SX3(I)*SXY(I)-SX1(I)**2*SX2Y(I))/DENOTE(I)
   71 FORMAT(//,*     I=*I4,*  A1=*,E12.5,*     A2=*,E12.5,*     A3= *E12.5
     1)
   50 CONTINUE

      INPUT THE T.G.M.S. EXPERIMENTAL DATA

      DO 210 I=1,N
      READ 11,Y3,YI,Y2,A,B,C,D
      READ 12,DINT,DTH,DMI,HOT,COLD
      READ 13,M,K,CL1,SM1,SM2,TIME
   11 FORMAT(3F10.9,4F10.7)
   12 FORMAT(F10.8,4F10.9)
   13 FORMAT(2I10,F10.10,3F10.9)
      CL(I)=CL1
      TH=(Y2-Y3)*(ABS(C-D)-ABS(A-B))/(YI-Y3)
      THICK(I)=(TH+ABS(A-B))*0.001-0.1
      READ 14,(DMR(J),J=1,M)
      READ 14,(EMF(J),J=1,M)
   14 FORMAT(8F10.9)
      THETA(I)=ATAN((ABS(C-D)-ABS(A-B))/(ABS(YI-Y3)*10000.))
      DO 200 J=1,M
      DMR2=(DMR(J)*25.4)/4.
```

```
      XT(J)=DMR2+DTH
      XI(J)=(DMI*25.4)/4.+DTH+DINT-XT(J)
      CALL TEMPCA(EMF(J),K,T(J))
 3002 FORMAT(5X,2F14.5)
  200 CONTINUE
C
C     CALCULATE THE INTERFACIAL TEMPERATURE
C
C
      CALL LSQS(XT,T,M,AI1,AI2,EI1)
  778 FORMAT(* X HOT STAGE,  EXP. TEMP.  LSQ FIT T. X FROM INTERFACE
     1  DT*)
  779 FORMAT(*     (MM)      (DEGREE C)     (DEGREE C)          (MM)*)
  775 FORMAT(5F12.4,5X,I4)
      TG(I)=ABS(AI1)*10.
      TIEX(I)=AI1*(25.4*DMI/4.+DINT+DTH)+AI2
  774 FORMAT(//,*  EXTRAP. INTERFACE TEMP.   =  *,5XF12.4,//)
      CALL TEMPCA(HOT,K,HO(I))
      CALL TEMPCA(COLD,K,CO(I))
      TGS(I)=(HO(I)-CO(I))/2.52
      SR(I)=((SM2-SM1)*2.54)/(4.*60.*TIME)
  210 CONTINUE
C
C     CALCULATE THE ANGLE INVOLVED
C
      DO 80 I=1,N
      I2=6*I-5
      DO 140 J=1,4
      XL1(J)=X(I2,J)
  140 YL1(J)=Y(I2,J)
      CALL LSQS(XL1,YL1,4,S1,C1,V1)
      I3=6*I-5
      DO 150 J=5,7
      XL2(J-4)=X(I3,J)
      YL2(J-4)=Y(I3,J)
  150 CONTINUE
      CALL LSQS(XL2,YL2,3,S2,C2,V2)
      IF(S1.EQ.S2) GO TO 148
      IF(S1.EQ.3434.7) 141,142
  141 ANGLE(I)=11./7.-ATAN(ABS(S2))
      GO TO 147
  142 IF(S2.EQ.3434.7) 143,144
  143 ANGLE(I)=11./7.-ATAN(ABS(S1))
      GO TO 147
  144 ANGLE(I)=ATAN(ABS((S1-S2)/(1.+S1*S2)))
  147 GR(I)=SR(I)*COS(ANGLE(I))
      GO TO 149
  148 GR(I)=SR(I)
      ANGLE(I)=0.
      S3=(-1.)/S1
  149 BETA(I)=ATAN(ABS(S2))
      IF(S1.EQ.3434.7) 151,152
  151 S3=0.
      GO TO 153
  152 S3=(-1.)/S1
  153 ALPHA(I)=ATAN(ABS(S3))
      ANGL(I)=(360.*7./44.)*ANGLE(I)
      BET(I)=360.*7.*BETA(I)/44.
      ALPH(I)=360.*7.*ALPHA(I)/44.
```

```
C
C     CALCULATE THE INTERFACIAL TEMPERATURE RISE
C
      DTS(I)=THICK(I)*CL(I)*(2.-(12.E-4-GR(I))*1.17/4.E-4)
      IF(GR(I).LT.1.E-4) DTT(I)=THICK(I)*CL(I)*(1.1+(GR(I)-1.E-4)*1.33/1
     1.5E-4)
      IF(GR(I).EQ.1.E-4) DTT(I)=THICK(I)*CL(I)*3.5
      IF(GR(I).GT.1.E-4) DTT(I)=THICK(I)*CL(I)*(3.5+(GR(I)-4.E-4)*0.3/1.
     1E-4)
      IF(DTS(I).LT.0.) DTS(I)=0.
      IF(DTT(I).LT.0.) DTT(I)=0.
      DELTI(I)=DTT(I)+DTS(I)
C
C     CALCULATE THE VERTICAL SPACING BETWEEN FRINGES IN X-Y COORDINATES
C
      SP=0.
      I1=6*I-4
      DO 120 J=1,6
  120 SP=SP+ABS(Y(I1,J+1)-Y(I1,J))
C
C     FIND THE FRACTION OF FRINGE SHIFT AT THE INTERFACE
C
      DELNT(I)=0.
      DO 440 J=1,3
      I4=6*I-4+J
      I5=6*I-4
      I6=8-J
      O2=(Y(I4+1,1)-Y(I4,1))**2
      O3=(X(I4+1,1)-X(I4,1))**2
      O1=ABS(O2+O3)
      OAA=SQRT(O1)
      OBB=Y(I5,I6)-Y(I4,1)
      OB2=OBB/COS(ANGLE(I))
      DEL=OB2/OAA
      DELNT(I)=DELNT(I)+DEL
  440 CONTINUE
      DELN(I)=DELNT(I)/3.
      SPA1(I)=(SP/6.)*FACTOR
  110 SPAV(I)=SPA1(I)/COS(ANGLE(I))
C***
C
C
C
C
C*****
      YO(I)=(A2(I*4-3)+A2(4*I-2)+A2(4*I-1)+A2(4*I))/4.
      TIACT(I)=TIEX(I)+DELTI(I)
C
C
C      CALCULATE THE DIFFUSIVITY OF THE MIXTURE AT INTERFACIAL TEMPERATURE
C
      DIFTS=EXP(CL(I)*ALOG(0.77)+(1.-CL(I))*ALOG(1.25))
      DIF(I)=DIFTS*1.E-6*(TIACT(I)+273.15)/300.15
C
C******
C     CALCULATE THE REFRACTIVE INDEX CHANGE VS TEMPERATURE AND TEMPERATURES
C
      YS(I)=CL(I)
      ITE=0
      DN(I)=(6.328E-4)*DELN(I)/(2.*THICK(I))
```

```
  993 DNDT(I)=-5.56883E-4+YS(I)*1.71362E-5+TIACT(I)*2.2E-6
      DNDY(I)=7.95434E-2+1.71362E-5*TIACT(I)-YS(I)*2.*1.31182E-2
C
C     CALCULATE THE CONCENTRATION GRADIENT, INTERFACIAL LIQUID AND SOLID CONC.
C
      DCDZD(I)=2.*SPAV(I)*THICK(I)*COS(ALPHA(I))*DNDY(I)*(SIN(BETA(I))+Y
     10(I)*COS(BETA(I)))
      DCDZ(I)=6328.E-7*Y0(I)/DCDZD(I)
      DN11(I)=(DN(I)-DNDT(I)*(+DELTI(I)))/DNDY(I)
      CYI(I)=CL(I)-(DN11(I))
      DFF=ABS(YS(I)-CYI(I))
      IF(DFF.LT.1.0E-3) 991,992
  992 YS(I)=CYI(I)
      ITE=ITE+1
      IF(ITE.GT.1000) GO TO 991
      GO TO 993
  991 CXI(I)=CYI(I)+(DIF(I)*DCDZ(I)/GR(I))*10.
      XIYI(I)=(DIF(I)*DCDZ(I)/GR(I))*10.
      GRY(I)=GR(I)/CYI(I)
      IF(CL(I).GT.0.58) AKI(I)=CXI(I)/CYI(I)
      IF(CL(I).LT.0.58) AKI(I)=(1.-CXI(I))/(1.-CYI(I))
      IF(CYI(I).LT.0.5765) TE(I)=49.8-79.198448*CYI(I)+38.322395*CYI(I)*
     1*2-26.323182*CYI(I)**3
      IF(CYI(I).GT.0.5765) TE(I)=-138.71831+489.01344*CYI(I)-503.51732*C
     1YI(I)**2+195.26180*CYI(I)**3
      ST(I)=TE(I)-TIACT(I)
      ST2(I)=ST(I)**2
      IF(TIACT(I).LT.13.) 222,223
  222 CYETI(I)=0.
      GO TO 224
  223 IF(CYI(I).GT.0.5765) CYETI(I)=5.6070045E-1-TIACT(I)*6.5955042E-3+T
     1IACT(I)**2*6.7787577E-4-TIACT(I)**3*6.478803E-6
      IF(CYI(I).LT.0.5765) CYETI(I)=7.9111099E-1-TIACT(I)*1.5782194E-2-T
     1IACT(I)**2*4.9189459E-5+TIACT(I)**3*1.0880115E-6
  224 PLANA1(I)=SQRT(CL(I)*GR(I))
      AKE=0.
      IF(CL(I).GT.0.58) AKE=1./CYETI(I)
      IF(CL(I).LT.0.58) AKE=1./(1.-CYETI(I))
C
C
C
C     LIQUDUS SLOPE
C
      IF(CL(I).LT.0.5765) LIQM(I)=-79.198448+2.*38.322395*CL(I)-3.*26.32
     13182*CL(I)**2
      IF(CL(I).GT.0.5765) LIQM(I)=489.01344-2.*503.51732*CL(I)+3.*195.26
     1180*CL(I)**2
      PLANAR(I)=SQRT(ABS(TG(I)*DIF(I)/LIQM(I)))
      HR7(I)=1./PLANA1(I)
      HL7(I)=SQRT(ABS((AKI(I)-1.)/(AKE-1.)))
      HR11(I)=PLANAR(I)/PLANA1(I)
C
C      CALCULATE THE FORWARD RATE COEFFICIENT
C
      T10=TIACT(I)
      T11=T10+273.15
      CC=-1./0.66
      IF(CL(I).LT.0.5) GO TO 410
      IF(CL(I).GT.0.5) GO TO 420
```

```
  410 DEST=(-8.3E-4)*(T10-9.6)+0.9816
      WT=6.3E-8
      DGT=(12.8-14.4*(1.-T11/(TE(I)+273.15))-1.987*ALOG(1.-CYI(I)))*ST(I)
     1)
      FT=DGT/(1.2*3.142*4160.)
      TEST10=GR(I)*(CYI(I)-CXI(I))
      TEST11=CYI(I)*(1.-CYI(I)-(1.-CXI(I))*(1.-CYETI(I)))
      FKT(I)=TEST10/TEST11
      CKF(I)=FKT(I)/(FT*WT)
      HVT=4160.
      TK1=0.21E11*T11*EXP((CC*HVT+T11*15.6)/(1.987*T11))
      TRANS(I)=CKF(I)/TK1
      GB=(TK1*1.0E-8*FT*WT)/GR(I)
      EKQB(I)=(GB*CYI(I)+1.)/(1.+GB*CYI(I)*(1.-CYETI(I)))
      XXX(I)=EKQB(I)*(1.-CYI(I))
      GB3(I)=GB
      TK3(I)=TK1
      FT3(I)=FT
      EKQN3(I)=GB*CYI(I)+1.
      EKQD3(I)=(1.+GB*CYI(I)*(1.-CYETI(I)))
      X111(I)=1.-CXI(I)
      GO TO 430
  420 DESS=(-8.77E-4)*(T10-45.)+1.17858
      DGS=(13.6-21.5*(1.-T11/(TE(I)+273.15))-1.987*ALOG(CYI(I)))*ST(I)
      FS=DGS/(1.2*3.142*4670.)
      WT=6.7E-8
      TEST12=GR(I)*(CXI(I)-CYI(I))
      TEST13=(1.-CYI(I))*(CYI(I)-CXI(I)*CYETI(I))
      FKT(I)=TEST12/TEST13
      CKF(I)=FKT(I)/(FS*WT)
      HVS=4670.
      SK1=0.21E11*T11*EXP((CC*HVS+T11*15.0)/(1.987*T11))
      TRANS(I)=CKF(I)/SK1
      GBS=(SK1*1.0E-8*WT*FS)/GR(I)
      EKQB(I)=(GBS*(1.-CYI(I))+1.)/(1.+GBS*(1.-CYI(I))*CYETI(I))
      XXX(I)=EKQB(I)*CYI(I)
      GB3(I)=GBS
      TK3(I)=SK1
      FT3(I)=FS
      EKQN3(I)=GBS*(1.-CYI(I))+1.
      EKQD3(I)=(1.+GBS*(1.-CYI(I))*CYETI(I))
C
C     CALCULATE THE ACTIVATION ENERGY
C
  430 CK2=(CKF(I)*4.8E-11)/(T11)
      CK3=ABS(CK2)
      DG(I)=1.987*T11*ALOG(CK3)*(-1.)
   80 CONTINUE
C
C
C     OUT PUT
C
C
      PRINT 555
      PRINT 501
  501 FORMAT(///,*        K          XI          YI          YTI         YO
     1      DCDZ        SR          GR/C        GR       K-PRED*)
      DO 500 I=1,N
  500 PRINT 502,I,AKI(I),CXI(I),CYI(I),CYETI(I),CL(I),DCDZ(I),SR(I),GRY(
     1I),GR(I),EKQB(I)
```

```
  502 FORMAT(I3,6F10.4,3E11.2,E14.6)
      PRINT 555
      PRINT 503
  503 FORMAT(///,*     TIEX      TI      TE      DELTI      TG     TGS      ST
     1     ST2      KF              DG            TRANS        FKT*)
      DO 505 I=1,N
  505 PRINT 506,I,TIEX(I),TIACT(I),TE(I),DELTI(I),TG(I),TGS(I),ST(I),ST2
     1(I),CKF(I),DG(I),TRANS(I),FKT(I)
  506 FORMAT(I3,8F7.2,4E14.3)
      PRINT 555
      PRINT 507
  507 FORMAT(///,*        YPRIME      GD/M        HL7,11     HR7
     1HR11       DIFF            DNDT              DNDY        X-PRED*)
      DO 510 I=1,N
  510 PRINT 511,I,Y0(I),PLANAR(I),HL7(I),HR7(I),HR11(I),DIF(I),DNDT(I),D
     1NDY(I),XXX(I)
  511 FORMAT(I3,F11.3,2E11.2,1F12.2,4E12.2,E14.6)
      PRINT 555
      PRINT 512
  512 FORMAT(///,*        ANGLE       ALPHA       BETA       THETA     COLD
     1     HOT          DN            THICK            SPACING*)
      DO 515 I=1,N
  515 PRINT 516,I,ANGL(I),ALPH(I),BET(I),THETA(I),CO(I),HO(I),DELN(I),TH
     1ICK(I),SPA1(I)
  516 FORMAT(2XI3,7F10.4,2F13.4)
      PRINT 555
      PRINT 517
  517 FORMAT(*          F                    K                  GB              KN
     1            KD              KEQ              X-PRED            XI*)
      DO 520 I=1,N
  520 PRINT 518,I,FT3(I),TK3(I),GB3(I),EKQN3(I),EKQD3(I),EKQB(I),XXX(I),
     1X111(I)
  518 FORMAT(I3,8E14.5)
  555 FORMAT(1H1)
10000 CONTINUE
      STOP
      END
```

```
      SUBROUTINE LSQS(X,Y,M,A,B,E1)
      DIMENSION X(20),Y(20)
      A=0.
      B=0.
      SX=0.
      SY=0.
      SXY=0.
      SX2=0.
      DO 10 I=1,M
      SX=SX+X(I)
      SY=SY+Y(I)
      SX2=SX2+X(I)**2
   10 SXY=SXY+X(I)*Y(I)
```

```
      AM=M
      IF((AM*SX-SX**2).EQ.0.) 30,40
   40 A=(AM*SXY-SX*SY)/(AM*SX2-SX**2)
      B=(SY*SX2-SX*SXY)/(AM*SX2-SX**2)
      E1=0.
      DO 20 I=1,M
   20 E1=E1+(Y(I)-(A*X(I)+B))**2
      GO TO 50
   30 A=3434.7
      B=SX/AM
      PRINT 100,B
  100 FORMAT(* LEST SQUARE FITTING LINE PARALLEL TO VERTICAL AXIS .
     1 X = B, WHERE B =*,E11.4)
   50 RETURN
      END
```

```
      SUBROUTINE TEMPCA(E,K,T)
      IF(E.GT.0.AND.E.LE.0.193)TI=0.+(E-0.)/0.0386
      IF(E.GT.0.193.AND.E.LE.0.389)TI=5.+(E-0.193)/0.0392
       IF(E.GT.0.389.AND.E.LE.0.587) TI=10.+(E-0.389)/0.0396
      IF(E.GT.0.587.AND.E.LE.0.787) TI=15.+(E-0.587)/0.04
      IF(E.GT.0.787.AND.E.LE.0.99) TI=20.+(E-0.787)/0.0406
      IF(E.GT.0.990.AND.E.LE.1.194) TI=25.+(E-0.990)/0.0408
      IF(E.GT.1.194.AND.E.LE.1.401) TI=30.+(E-1.194)/0.0414
      IF(E.GT.1.401.AND.E.LE.1.610) TI=35.+(E-1.401)/0.0418
      IF(E.GT.1.610.AND.E.LE.1.821) TI=40.+(E-1.610)/0.0422
      IF(E.GT.1.821.AND.E.LE.2.035) TI=45.+(E-1.821)/0.0428
      IF(E.GT.2.035.AND.E.LE.2.250) TI=50.+(E-2.035)/0.0430
      IF(E.GT.2.250.AND.E.LE.2.467) TI=55.+(E-2.250)/0.0434
      IF(E.GT.2.467.AND.E.LE.2.687) TI=60.+(E-2.467)/0.0440
      IF(E.GT.2.687.AND.E.LE.2.908) TI=65.+(E-2.687)/0.0442
      IF(E.GT.2.908.AND.E.LE.3.132) TI=70.+(E-2.908)/0.0448
      IF(E.GT.3.132.AND.E.LE.3.357) TI=75.+(E-3.132)/0.0450
      IF(E.GT.3.357.AND.E.LE.3.813) TI=80.+(E-3.357)/0.0456
      IF(E.GT.3.813.AND.E.LE.4.277) TI=90.+(E-3.813)/0.0464
      IF(E.GT.4.277.AND.E.LE.4.749) TI=100.+(E-4.277)/0.0472
      IF(E.GT.4.749.AND.E.LE.5.227) TI=110.+(E-4.749)/0.0478
      IF(E.GT.5.227.AND.E.LE.5.712) TI=120.+(E-5.227)/0.0485
      IF(E.GT.5.712.AND.E.LE.6.204) TI=130.+(E-5.712)/0.0492
      IF(E.GT.6.204.AND.E.LE.6.703) TI=140.+(E-6.204)/0.0499
      IF(E.GT.6.703.AND.E.LE.7.208) TI=150.+(E-6.703)/0.0505
      IF(E.GT.7.208.AND.E.LE.7.719) TI=160.+(E-7.208)/0.0511
      IF(E.GT.7.719.AND.E.LE.8.236) TI=170.+(E-7.719)/0.0517
      IF(E.GT.8.237) PRINT 1
    1 FORMAT(* TEMPERATURE RANGE OVER THE TABLE---INPUT DATA WRONG*)
      IF(K.EQ.1) T=TI-((TI-40.)*0.003+0.14)
      IF(K.EQ.2) T=TI-((TI-40.)*0.002+0.16)
      IF(K.EQ.3) T=TI-((TI-40.)*0.003+0.14)
      IF(K.EQ.4) T=TI-((TI-40.)*0.002+0.16)
      IF(K.EQ.8) T=TI-0.035
      IF(K.EQ.9) T=TI-0.1125
      RETURN
      END
```

LEGAL NOTICE

This report was prepared as an account of work sponsored by the United States Government. Neither the United States nor the United States Atomic Energy Commission, nor any of their employees, nor any of their contractors, subcontractors, or their employees, makes any warranty, express or implied, or assumes any legal liability or responsibility for the accuracy, completeness or usefulness of any information, apparatus, product or process disclosed, or represents that its use would not infringe privately owned rights.

TECHNICAL INFORMATION DIVISION
LAWRENCE BERKELEY LABORATORY
UNIVERSITY OF CALIFORNIA
BERKELEY, CALIFORNIA 94720